UNIVERSITÉ DE GENÈVE

Archive ouverte UNIGE
https://archive-ouverte.unige.ch

Thèse 2019

Open Access

This version of the publication is provided by the author(s) and made available in accordance with the copyright holder(s).

Complementarity of decoupling elements with respect to spectral quality in 2D pure-shift homonuclear experiments

Brucka, Marta

How to cite

BRUCKA, Marta. Complementarity of decoupling elements with respect to spectral quality in 2D pure-shift homonuclear experiments. Doctoral Thesis, 2019. doi: 10.13097/archive-ouverte/unige:127380

This publication URL: https://archive-ouverte.unige.ch/unige:127380
Publication DOI: 10.13097/archive-ouverte/unige:127380

© This document is protected by copyright. Please refer to copyright holder(s) for terms of use.

UNIVERSITE DE GENEVE FACULTE DES SCIENCES

Section de chimie et biochimie
Département de chimie organique Dr. Damien Jeannerat

Complementarity of decoupling elements with respect to spectral quality in 2D pure-shift homonuclear experiments

THÈSE

présentée à la Faculté des sciences de l'Université de Genève
pour obtenir le grade de Docteur ès sciences, mention chimie

par

Marta Brucka

de

Międzyzdroje (Pologne)

Thèse N° 5372

GENÈVE

Centre d'impression de l'Université de Genève, ReproMail, Unimail

2019

UNIVERSITÉ DE GENÈVE

FACULTÉ DES SCIENCES

DOCTORAT ÈS SCIENCES, MENTION CHIMIE

Thèse de Madame Marta BRUCKA

intitulée :

«Complementarity of Decoupling Elements with Respect to Spectral Quality in 2D Pure-shift Homonuclear Experiments»

La Faculté des sciences, sur le préavis de Monsieur D. JEANNERAT, docteur et directeur de thèse (Département de chimie organique), Monsieur F. COUGNON, docteur (Département de chimie organique), Madame S. HOOGENDOORN, professeure (Département de chimie organique), Monsieur J.-N. DUMEZ, professeur (Faculté des sciences et techniques, CEISAM (Chimie et Interdisciplinarité, Synthèse, Analyse, Modélisation, Nantes, France), autorise l'impression de la présente thèse, sans exprimer d'opinion sur les propositions qui y sont énoncées.

Genève, le 14 juin 2019

Thèse - 5372 -

p.o. **Le Décanat**

N.B. - La thèse doit porter la déclaration précédente et remplir les conditions énumérées dans les "Informations relatives aux thèses de doctorat à l'Université de Genève".

Abstract

The work presented in this thesis was aimed at exploring the homodecoupling methods implemented in different two-dimensional NMR experiments. The main goal was to demonstrate the advantages of these experiments in terms of resolution and the information content they provide with respect to "routinely" used experiments. Furthermore, the limitations and complementarity of the methods were investigated.

The first part of the work consisted in assembling a toolbox of two-dimensional homonuclear high-resolution experiments homodecoupled in the F1 indirect dimension (DIAG, CLIP-COSY, TOCSY). The homodecoupling leads to elimination of the *J*-scalar coupling splitting in the F1 dimension, significantly simplifying the multiplet pattern and reducing the signal overlap probability. The full multiplets, being invaluable providers of structural information, are preserved in the direct F2 dimension, where high resolution and thus complete separation of the multiplet components comes usually with no cost in experimental time. In our toolbox, the presence of the *J*-coupling constants in at least one dimension has been considered more important than the possible further increase in resolution by decoupling the signals in both spectral dimensions.

The specific experiments were built upon a common template sequence, which facilitated their implementation and use. The general scheme was introduced by Thrippleton and Keeler, where the mixing sequence - if present - is embraced by two *z*-filters that serve to purge the desired magnetization from any other unwanted contributions - mainly the zero-quantum coherences. All the experiments exploit the in-phase magnetization, which ensures that the signals belonging to one multiplet will be all positive and thus not prone to cancellation – in contrast to many routinely used experiments such as the DQF-COSY.

A particular attention has been put on the modularity of the whole structure. The experiments, employing decoupling elements based on different mechanisms, are complementary to each other and can be used to access the maximum of structural information, not easily available by other methods. The particular information that can be obtained from the spectra provided by each of the experiment depends mainly on the type of the mixing, if present.

The DIAG experiment lacks any mixing and thus, *in principle,* produces only diagonal signals. If decoupled in the F1 indirect dimension, it primarily aims at separating the chemical shift and *J*-coupling interactions while not providing any information about the correlations between spins. This experiment largely benefits from the possibility to drastically reduce the spectral window in F1. The much more recently proposed F1-decoupled and aliased DIAG can

be compared to the *J*-resolved spectroscopy introduced in the solution NMR methodology much earlier. Experiments separating interactions are highly desirable as they offer the possibility to simplify the spectra and to facilitate the precise measurement of the *J* - coupling in isolated multiplets.

In order to tackle more complex structural problems, we propose the insertion of in-phase based mixing sequences in the toolbox to provide the F1-decoupled CLIP-COSY and TOCSY experiments.

The CLIP-COSY provides in-phase multiplets of a regular lineshape for both diagonal and cross-peaks and it is compatible with the homonuclear decoupling. While the use of the selective modulated pulse *nemoZS* or the PSYCHE element to decouple the indirect dimension of the CLIP-COSY ensures its optimal sensitivity, the application of the BIRD filter introduces some novel and interesting features in this experiment and can be used to fully reveal the multiplet structure of signals not easily reachable by other methods.

The second, main part of the work, was dedicated to exploiting the toolbox experiments as model sequences in order to examine the spectral artifacts. This turned out to be a good occasion to explore more theoretical aspects of NMR spectroscopy in general and homodecoupling in particular. The path of building the theoretical structure allowing to approach the question of artifacts in these “toolbox experiments” was greatly facilitated by numerical simulations performed in the Spinach simulation package.

Le travail présenté dans cette thèse visait à explorer les méthodes de homodécouplage mises en œuvre dans différentes expériences de RMN bidimensionnelle. L'objectif principal était de démontrer les avantages de ces expériences en termes de résolution et du niveau d'information qu'elles fournissent par rapport aux expériences utilisées “en routine”.

La première partie du travail consistait à assembler une série d'expériences homonucléaires bidimensionnelles à haute résolution homodécouplé dans la dimension indirecte F1. L’homodécouplage conduit à l’élimination du dédoublement du couplage scalaire dans la dimension F1, simplifiant considérablement les multiplets et réduisant la probabilité de chevauchement des signaux. Les structures de couplage sont conservées dans la dimension directe F2, où une résolution élevée et une séparation complète des composantes du multiplet sont généralement obtenues sans augmentation du temps expérimental. Dans notre série d’expérience, la présence des constantes de couplage dans au moins une dimension a été jugée préférable par rapport à un découplage dans les deux dimensions spectrales.

Les expériences sont construites sur une séquence modèle commune, ce qui facilite leur mise en œuvre et leur utilisation. Le schéma général a été introduit par Thrippleton et Keeler, où la séquence de mélange - quand elle est présente - est entourée de deux filtres *z* qui servent à isoler l’aimantation souhaitée de toute autre contribution - principalement les cohérences de zéro quanta.

Toutes les expériences exploitent l'aimantation « en-phase », ce qui garantit que les signaux appartenant à un multiplet soient tous positifs et ne risquent donc pas d'être annulés - contrairement à ce qui se produit dans de nombreuses expériences couramment utilisées telles que la DQF-COSY.

Un soin particulier a été apporté pour assurer une modularité des expériences. Les informations spécifiques pouvant être obtenues à partir des spectres fournis par chacune des expériences dépendent donc principalement du type de mélange, le cas échéant.

Les expériences qui utilisent des éléments de découplage basés sur différents mécanismes sont complémentaires et permettent d’accéder à un maximum d’informations structurelles, difficiles à obtenir par d’autres méthodes.

L’expérience DIAG est dépourvue de tout mélange et peut donc, en principe ne produire que des signaux diagonaux. Découplée dans la dimension indirecte F1, elle vise principalement à séparer les interactions de déplacement chimique et de couplage sans fournir d'information sur les corrélations entre les spins. Cette expérience bénéficie largement de la possibilité de réduire considérablement la fenêtre spectrale en F1. On peut comparer la DIAG - aliasée et découplée à l’expérience *J*-résolu, spectroscopie introduite beaucoup plus tôt dans la méthodologie de RMN en solution. De telles expériences sont très intéressantes, car elles offrent la possibilité de simplifier les spectres et de faciliter la mesure précise du couplage dans des multiplets qui sont désormais isolés.

Afin de résoudre des problèmes structurels plus complexes, nous proposons l'insertion de séquences de mélange basées sur le transfert d'aimantation “en-phase” pour obtenir des expériences CLIP-COSY et TOCSY découplées en F1.

La CLIP-COSY, qui est particulièrement intéressante, fournit des multiplets en forme “en-phase” pour les signaux diagonaux et croisés et est compatible avec le découplage homonucléaire. L'impulsion sélective modulée *nemoZS* ou l'élément PSYCHE, permettant de découpler la dimension indirecte de la CLIP-COSY, garantissent une sensibilité optimale. L’application du filtre BIRD, introduit quelques caractéristiques nouvelles et intéressantes dans cette expérience et peut être utilisée pour révéler pleinement la structure multiplet de signaux difficilement accessibles par d’autres méthodes.

La deuxième partie du travail était consacrée à l’exploitation des expériences de la série en tant que séquences modèles afin d’examiner les artéfacts spectraux. Ce fut une bonne occasion d’explorer des aspects plus théoriques de la spectroscopie RMN en général et du découplage homonucléaire en particulier. La voie vers la construction de la structure théorique permettant d’aborder la question des artéfacts dans ces expériences a été grandement facilitée par les simulations numériques effectuées avec le logiciel de simulation “Spinach”.

Acknowledgements

I would like to especially acknowledge my thesis director, Dr. Damien Jeannerat, for making me fascinated about NMR spectroscopy and rendering my research experience in his group to be very unique.

I would like to thank Dr. Jean-Nicolas Dumez and Dr. Fabien Cougnon for accepting to be a part of my examination committee and reading my thesis.

I would like to express my gratitude to Marion Pupier, who is not only a very talented NMR engineer a good friend.

I am deeply grateful to my close friend Kirill Sheberstov, who brought a lot of inspiration and enthusiasm to my work. I am particularly thankful for the long and exciting discussions I had with him on NMR topics and many others.

I would like to thank Sonia Candolfi, Sonya Torche, Stéphane Grass, Patrick Romanens, Amalia Poblador-Bahamonde, Eduard Sistaré Guardiola and many other wonderful people who made my every day at work very pleasant.

Most importantly, I would like to thank my family and friends.

Abbreviations and Symbols

AQ	Acquisition time
BBHD	Broadband Homodecoupling
BIRD	Bilinear Rotation Decoupling
COSY	Correlation Spectroscopy
CLIP-COSY	Clean In-phase Correlation Spectroscopy
DIAG	2D experiment generating only diagonal signals
DOSY	Diffusion Ordered Spectroscopy
DQF-COSY	Double-Quantum Filtered Correlation Spectroscopy
HSQC	Heteronuclear Single Quantum Coherence
*nemo*ZS	Zangger-Sterk element with non-equidistantly modulated selective refocusing pulse
PSYCHE	Pure Shift Yielded by Chirp Excitation
rf	Radio-frequency irradiation
SERF	Selective Refocusing experiment
TOCSY	Total Correlation Spectroscopy
ZS	Zangger-Sterk element

$\|\alpha\rangle$, $\|\beta\rangle$	Eigenstates of $\hat{I}_z$ for a single uncoupled spin $^1/_2$;
γ	Gyromagnetic ratio;
δ	Chemical shift;
ΔF	Chirp pulse sweep width;
$\hat{H}$	Hamiltonian operator;
θ	Flip angle of a pulse;
$\hat{I}_x$, $\hat{I}_y$, $\hat{I}_z$	Operators corresponding to *x*, *y* and *z* components of angular momentum;
p	Coherence order;
$\hat{\rho}$, ρ	Density operator and its corresponding matrix, respectively;
ϱ	Angle expressing the tilt of the rotation axis - around which magnetization precesses - from the *z* axis of the rotating frame, if off-resonance effects are relevant;
ϕ_p	Phase of a pulse defined as an axis in the transverse plane in the rotating frame of reference;
ψ	Wavefunction describing the wave characteristics of a spin;
$\|\psi\rangle$	*Ket* in the Dirac notation representing wavefunction in a matrix form;
$\langle\psi\|$	*Bra* in the Dirac notation representing the matrix adjoint of the *ket*;
ω_0	Larmor frequency;
ω_1	Nutation frequency expressing the speed of rotation of spins around the *rf* field applied from the transverse plane in the rotating frame of reference;
ω_{eff}	Effective frequency expressing the speed of rotation of spins around the applied *rf* field if its direction lies off the transverse plane in the rotating frame of reference;
Ω	Offset frequency;
F1, F2	Frequency axis of indirect and direct dimension, respectively;
R	Rate of the chirp pulse;
U	Propagator of the density matrix;

Contents

I. Introduction, context, motivation

The through-chemical bond interaction between spins of the same - or different - type leads to the splitting of the observed NMR signals into multiplets.

Suppressing the effect of this interaction is a common practice when acquiring, for example, ^{13}C spectra, where the knowledge of the values of the heteronuclear $J(^{1}H\text{-}^{13}C)$ couplings are usually redundant and removing them simplifies and facilitates the interpretation of the spectra and increases sensitivity. In this case, each such recovered singlet line corresponds to a chemically distinct spin site in a molecule. Heteronuclear decoupling is achieved by saturating the magnetization of one of the isotopes to be decoupled, which is simple if their Larmor frequencies are significantly different.

The homonuclear decoupling, particularly in the case of ^{1}H NMR spectroscopy, brings even bigger advantages, as the chemical shift range of the isotope is relatively narrow. The overlapping multiplets, often complicated and extended, hinder or even prevent spectra interpretation. The quest for the methodology allowing the suppression of the homonuclear couplings in order to obtain pure-shift spectrum started already in 1960s[1]. However, homonuclear decoupling is much more challenging than its heteronuclear correspondent, as in this case, spins of the same isotope must be manipulated separately and differently.

The first broadband decoupled proton spectrum was obtained indirectly from the projection of the *J*-resolved spectrum[2]. Among other methods that were proposed over the decades, it is compulsory to mention the Pines BIRD element[3] allowing to distinguish between protons on the basis of the presence/absence of a chemical bond with a ^{13}C isotope (Section III.B.3) and the revolutionary, in this field, spatial encoding proposed by Zangger and Sterk (Section III.B.1). Several years ago, a novel element for broadband homonuclear decoupling, called PSYCHE[4], has been proposed by Mohammadali Foroozandeh (Section III.B.2.b)). More detailed description of these methods, their principles and characteristics will be discussed in Section III.B, after introducing the necessary quantum mechanical description of NMR in Section II. Deriving from these methods, the work of Morris and his coworkers[5-8] as well as many other groups, in the last decade, contributed to a design of a plethora of pure-shift experiments, within different categories, for example: 1D ^{1}H pure-shift experiments[9], 2D homonuclear experiments decoupled in indirect and/or direct dimension[4, 10], pure-shift HSQC[11], pure-shift experiments for ^{13}C enriched compounds[12, 13], pure-shift DOSY[14], homodecoupled band-selective experiments[15] and many others.

In this thesis, the first part of the work consisted in assembling a toolbox of two-dimensional homonuclear high-resolution experiments homodecoupled in the F1 indirect dimension (DIAG[10] CLIP-COSY[16], TOCSY[17]), see the green part in Figure 1. The

homodecoupling serves to reduce the signal overlap probability. However, the full multiplets, being an invaluable provider of structural information, are preserved in the direct F2 dimension, where high resolution and thus complete separation of the multiplet components comes usually with no cost in experimental time. In our toolbox, the presence of the *J*-coupling constants in at least one dimension has been considered more important than the possible further increase in resolution by decoupling the signals in both spectral dimensions[5].

The specific experiments were built upon a common template sequence, which facilitated their implementation and use (Figure 1). The scheme was introduced by Thrippleton and Keeler[18], where the mixing sequence (if present) is embraced by two *z*-filters that serve to purge the desired magnetization, stored along the *z* direction prior to detection, from any other unwanted contributions - mainly the zero-quantum coherences. All the experiments exploit the in-phase magnetization (in the product operator formalism), which ensures that the signals belonging to one multiplet will be all positive and thus not prone to cancellation (Figure 2).

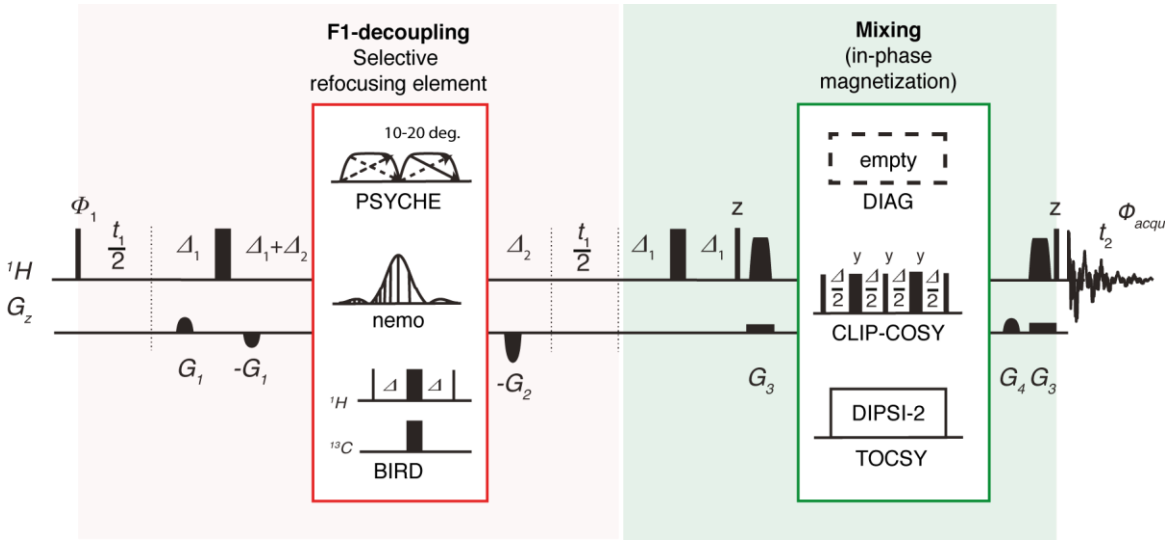

Figure 1. The template sequence for the z-filtered experiments of the toolbox with the optional decoupling and mixing elements.

When analyzing the structure of small molecules or their mixtures by NMR, very often it is necessary to complement the 1D spectra with different 2D experiments. In this work, a particular attention has been put on the modularity of this toolbox. The experiments, employing decoupling elements based on different mechanisms, are complementary to each other and can be used to access the maximum of structural information, not easily available by other methods. The particular information that can be obtained from the spectra provided by each of the experiment depends mainly on the type of the mixing (if present). The choice of the

elements of the toolkit will depend on the problem at hand so that the user can optimally benefit from the specific advantages of each of the experiments.

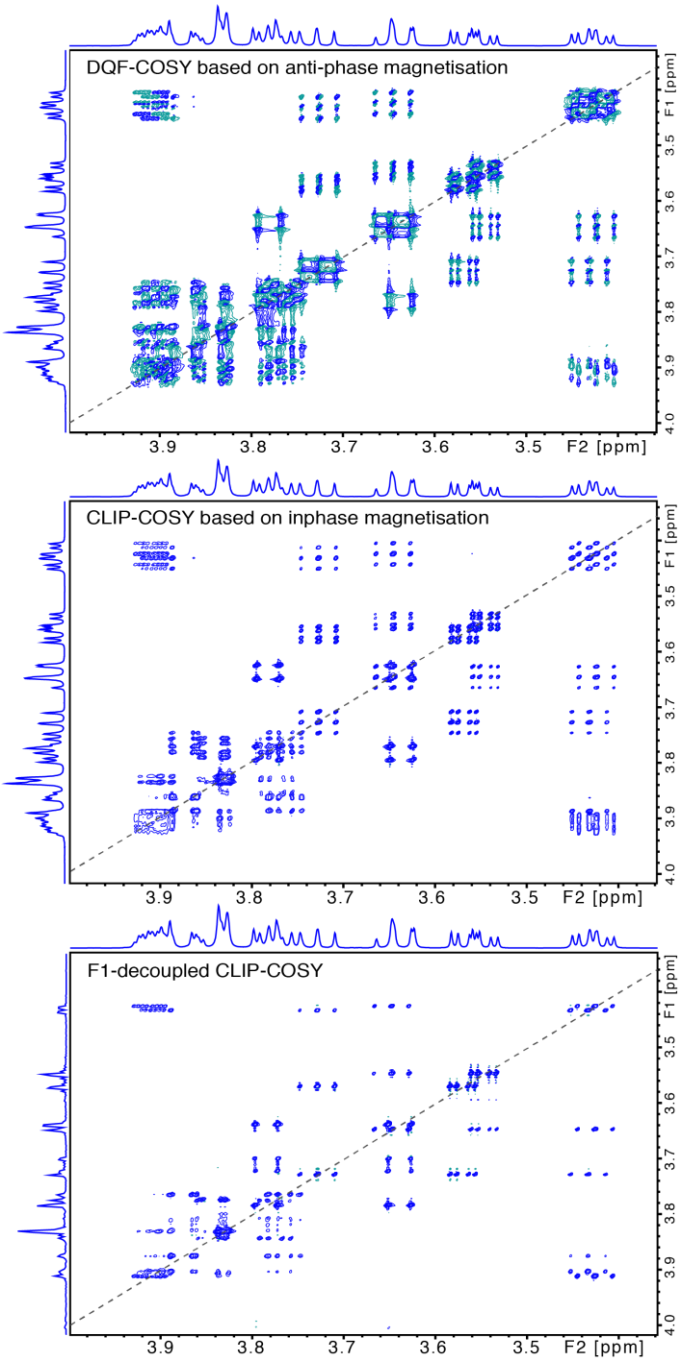

Figure 2. DQF-COSY (top) and CLIP-COSY (middle) spectra of melezitose showing signals with antiphase and in-phase patterns, respectively. In the formal description, distinct product operators describe the two types of signals. Generally, experiments based on in-phase magnetization are compatible with homonuclear decoupling: the spectrum at the bottom shows F1-nemoZS decoupled CLIP-COSY. The CLIP delay in the CLIP-COSY experiments was set to Δ = 25 ms. The selective pulse used for decoupling was a 120 ms rsnob with 2x40 irradiation sites.

The DIAG experiment (similar to the δ-resolved experiment[19]) lacks any true mixing and thus, *in principle,* produces only diagonal signals. Even though the sequence ends up with a 90° hard pulse, which often plays the role of a minimalistic mixing element, the conditions here are not fulfilled for the transfer of magnetization between coupled spins to take place, since all spins are aligned with the *z* direction prior to the pulse.

If decoupled in the F1 indirect dimension, it primarily aims at separating the chemical shift and *J*-coupling interactions while not providing any information about the correlations between spins. This experiment largely benefits from the possibility to drastically reduce the spectral window in F1 (typically by two orders of magnitude, e.g. from 5000 Hz to 50 Hz). This causes the so-called "spectral aliasing" and consequently the increase in resolution by the factor of the spectral width reduction - in the same experimental time. This comes however with the disarranging of the resonance frequencies (chemical shifts) in F1. The usually undesired ambiguity, in this case becomes insignificant, as the chemical shift of the diagonal signals is obviously the same in F1 and F2 and thus apparent from the direct dimension, see Section IV.A.1.

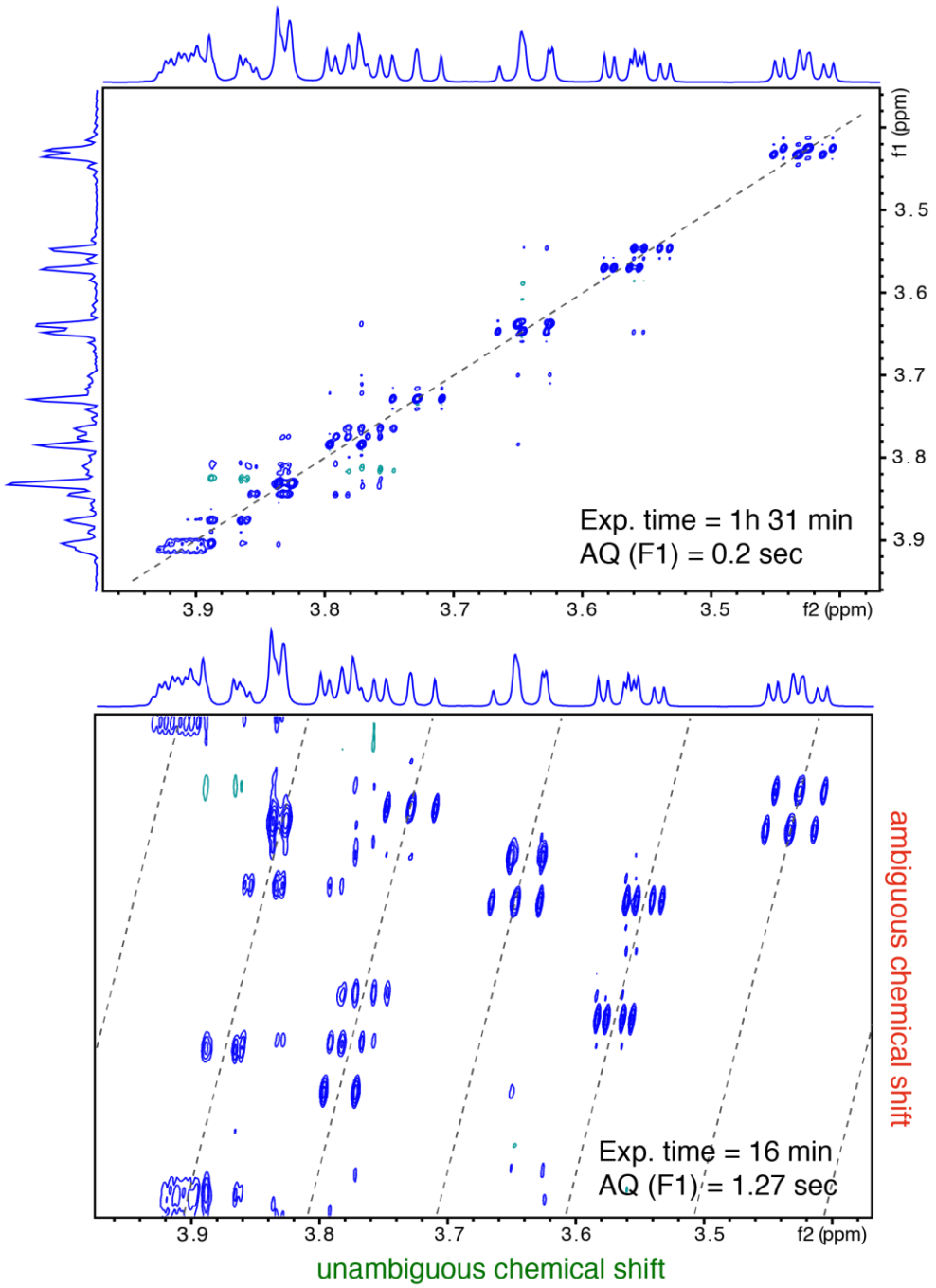

Figure 3. The non-aliased (top) and aliased (bottom) DIAG spectra of melezitose.

The much more recently proposed F1-decoupled and aliased DIAG can be compared to the *J*-resolved spectroscopy[2] introduced in the solution NMR methodology as soon as in the 1970s with the same main goal to separate the interactions and obtain the (J, δ)-representation. The motivation to design an experiment separating the shifts and the couplings, which appeared so early in NMR, is easily understood, as the simplification of the spectra and

the possibility to study each multiplet in the isolation from others is very appealing to facilitate the spectra interpretation.

Recent methodological advances contributed to significant improvement of the two, fundamentally different, experiments, making the comparison of the resulting spectra interesting and quite challenging. First of all, it is quite recent that the homodecoupling methods have been improved to the extent as to provide the decoupled spectra with a reasonable quality and sensitivity. Secondly, the treatment of aliased 2D spectra, where the spectral window in F1 is reduced to the value of tens of Hertz, is well elaborated[20] may facilitate the work with such spectra. The limit of tens of Hertz in F1 is kept so to ensure the embedding of the most extended multiplets expected in the spectra, just as in the *J*-resolved spectroscopy. Thus, the two classes of experiments (δ- and *J*-resolved), can be acquired with similar experimental parameters for better comparison. Thirdly, sophisticated methods to improve the coherence selection in modern experiments (gradients, adiabatic pulses combined with gradients, optimized pulses, *etc.*) are routinely employed. The upgraded coherence selection influences the lineshapes of the signals and overall quality of the spectra, also (and importantly) in the presence of strong coupling. All the factors listed above contribute to the high competitiveness of experiments such as the the F1-decoupled DIAG and the *J*-resolved (*J*-res) and their precise comparison becomes a challenging task, as it requires the knowledge and suitable tools to question and examine the *nuances* that could tip the balance in favor of one of those experiments.

One important difference that sets the DIAG experiment apart from the *J*-res is that it is a two-dimensional experiment based on the quadrature detection and in principle any mixing sequence based on the in-phase magnetization may be inserted in-between the two final Keeler's *z*-filters in the pulse sequence in order to restore the spin-spin correlations. This makes it very attractive as an alternative to the *J*-resolved experiment, which does not offer this flexibility. In fact, the DIAG underpins the presented toolkit. It can be run as a sort of diagnostic experiment to provide highly resolved multiplets in a minimum of experimental time – when aliased. It can be used to measure couplings in the F2 dimension[10] and can be useful to identify strongly coupled spins as those will certainly generate of out-of-diagonal signals[21].

However, in order to facilitate the assignment and tackle more complex structural problems, a COSY-like experiment, making it possible to track the connectivity between spins, is vitally important. We inserted in our toolbox the perfect echo mixing sequence[22], which forms the basis of the recently proposed CLIP-COSY experiment[16]. The perfect echo block transfers the magnetization between directly coupled spins through the *J* coupling in a manner analogous to the INEPT transfer, ubiquitous in heteronuclear experiments. Since the efficiency of the transfer depends on the CLIP delta delay (Figure 1) and the *J* couplings underlying a given signal multiplicity, the intensity of signals in the spectrum will vary. This fickle intensity behavior

is however not the only feature that makes the experiment distinct from most of other common versions of the COSY experiment. Most importantly, to a great advantage, the CLIP-COSY provides in-phase multiplets of a regular lineshape for both diagonal and cross-peaks and it is compatible with the homonuclear decoupling. While the use of the selective modulated pulse (*nemoZS*[10], Section III.B.1.c) or the PSYCHE element[9] (Section III.B.2.b)) to decouple the indirect dimension of the CLIP-COSY ensures its optimal sensitivity, the application of the BIRD filter[3] (Section III.B.3) introduces some novel and interesting features in this experiment. It will be shown how the BIRD-CLIP-COSY can be used to fully reveal the multiplet structure of signals not easily reachable by other methods.

Finally, the F1-decoupled TOCSY[17] experiment, based on the extensive transfer of in-phase magnetization between spins in the entire spin system, turns out to be often complementary to the CLIP-COSY experiment, as it shows correlations that may accidentally be missing/or be of a very low intensity in the latter one. TOCSY is an invaluable experiment in the assignment of compounds like carbohydrates, as it makes the distinction between separate rings straightforward. The additional increase in the resolution due to the homodecoupling renders the spectral assignment even easier.

The second, main part of the work, was dedicated to exploiting the toolbox experiments as a model sequences in order to examine the spectral artifacts. This turned out to be a good occasion to explore more theoretical aspects of the NMR spectroscopy in general and the homodecoupling in particular. The path of building the theoretical structure facilitating the approach to the question of artifacts in these “toolbox experiments” was greatly facilitated by numerical simulations performed in the Spinach simulation package[23, 24].

The study of artifacts is not a particularly trivial task. First of all, there is a variety of possible sources of artifacts, not all being of interest to NMR methodologists. Secondly, artifacts are usually much less intense than the desired signals and so their investigation - either experimental or by simulations - is quite of a challenge. Finally, the rigorous study of artifacts requires rather advanced understanding of a theory of spin dynamics and the mechanism of the applied NMR methods. The cost of such study would be probably not rewarded even by finding a method to clean spectra coming from a given pulse sequence from the spurious responses and it is definitely not of a main interest for most of the users of the “routine” NMR spectroscopy. However, the focus that was given to artifacts in this PhD work was beneficial, as it resulted in a deeper understanding of some very recent homodecoupling methods and pointing out the difficulties associated with their use, which paves the way for a search of better solutions.

As the homodecoupling relies on separation of interactions, the presence of the strong coupling phenomenon, which inherently *mixes* the coupled spins, causes an evident limitation in making the separation ideal. Moreover, the use of novel methods providing an improvement

in sensitivity of the decoupled experiments may be disadvantageous in other aspects. For example, the employment of multiple-modulated selective pulses or small flip angle adiabatic pulses in the middle of the evolution of the indirect dimension, causes transfers of magnetization which will behave differently than the (usually main) desired one. This magnetization will not contribute to the expected signals but will rather be dispersed in the 2D spectrum with an unpredictable phase in the form of what is often referred to as "artifacts".

The precise indication of the sources (imperfections of hard pulses, performance of the shaped pulses, the choice of the flip angle and its accuracy, periods of free evolution under the action of strong coupling Hamiltonian, mixing period, *etc*.) of the magnetization evolving differently than expected, would allow to assess the frequencies, phases and intensities of these artifacts in the 2D spectrum. Obviously, these measurable characteristics of the artifacts are a final result deriving from the combination of the different contributions. The decomposition of this final result into the distinct steps occurring in time would be a challenge. Spin dynamics simulations are necessary for this purpose.

Some manual calculations have been done for simple cases (two coupled spins) as a method to understand the logic underlying the transformations of the density matrix upon different propagators. The aim of reproducing the exact path of the magnetization with the help of a simulator should be deliberated over:

1. One possible benefit of this approach would be to get an insight into the physics of the spin interactions (also with regard to a particular method). This is attractive when new and not completely understood methods are studied. Doing it in the context of 2D experiments that allow probing the magnetization transfers in the 2D map is much more convenient and informative (if not to say: the only way) than to study those effects only from the phase distortion in the one-dimensional spectra.

2. Another tempting use of a detailed understanding and analysis of the artifacts would be to develop a method to eliminate or reduce them and produce improved spectra.

For example, formal theoretical analysis concerning the density matrix transformations upon different (time-independent and time-dependent Hamiltonians) have been performed, with the help of a simulation program, and published for more simple experiments (e.g. *J*-resolved experiment[25] and SERF experiment[26]). It consequently led to finding the (partial) solution to remove the spectral artifacts: either by an optimized coherence selection (the SERF) or smartly designed averaging - Keeler's trick of substituting the only 180° hard pulse in the sequence by a chirp pulse combined with a weak gradient (the *J*-res).

Regarding the strong coupling artifacts present in the spectra of the toolbox experiments, a methodological trick – similar to the one used to eliminate these artifacts in the *J*-res – could likely be proposed to achieve their elimination or reduction. However, considering the main differences between *J*-res and DIAG: the presence of the mixing pulse(s) and the

necessity to cycle the sequence for the quadrature, the methodology in this case may require some adjustments. The understanding and treatment of artifacts different than the strong coupling ones may be more difficult, because they are probably much less systematic. If they are related to the hardware or some experimental (but not methodological) issues, there is no interest of them in the context of this thesis. On the other hand, artifacts related to the imperfections of the pulses will be generally discussed and are of an interest in the perspective of designing optimized pulses.

3. Yet another application of the study and simulations of artifacts would be to facilitate the conception of a software for a fully/semi - automatic spectral analysis.

II. Quantum mechanical description of the NMR experiments

In order to compare rigorously the properties of the different decoupling elements and their performances in the studied experiments as well as to demonstrate their *complementarity*, a method for a precise analysis of the magnetization is essential. The formalism of quantum mechanics provides a very convenient tool to describe the NMR spectroscopy and will be used for the theoretical analysis of the experiments (or its elements) studied in this PhD thesis. The aim to write such a formal section is to construct a general framework to refer to, when discussing in detail the experiments. Moreover, quantum mechanical calculations lie at the core of programs allowing the simulation of the spin dynamics and consequently the NMR experiments. It was then necessary to introduce the basic theoretical treatment to pave the way for the future developments in the context of this work, which can greatly profit from simulations (Spinach simulations of the experiments, with the focus on the artifacts analysis, are currently under preparation).

A. The Hamiltonian operator and the density operator

In NMR, one measures frequencies at which the nuclear spins "precess", which is directly proportional to the differences between the energy levels of the spin system. *This section serves to demonstrate that the energy may not only be measured in an NMR experiment, but can also be calculated as the eigenvalues of a quantum mechanical operator called* ***Hamiltonian****.* This approach turns out to be very useful to understand spectra containing signals whose source may not be easily identified, for example the spectral ***artifacts*** often associated with some imperfections of the pulse sequence. However, the origin of such signals is sometimes intrinsic to the spin system and the spin interactions within it. Thus, if the frequency of the "artifacts" (and so the energy of the spin system) can be calculated and translated to their root, one can have an access to a (beneficial) manipulation of these signals.

An arbitrary state of any physical system, for example an ***atomic nucleus in a magnetic field***, is labelled by a *vector of a vectorial space* called a Hilbert space[27]. A state, labeled by the vector and described by a corresponding wavefunction can be written as a linear combination (superposition) of some basis states:

$$|\psi\rangle = c_1|1\rangle + c_2|2\rangle, \quad (1)$$

where $|\psi\rangle$ is the ket (in the Dirac notation) specifying this state. The basis states $|1\rangle$, …, $|n\rangle$ can be represented by orthogonal unit vectors and the coefficients c_1, …, c_n express the contribution of each of the basis state in the superposition. These coefficients play a central role in the link between the formal description and the experiment, as will be shown.

Operators act on vectors in this Hilbert space and, in general, transform them to different vectors. There is a special class of operators that do not modify the vectors, but at most scale them. Those vectors are called ***eigenvectors*** (***eigenstates***) of the operators and the scaling factors are called the ***eigenvalues*** associated with these eigenvectors. The crucial point is that these eigenvalues correspond to physical variables (like the energy for example) and can be measured in an experiment.

The very important ***Hamiltonian operator*** $\widehat{H}$ determines the total energy of a quantum-mechanical system, according to

$$\widehat{H}|\psi\rangle = \varepsilon|\psi\rangle \tag{2}$$

where ε is the energy (the measurable eigenvalue of the Hamiltonian operator acting on a wavefunction describing a given state of the system).

Noteworthy, in NMR, all spin interactions: with the static magnetic field, the *rf* pulses, the other spins *etc.* can be represented by a corresponding Hamiltonian operator. Any pulse sequence (like COSY, HSQC etc.) can be seen in this context as a series of different Hamiltonians applied sequentially - to a given state of a spin system that changes under each action of any Hamiltonian - that altogether lead to the final state which will be manifested in the form of the spectrum after the Fourier Transform.

The calculation of the energy values measured in an experiment is equivalent to the calculation of the so-called ***expectation value*** of a quantum mechanical operator, given by a scalar product of $\langle\psi|$ and $\widehat{H}|\psi\rangle$:

$$\langle\widehat{H}\rangle = \langle\psi|\widehat{H}|\psi\rangle \tag{3}$$

where $\langle\psi| = \langle 1|c_1^* + \langle 2|c_2^* + \cdots + \langle n|c_n^*$ and the asterisk indicates the complex conjugate, as the c_1, …, c_n are complex numbers. After performing simple calculations and knowing that states and operators can be expressed as vectors/matrices, it can be shown that this is equivalent to:

$$\langle \hat{H} \rangle = Tr(\rho \cdot H) = Tr\left(\begin{pmatrix} c_1 c_1^* & \cdots & c_1 c_n^* \\ \vdots & \ddots & \vdots \\ c_n c_1^* & \cdots & c_n c_n^* \end{pmatrix} \cdot \begin{pmatrix} \langle 1|\hat{H}|1\rangle & \cdots & \langle 1|\hat{H}|n\rangle \\ \vdots & \ddots & \vdots \\ \langle n|\hat{H}|1\rangle & \cdots & \langle n|\hat{H}|n\rangle \end{pmatrix} \right) \tag{4}$$
$$= c_1^* c_1 \langle 1|\hat{H}|1\rangle + c_1^* c_2 \langle 1|\hat{H}|2\rangle + \cdots + c_n^* c_{n-1} \langle n|\hat{H}|n-1\rangle + c_n^* c_n \langle n|\hat{H}|n\rangle$$

where ρ is the matrix representation of the so-called density operator $\hat{\rho}$. The density matrix describes how the basis states superpose to form a state. This information is coded in the form of *products of the coefficients* (elements of the density matrix). Importantly, as the c_1, …, c_n are complex numbers, they carry an information not only about the amplitude, but also the relative phase of the basis states in the superposition. In other words, in order to calculate the energy values of a given state of a system under a given Hamiltonian *(e.g. to simulate the NMR spectrum)*, **it is necessary to know how this Hamiltonian acts on the basis states and what is exactly their superposition in the state.**

In the *special* case when the *basis* states $|1\rangle$, …, $|n\rangle$ are the *eigenstates* of a given Hamiltonian $\hat{H}$, its expectation value is:

$$\langle \hat{H} \rangle = \varepsilon_1 \cdot c_1^* c_1 + \cdots + \varepsilon_n \cdot c_n^* c_n. \tag{5}$$

For example, the influence of an external magnetic field on a spin system such as two coupled spins, each with a spin ½, can be expressed as the Hamiltonian: $\hat{H} = -\gamma B_0 \cdot \hat{I}_z = \omega_0 \cdot \hat{I}_z$ acting on a wavefunction: $|\psi\rangle = c_{\alpha\alpha}|\alpha_I \alpha_S\rangle + c_{\alpha\beta}|\alpha_I \beta_S\rangle + c_{\beta\alpha}|\beta_I \alpha_S\rangle + c_{\beta\beta}|\beta_I \beta_S\rangle$. In this case, the four basis states superposing to form the $|\psi\rangle$ are also the eigenstates of the Hamiltonian and the corresponding eigenvalues are: $\varepsilon_{\alpha_I \alpha_S} = {}^1/_2$, $\varepsilon_{\alpha_I \beta_S} = 0$, $\varepsilon_{\beta_I \alpha_S} = 0$, $\varepsilon_{\beta_I \beta_S} = {}^1/_2$. The eigenvalues of a Hamiltonian are the energies of the associated eigenstates (commonly called energy levels) and determine the energy separation between these levels. This has a direct impact on the probabilities of transition between the levels and consequently on what is observed in a NMR experiment. The possibility to calculate these probabilities allows accounting for a *frequency*, *an amplitude (intensity)* and *a phase* of each signal in a 1D spectrum. It is important to add, that the transitions between the states may or may not happen – this depends on a specific Hamiltonian, which acts on a system. This issue is addressed in the following section.

B. Evolution of the density matrix

As described in the previous section, the eigenstates and eigenvalues of the Hamiltonian $\hat{H} = -\gamma B_0 \cdot \hat{I}_z$ acting upon a spin system are used to formally describe the energy quantization (energy levels degeneracy) in a quantum-mechanical system, ***at equilibrium***. The NMR spectroscopy is possible only if the system is dragged away from the equilibrium and changes over time. The information about this change can be retrieved from the time-dependent Schrödinger equation:

$$\frac{d}{dt}|\psi\rangle = -i\hat{H}|\psi\rangle, \tag{6}$$

which states that the integral of the wavefunction with respect to time is equal to the output of the action of the Hamiltonian operator $\hat{H}$ on this wavefunction multiplied by $-i$ imaginary number. This time evolution of a system can be accurately described by the evolution of the density matrix, since, what changes in time, are the coefficients (probabilities) and not the basis states themselves.

The equation that relates the evolution of the density operator to the Hamiltonian, is called *Liouville-von Neumann equation*:

$$\frac{d\hat{\rho}}{dt} = -i[\hat{H}, \hat{\rho}]. \tag{7}$$

This equation provides the fundamental criterion for the evolution of a system to take place at all, which is only when the commutator of the density operator and the Hamiltonian operator is non-zero.

The understanding of the rules underlying the evolution of the density matrix in time, under different Hamiltonians, is the core of the NMR methodology development. The ability to find an algorithm to optimize any chosen elements of the density matrix (while it is evolving under a series of Hamiltonians in time) is equivalent to designing a way to control the evolution of the magnetization up to the final desired state.

When the Hamiltonian is time-independent, the solution of the *Liouville-von Neumann equation* (as it requires the integration of equations including the imaginary unit $-i$ present in the coefficients in the density matrix) can be written in terms of the operator exponentials:

$$\hat{\rho}(t) = e^{-i\hat{H}t}\hat{\rho}(0)e^{+i\hat{H}t} \tag{8}$$

The general notation is also often used: $\hat{\rho}(t) = U\hat{\rho}(0)U$, where U represents the exponential function in Eq (8) is called the propagator.

Solving this equation requires the calculation of a matrix exponential, which is straightforward when a diagonal matrix represents the Hamiltonian, and it is more demanding when the matrix is not diagonal.

In the above equation, if the Hamiltonian operator $\hat{H}$ is represented by a diagonal matrix, the matrix exponential is also a diagonal matrix such that, e.g.:

$$\hat{H} = \begin{pmatrix} \varepsilon_1 & 0 \\ 0 & \varepsilon_2 \end{pmatrix};\ e^{\hat{H}} = \begin{pmatrix} e^{\varepsilon_1} & 0 \\ 0 & e^{\varepsilon_2} \end{pmatrix}; \tag{9}$$

The evolution of the density matrix in this particular case is as simple as its elements acquiring a phase label determined by the energy levels of the system (*phase modulation*), for example, if an uncoupled spin is considered in the Hilbert space:

$$\rho = \begin{pmatrix} \rho_{11} & \rho_{12} \\ \rho_{21} & \rho_{22} \end{pmatrix} \tag{10}$$

$$\rho(t) = e^{-i\hat{H}t} \cdot \begin{pmatrix} \rho_{11} & \rho_{12} \\ \rho_{21} & \rho_{22} \end{pmatrix} e^{+i\hat{H}t}. \tag{11}$$

Then, the evolution of the element ρ_{12} can be expressed as:

$$\rho_{12} \overset{\hat{H}t}{\rightarrow} \rho_{12} \cdot e^{i(\varepsilon_2 - \varepsilon_1)t} \tag{12}$$

and generally:

$$\rho_{ij} \overset{\hat{H}t}{\rightarrow} \rho_{ij} \cdot e^{i(\varepsilon_j - \varepsilon_i)}. \tag{13}$$

In the case where the Hamiltonian is represented by a non-diagonal matrix, it must first be *diagonalized* by solving the *secular equation*, which enables the matrix exponential to be calculated. In this case, the matrix exponential consists of non-zero diagonal and off-diagonal elements equal to $\cos(\omega t)$ and/or $\sin(\omega t)$ (*amplitude modulation*) where ω corresponds to a frequency (energy) determined by the given Hamiltonian.

C. Radio-frequency pulse

1. General description and a hard pulse

As mentioned above and in accordance with the *Liouville-von Neumann equation* (Eq (7)), a quantum mechanical system evolves in time only if the density operator that describes the system and the acting/propagating Hamiltonian do not commute. It is very common to choose the propagators of the density matrix in a way that $\widehat{H}$ and $\hat{\rho}$ are orthogonal (in addition to the fact that they do not commute). For example, operators like $\hat{I}_x$ or $\hat{I}_y$ do not commute with $\hat{I}_z$, they are orthogonal to each other and to $\hat{I}_z$ and the following commutation relationships hold:

$$\begin{aligned}\left[\hat{I}_x, \hat{I}_z\right] &= -i\hat{I}_y \\ \left[\hat{I}_y, \hat{I}_z\right] &= +i\hat{I}_x\end{aligned} \tag{14}$$

Moreover, the $\hat{I}_x$ or $\hat{I}_y$ ensure the *full interconversion* of the $\hat{I}_z$ eigenstates.

$$\begin{aligned}\hat{I}_x \left|\, \alpha\right\rangle &= +\tfrac{1}{2}\left|\, \beta\right\rangle \qquad \hat{I}_x \left|\beta\right\rangle = +\tfrac{1}{2}\left|\, \alpha\right\rangle \\ \hat{I}_y \left|\, \alpha\right\rangle &= +\tfrac{1}{2}i\left|\, \beta\right\rangle \qquad \hat{I}_y \left|\beta\right\rangle = -\tfrac{1}{2}i\left|\, \alpha\right\rangle\end{aligned} \tag{15}$$

This explains why the *rf* pulses are usually applied from the transverse plane in the rotating frame. It will be shown below, that on-resonance *rf* pulses are in fact described by the quantum-mechanical operators corresponding to the *x* and *y* components of the angular momentum $\hat{I}_x$ and $\hat{I}_y$. Importantly, the interconversion of the basis states corresponds to the generation of a *coherence*.

It is however noteworthy that the operators that are neither perpendicular nor parallel (the latter is the extreme case when the commutator is zero) to a given density operator, will still trigger the evolution of the system.

It is essential for the analysis carried out in this thesis to provide the formal description of the action of *rf* pulses on the magnetization in a given state. Since pulses are oscillating signals, the full Hamiltonian is time-dependent:

$$\widehat{H} = \omega_0 \hat{I}_z + \widehat{H}_{RF}(t) \tag{16}$$

where: $\widehat{H}_{RF}(t) \cong -\frac{1}{2}\gamma B_{RF} \cdot \left\{\cos\left(\omega_{ref}t + \phi_p\right)\hat{I}_x + \sin\left(\omega_{ref}t + \phi_p\right)\hat{I}_y\right\}$.

The rotating frame transformation, based on adjusting the frequency of the oscillation of the *rf* pulse (ω_{ref}) to the Larmor frequency (± the chemical shift) of the spins in a given magnetic field, allows to remove the time-dependence from the above expression and the Hamiltonian becomes:

$$\hat{H}_{rot} \cong \Omega \hat{I}_z + \omega_1 \cdot \{\cos(\phi_p)\hat{I}_x + \sin(\phi_p)\hat{I}_y\} \tag{17}$$

where Ω is the offset frequency and $\omega_1 = \left|\frac{1}{2}\gamma B_{RF}\right|$ is the nutation frequency (labeled sometimes as ω_1) and it is always positive. The nutation frequency is the measure of the *rf* field amplitude. ϕ_p is the phase of the pulse - the axis in the rotating frame along which the pulse is applied. The $\hat{H}_{rot}$ is a sum of the Hamiltonian describing the interaction of the spins with the external magnetic field and the time-independent $\hat{H}_{RF\_rot}$ contribution. In case of an on-resonance (no offset frequency) *x* pulse, the Hamiltonian is as simple as:

$$\hat{H}_{rot} = \hat{H}_{RF\_rot} = \omega_1 \hat{I}_x \tag{18}$$

It is worth to highlight that the exact form of the Hamiltonian will depend on the *phase* of the pulse ϕ_p, since the matrix representation of $\hat{I}_{\phi_p}$ (operator corresponding to angular momentum component along axis defined by ϕ_p angle) depends on ϕ_p and consequently, the rotation induced by the propagator $e^{-i\omega\hat{I}_{\phi_p}t}$ is sensitive to the phase of the pulse (note that ω may not always be ω_1 but may be ω_{eff}). In order to calculate what happens with a physical system under the Hamiltonian $\hat{H}_{RF\_rot} = \omega_1\hat{I}_x$, it is sufficient to calculate this *"sandwich"* relationship:

$$\hat{\rho}(t) = e^{-i\hat{H}_{RF\_rot}\cdot t}\hat{\rho}(0)e^{+i\hat{H}_{RF\_rot}\cdot t} \tag{19}$$

$$\hat{\rho}(t) = e^{-i\omega_1 t\cdot\hat{I}_x}\hat{\rho}(0)e^{+i\omega_1 t\cdot\hat{I}_x} \tag{20}$$

In the case of the hard pulse, the duration t of the pulse and its amplitude ω_1 can be directly related to the flip angle $\theta = \omega_1 t$.

$$\hat{\rho}(t) = e^{-i\theta\cdot\hat{I}_x}\hat{\rho}(0)e^{+i\theta\cdot\hat{I}_x} \tag{21}$$

The pulse propagator is thus:

$$U = e^{-i\theta \cdot \hat{I}_x} \tag{22}$$

The particular combination of the *duration*, *amplitude* and *phase* of the pulse will all contribute together to produce the unique propagation of the density operator from an arbitrary state *n* to another arbitrary state *m*.

The equation above can be generalized for a pulse applied from an arbitrary axis in the transverse plane:

$$U = e^{-i\phi \cdot \hat{I}_z} \cdot e^{-i\omega_1 t \cdot \hat{I}_x} \cdot e^{+i\phi \cdot \hat{I}_z} \tag{23}$$

or, going further, for a pulse applied from an arbitrary axis, which may not lie in the transverse plane of the rotating frame:

$$U = e^{-i\phi \cdot \hat{I}_z} \cdot e^{-i\varrho \cdot \hat{I}_y} \cdot e^{-i\omega_{eff} t \cdot \hat{I}_z} \cdot e^{+i\varrho \cdot \hat{I}_y} \cdot e^{+i\phi \cdot \hat{I}_z} \tag{24}$$

where: $\omega_{eff} = \sqrt{\omega_1^2 + \Omega^2}$ and $\varrho = arctan\left(\frac{\omega_1}{\Omega}\right)$; ϱ is the angle expressing the tilt of the rotation axis from the *z* axis (or equivalently 90° - δ from the transverse plane).

It is evident from the equations above that if the *rf* pulse is applied from an arbitrary axis and the offset effect is not negligible, the rotation of the density matrix (or in other words the *trajectory* of the magnetization) will be more complex than when a hard *x* pulse is applied. Here, the propagator is not directly perpendicular to the density operator (if we assume that $\hat{\rho}(0)$ represents magnetization in equilibrium along *z*) but yet it is composed of rotations along several perpendicular axes. The two operators: $\hat{\rho}(0)$ and $\hat{H}_{RF\_rot}$ do not commute but they are not orthogonal either. The interconversion of the eigenstates of the operators along *z* (for example α/β for $\hat{I}_z$ or $\alpha\beta/\beta\beta$ for $\hat{I}_z$+$\hat{S}_z$ etc.) is not the same as in case when operators orthogonal to the *z* direction are involved in the propagation. There will be less coherence with order ± 1 generated (less of the transverse magnetization) and moreover, some elements of the density matrix may acquire an additional phase as the interconversion of the basis states can be thought of as "partial".

If the dependence of each of the rotation in a composite propagator could be precisely controlled and the overall effect for all possible combinations of the parameters influencing the rotations could be predicted, it would be then possible to better design the propagation path and manipulate the magnetization in a more controlled way.

2. Soft pulses

A soft pulse (selective pulse) is an *rf* pulse with a small *rf* amplitude, e.g. small value of the nutation frequency relative to isotope bandwidth (see Eq (17)). The amplitude of the *rf* pulse is inversely proportional to its duration and so the selective pulses are much longer than the hard pulses (order of *ms* rather than *μs* for isotopes such as ^{1}H and ^{13}C in a typical NMR magnet with a field strength of 5-20 T). Soft pulses are also more frequency selective (act on a narrower bandwidth) than the hard ones. A very selective pulse, for example a 120 ms 1% truncated Gaussian[28] can excite a bandwidth as small as 18 Hz. Rsnob pulse[29] of the same duration can selectively refocus magnetization in a bandwidth of 20 Hz. This means that only a small portion of the spins of a given isotope, having their chemical shift in this narrow frequency range, will be *precessing with the rf field*. In other words, only the spins *on-resonance* with this pulse and will be affected by its action similarly to as was described above in the context of the hard pulses – regarding the geometry of the rotations *etc*. For all other spins, the offset $\Omega\hat{I}_z$ term will be largely dominating and so their trajectories will be quite different than for the *on-resonance* spins. Ideally, they should be barely affected by the pulse and a minimum trajectory should be induced. In terms of the rotating frame model, the selective pulse seems static only for the small portion of the *on-resonance* spins. For all the other spins, the pulse will seem as "moving" or - in the vector model - the axis around which they will precess is not fixed and may not lie in the transverse plane. This situation can be thought of either as the frequencies of the spin precession and the moving pulse being so different that the spins are not affected, or that the Hamiltonian representing the magnetization and the pulse are (almost) parallel and, if indeed parallel, they *do* commute, preventing any spin evolution.

For soft pulses, the *on-resonance* frequency can be chosen by the user. On Bruker spectrometer, this is done either by the SPOFFS parameter, which shifts the carrier frequency of the soft pulses generator, or by directly multiplying the shape of the pulse by a complex exponential with the chosen frequency.

If, on the other hand, the pulse shape is modulated by a function like $\cos(\omega_1)$, equivalent to adding two shapes each modulated by $exp(+\omega_1)$ and $\exp(-\omega_1)$, respectively, spins at the two symmetrical frequencies $+\omega_1$ and $-\omega_1$ will be instantaneously on-resonance. Similarity can be drawn between such a pulse modulation and the amplitude modulation of the two-dimensional dataset, which causes the lack of the frequency discrimination and the mirror effect in the corresponding spectrum after the FT.

3. Chirped pulse

A chirped pulse (in its most basic form) is a frequency-modulated pulse. For such pulses, the "*on-resonance* situation" constantly changes during the duration of the pulse, so that there *cannot* be a one fixed frequency chosen for the rotating frame transformation. In order to consider the spin dynamics under the action of the frequency-modulated pulse in the static vector model, the rotating frame should accelerate together with the pulse rather than having a fixed rotation frequency. This pulse, at each given instant of time $t'_{(1)}$ has an instantaneous frequency ($\omega'_{c(1)}$technically equivalent to a specific $SPOFFS'_{(1)}$), which will be *on-resonance* with a portion of spins precessing with a frequency equal to this instantaneous frequency of the pulse. An instant later $t'_{(2)}$, this instantaneous pulse frequency $\omega'_{c(2)}$, will be different and a different portion of spins will be affected by the pulse. Moreover, since the rotating frame is moving, at each time instant t', there is the corresponding instantaneous phase ϕ'. The latter is the fixed axis in the transverse plane of this *instantaneous rotating frame* along which the pulse is applied to a particular fraction of spins that will rotate around this axis up to the desired flip angle is reached according to the pulse calibration.

A phase-modulated chirped pulse, in contrast to a general hard pulse represented by Eq (17), is described by the time-dependent equation:

$$\widehat{H}_c(t) \cong \Omega\hat{I}_z(t) + \omega_1(t) \cdot \{cos(\phi_c(t))\hat{I}_x + sin(\phi_c(t))\hat{I}_y\} \tag{25}$$

And *only* upon the *instantaneous rotating frame* transformation it becomes:

$$\widehat{H}_{instant\_rot} \cong \Omega\hat{I}_z + \omega_1(t) \cdot \{cos(\phi_c)\hat{I}_x + sin(\phi_c)\hat{I}_y\}, \tag{26}$$

with the $\omega_1(t)$ being a slowly varying amplitude, as shown in Figure 4.

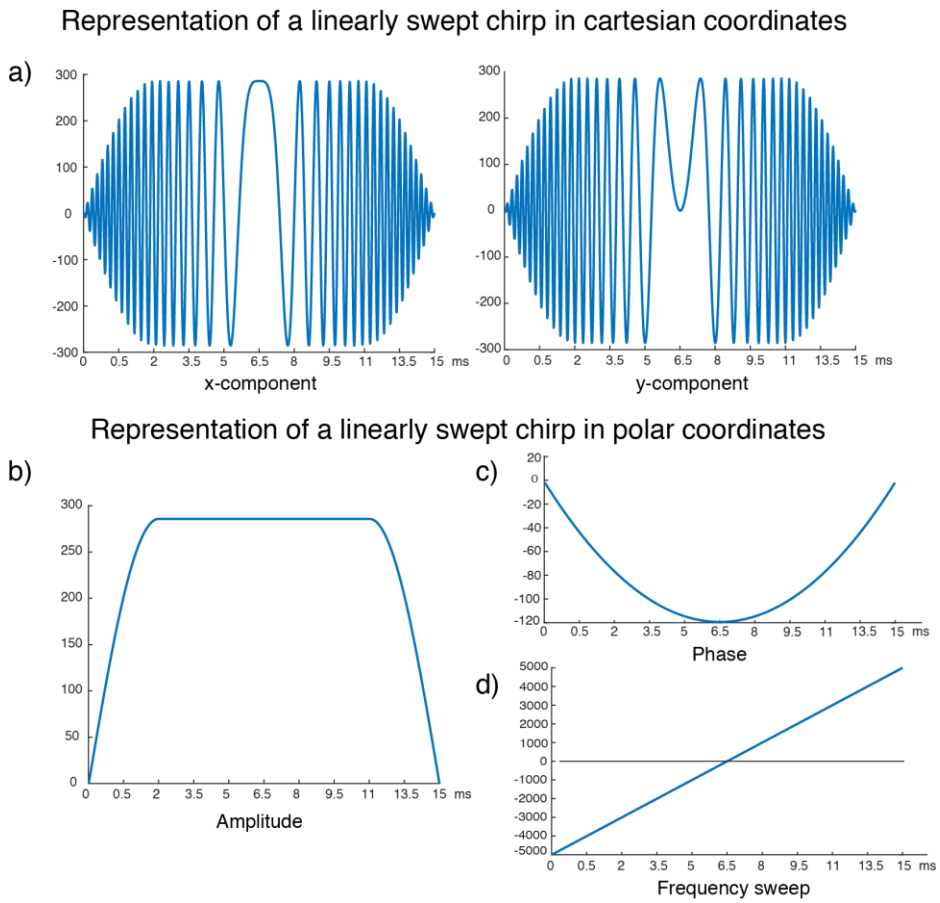

Figure 4. Features of linearly swept chirp: x and y components of the RF field (a), amplitude envelope (b), chirp's phase (c), chirp's instantaneous frequency (d).

The chirped pulse can be described by the basic equations of motion for the *constant acceleration motion*, where the position is given by the integral over the velocity increasing/decreasing linearly in time (and analogically for the chirp: the position is given by the integral over the frequency linearly changing in time). The formula describing the position (phase) must have a quadratic time-dependence to ensure the linearity of the velocity (frequency) change.

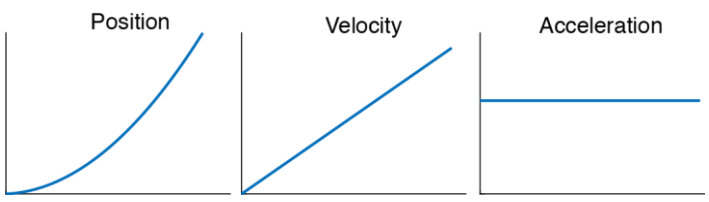

Figure 5. First and second derivatives of the motion resulting in a linear velocity sweep and a constant acceleration.

The phase, frequency and the rate of the chirp are thus given by:

$$\phi_c(t_c) = \int_0^t \omega_c'(t_c')dt' \tag{27}$$

$$\omega_c(t_c) = \frac{d\phi_c}{dt_c} \tag{28}$$

$$\omega_c(t_c) = F_{init} + Rt_c \tag{29}$$

$$\phi_c(t_c) = \phi_0 + Rt_c{}^2 \tag{30}$$

where $\phi_c(t)$ is the overall phase of the chirp pulse accumulated during its entire duration, ϕ_0 is the initial phase, ω_c' is the instantaneous frequency and the $\omega_c(t)$ is a time-dependent frequency of the chirp equal to the initial frequency F_{init} that varies in time according to the pulse rate $R = \frac{\Delta F}{t_c}$, equal to the ratio between the range of all affected frequencies and the time in which it happens.

Knowing all the parameters of the chirp, it is then possible to determine the exact moment during the pulse duration in which a given portion of spins is affected by the pulse and to relate it to the phase of the pulse at this moment. With this information, it is possible to make a first step into modeling of the spin dynamics during the chirp by assuming that during the considered very short time interval, everything happens as if the pulse behaved as a hard pulse. This simplification of the actual situation makes it possible to consider the exact matrix form of the propagator and analyze the mechanism of certain pulse sequence elements crucial for the experiments studied in this thesis.

a) Phase-modulated vs saltire chirp

Expressing the phase of a chirp as: $\phi_c = R \cdot (t - t_0)^2 = \frac{\Delta F}{t_p} \cdot (t - t_0)^2$, where $t_0 = 0$ and t varies from $-t_c/2$ to $+t_c/2$, allows to rewrite the general Eq omitting the offset, as:

$$\begin{aligned} \widehat{H}_{c\_LH}(t) &\cong \omega_1(t) \cdot \left\{ cos\left(\pi \cdot \frac{\Delta F}{t_c} \cdot (t - t_0)^2\right) + i \cdot sin\left(\pi \cdot \frac{\Delta F}{t_c} \cdot (t - t_0)^2\right)\right\} \\ &= \omega_1(t) \cdot e^{i \cdot \pi \cdot \frac{\Delta F}{t_c}(t - t_0)^2} \end{aligned} \tag{31}$$

for a chirp pulse with a linear low-to-high frequency sweep and

$$\widehat{H}_{c\_HL}(t) \cong \omega_1(t) \cdot \left\{ cos\left(\pi \cdot \frac{\Delta F}{t_c} \cdot (t - t_0)^2\right) - i \cdot sin\left(\pi \cdot \frac{\Delta F}{t_c} \cdot (t - t_0)^2\right)\right\} \tag{32}$$
$$= \omega_1(t) \cdot e^{-i \cdot \pi \cdot \frac{\Delta F}{t_c} \cdot (t - t_0)^2}$$

for a chirp pulse with a linear high-to-low frequency sweep[30].

Just as several soft pulses with different offset frequencies (with respect to the transmitter frequency) can be added together in order to excite simultaneously several different frequencies – with the special case being the biselective pulse where the two shapes with offsets $\exp(+\omega_1)$ and $\exp(-\omega_1)$ are added resulting in $\cos(\omega_1)$ modulation of the pulse – in the same way, two chirped phase-modulated pulses can be added to produce the amplitude-modulated chirped pulse (called *saltire pulse*):

$$\widehat{H}_{c\_saltire}(t) \cong \omega_1(t) \cdot \left\{ cos\left(\pi \cdot \frac{\Delta F}{t_c} \cdot (t - t_0)^2\right)\right\}. \tag{33}$$

D. Coherence orders and single transition operators

As already mentioned (Section II.A), the density matrix elements correspond to the coefficients that describe how the basis states superpose in a given state. A given Hamiltonian operator acting on the density matrix will modify the superposition of the basis states. In order to find the matrix representation of any operator (density operator or operator representing a pulse or free precession) it is necessary to consider the action of a given operator on all basis states that superpose and fully describe the system. For example, if two weakly coupled spins are considered in a Hilbert space, the general matrix form A of any operator $\hat{A}$ acting on such a system is:

$$A = \begin{pmatrix} \langle\alpha_I\alpha_S|\hat{A}|\alpha_I\alpha_S\rangle & \langle\alpha_I\alpha_S|\hat{A}|\alpha_I\beta_S\rangle & \langle\alpha_I\alpha_S|\hat{A}|\beta_I\alpha_S\rangle & \langle\alpha_I\alpha_S|\hat{A}|\beta_I\beta_S\rangle \\ \langle\alpha_I\beta_S|\hat{A}|\alpha_I\alpha_S\rangle & \langle\alpha_I\beta_S|\hat{A}|\alpha_I\beta_S\rangle & \langle\alpha_I\beta_S|\hat{A}|\beta_I\alpha_S\rangle & \langle\alpha_I\beta_S|\hat{A}|\beta_I\beta_S\rangle \\ \langle\beta_I\alpha_S|\hat{A}|\alpha_I\alpha_S\rangle & \langle\beta_I\alpha_S|\hat{A}|\alpha_I\beta_S\rangle & \langle\beta_I\alpha_S|\hat{A}|\beta_I\alpha_S\rangle & \langle\beta_I\alpha_S|\hat{A}|\beta_I\beta_S\rangle \\ \langle\beta_I\beta_S|\hat{A}|\alpha_I\alpha_S\rangle & \langle\beta_I\beta_S|\hat{A}|\alpha_I\beta_S\rangle & \langle\beta_I\beta_S|\hat{A}|\beta_I\alpha_S\rangle & \langle\beta_I\beta_S|\hat{A}|\beta_I\beta_S\rangle \end{pmatrix} \tag{34}$$

The numerical value of each of the element can be calculated by considering the effect of an acting operator(s) on the orthogonal basis states, as given in Eq (15); importantly, when operators such as: $\hat{I}_x$, $\hat{S}_x$, $\hat{I}_y$, $\hat{S}_y$ act on basis states, they interconvert them. The $\hat{I}$ operators do

not affect the spin S and vice versa. The orthogonality implies: $<\alpha|\alpha>=1, <\alpha|\beta>=0$, etc. For example:

- $<\alpha\alpha\left|\hat{I}_z+\hat{S}_z\right|\alpha\alpha>=<\alpha\alpha\left|\hat{I}_z\right|\alpha\alpha>+<\alpha\alpha\left|\hat{S}_z\right|\alpha\alpha>=\frac{1}{2}<\alpha\alpha|\alpha\alpha>+\frac{1}{2}<\alpha\alpha|\alpha\alpha>=1$;
- $<\alpha\alpha\left|\hat{I}_x+\hat{S}_x\right|\alpha\alpha>=<\alpha\alpha\left|\hat{I}_x\right|\alpha\alpha>+<\alpha\alpha\left|\hat{S}_x\right|\alpha\alpha>=\frac{1}{2}<\alpha\alpha|\beta\alpha>+\frac{1}{2}<\alpha\alpha|\alpha\beta>=0$; (35)
- $<\alpha\alpha\left|\hat{I}_x\right|\alpha\alpha>=<\alpha\alpha\left|\frac{1}{2}\right|\beta\alpha>=\frac{1}{2}<\alpha\alpha|\beta\alpha>=0$;
- $<\alpha\alpha\left|\hat{I}_x+\hat{S}_x\right|\alpha\beta>=<\alpha\alpha\left|\hat{I}_x\right|\alpha\beta>+<\alpha\alpha\left|\hat{S}_x\right|\alpha\beta>=\frac{1}{2}<\alpha\alpha\left|\beta\beta\right.>+\frac{1}{2}<\alpha\alpha\left|\alpha\alpha\right.>=\frac{1}{2}$;

etc.

And thus, for example:

$$I_z+S_z=\begin{pmatrix}1&0&0&0\\0&0&0&0\\0&0&0&0\\0&0&0&-1\end{pmatrix}\text{ and }I_x+S_x=\begin{pmatrix}0&\frac{1}{2}&\frac{1}{2}&0\\\frac{1}{2}&0&0&\frac{1}{2}\\\frac{1}{2}&0&0&\frac{1}{2}\\0&\frac{1}{2}&\frac{1}{2}&0\end{pmatrix}. \quad (36)$$

It is interesting to note that the I_x+S_x sum can either correspond to a density matrix describing the magnetization vector aligned along the x axis or a hard pulse applied from the x axis of the rotating frame and acting on both spins. The apparent equivalency of these two entities - adverted by the same notation - is somewhat striking.

The most common starting point of any NMR experiment is the generation of the transverse magnetization by a 90° pulse applied along a non-arbitrary axis such as *x* or *y*. As mentioned earlier (Section II.C.1), the interconversion of the α and β states when using such pulse is complete and the generated magnetization will be represented by a matrix, which has eight equal non-vanishing elements (four of them may just differ by the sign). They all correspond to "transitions" between two states differing in the magnetic quantum numbers by: ±1. For example, the element $\rho_{21}=\langle\alpha_I\beta_S|\hat{\rho}|\alpha_I\alpha_S\rangle$, if non-zero, is associated with the "transition" between the two states $|\alpha_I\beta_S\rangle$ and $|\alpha_I\alpha_S\rangle$. The difference in the magnetic quantum numbers between the two states is: $M_{|\alpha_I\beta_S\rangle}-M_{|\alpha_I\alpha_S\rangle}=0-1=-1$, i.e. it is anallowed transition. The "transition" is here referred to the interconversion of the states α and β and named also, as already mentioned, a *"coherence"*.

Generally, the ΔM_{rs} between two states $|r\rangle$ and $|s\rangle$ refers to the ***order of coherence p***, so that $\Delta M_{rs} = p_{rs}$.

It is clear now that a density matrix (and importantly the observable magnetization) can be described in terms of **single-element basis operators**. Each of them will correspond to a single line belonging to a given multiplet. For example, the element $\rho_{21} = \langle \alpha_I \beta_S | \hat{\rho} | \alpha_I \alpha_S \rangle$ corresponds to $\hat{I}_\alpha \hat{S}_-$ operator as it is the spin S polarization that is "inverted" and leads to the generation of a coherence of order $p = -1$. In this notation, the spin on which there is the coherence is called the ***active spin*** and its coupling partner is called the ***passive spin***. On the other hand, an element like for example $\rho_{32} = \langle \beta_I \alpha_S | \hat{A} | \alpha_I \beta_S \rangle$ corresponds to $\hat{I}_- \hat{S}_+$ operator which represents the zero-quantum coherence $p = 0$, *etc*. From the Figure 6 it is clear that when a system of two coupled spins is considered in the Hilbert space, there are eight elements corresponding to single-quantum coherences - and other two, two and four - corresponding to zero-quantum, double-quantum and populations, respectively.

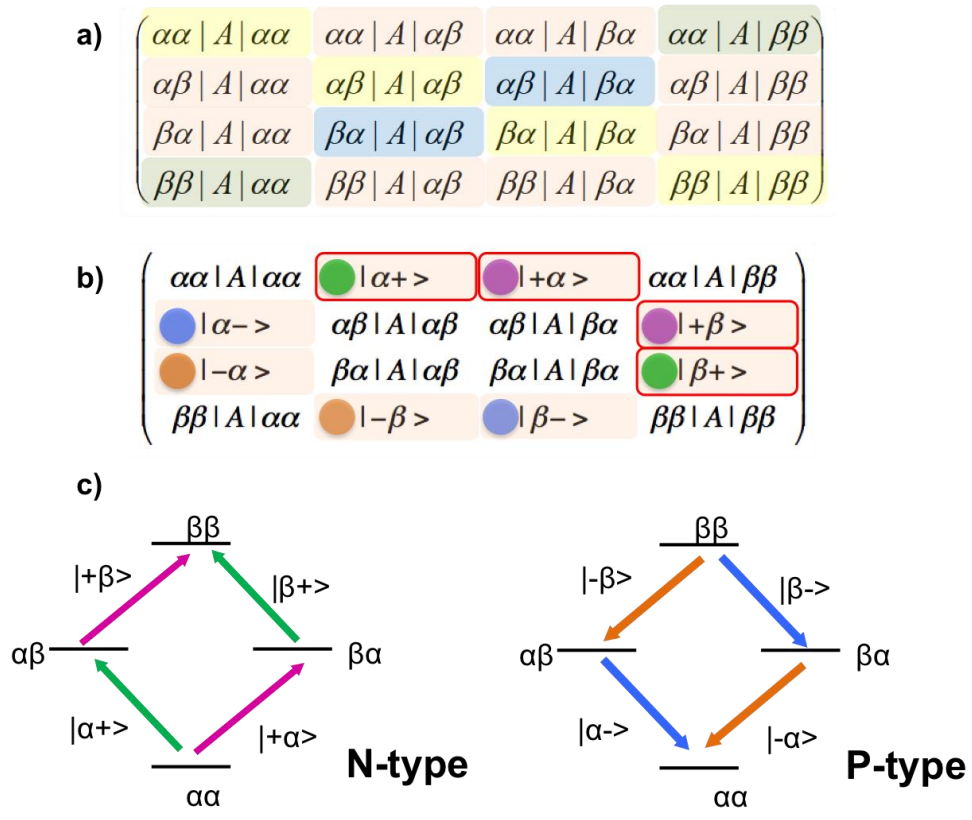

Figure 6. (a) General form of a density matrix for two coupled spins in a Hilbert space with elements labeled with a color code according to coherence order it represents, if the given transition takes place. (b) Density matrix with eight non-vanishing elements corresponding to single quantum coherences with $\Delta M_{rs} = +1$ and $\Delta M_{rs} = -1$, respectively. (c) Corresponding energy levels diagrams with a simplified, graphical representation of the eight single quantum coherences with coherence order +1 and -1 (generating N-type and P-type spectra, respectively, if two-dimensional spectroscopy with mixing is considered).

The transverse magnetization is then described by eight single transition operators forming the corresponding base:

$$B^{(\pm)} = \{\hat{I}_+\hat{S}_\alpha, \hat{I}_+\hat{S}_\beta, \hat{I}_-\hat{S}_\alpha, \hat{I}_-\hat{S}_\beta, \hat{I}_\alpha\hat{S}_+, \hat{I}_\beta\hat{S}_+, \hat{I}_\alpha\hat{S}_-, \hat{I}_{1\beta}\hat{S}_-\} \tag{37}$$

It is conventionally assumed that only a coherence with order -1 is observable. Thus, in the one-dimensional spectrum, only the four terms: $\hat{I}_-\hat{S}_\alpha$, $\hat{I}_-\hat{S}_\beta$, $\hat{I}_\alpha\hat{S}_-$, $\hat{I}_\beta\hat{S}_-$, corresponding to the density matrix elements: ρ_{31}, ρ_{42}, ρ_{21} and ρ_{43}, respectively, result in observable signals. When two-dimensional spectroscopy is considered, it is necessary to retain all the terms, as will be discussed in the following Section II.F.

While in the description of most of the NMR experiments it is not necessary to consider separately each single transition (it is sufficient to look at the entire multiplet at once), this approach turns out to be convenient in certain situations, for example when analyzing spectra of strongly coupled spins or spectra resulting from experiments utilizing pulses that may lead to transfers of magnetization escaping the standard selection rules (for example biselective pulses[26]). It also allows analyzing experiments that employ small flip angle pulses. In these situations, different components of a given multiplet may experience different rotations, which leads to differences in the phase and/or amplitude of signals within one multiplet.

E. Free precession

It was stated above that the difference ΔM_{rs} between two states $|r\rangle$ and $|s\rangle$ involved in a transition, refers to the ***order of coherence*** $\boldsymbol{p}$. The coherence order can also be defined by what happens to an operator (or product of operators) when a *z*-rotation through an angle ϕ is applied. If, as a result of this rotation, the operator acquires a phase of $(-p \cdot \phi)$, the operator is classed as having order p[31]:

$$\hat{\rho}^{(p)} \xrightarrow{\text{rotation by } \phi \text{ about z}} \hat{\rho}^{(p)} \cdot \exp(-ip\phi). \tag{38}$$

During the free precession, a system of two weakly coupled spins experiences only a *z*-rotation, as the weak coupling Hamiltonian is given by:

$$\hat{H}_{IS_{weak}} = \Omega_I\hat{I}_z + \Omega_S\hat{S}_z + 2\pi J \cdot \hat{I}_z\hat{S}_z \tag{39}$$

The matrix representation of this Hamiltonian is a diagonal matrix as the basis states: $|\alpha\alpha\rangle$, $|\alpha\beta\rangle, |\beta\alpha\rangle$ and $|\beta\beta\rangle$ are the eigenstates of this Hamiltonian. When it acts on them, it does not change them as the density operator and $\widehat{H}_{IS}$ commute.

$$\widehat{H}_{IS_{weak}} = \begin{pmatrix} \frac{1}{2}(\Omega_I + \Omega_S) + \frac{1}{2}\pi J & 0 & 0 & 0 \\ 0 & \frac{1}{2}(\Omega_I - \Omega_S) - \frac{1}{2}\pi J & 0 & 0 \\ 0 & 0 & -\frac{1}{2}(\Omega_I - \Omega_S) - \frac{1}{2}\pi J & 0 \\ 0 & 0 & 0 & -\frac{1}{2}(\Omega_I + \Omega_S) + \frac{1}{2}\pi J \end{pmatrix} \tag{40}$$

with the diagonal elements being: ε_1, ε_2, ε_3 and ε_4, respectively.

However, what evolves under this Hamiltonian is the transverse magnetization. The matrix exponential of the diagonal matrix in Eq (40) is also diagonal. Thus, the propagation of $I_x + S_x$:

$$(t) = e^{-iH_{IS_{weak}}\boldsymbol{t}} \cdot \begin{pmatrix} 0 & \frac{1}{2} & \frac{1}{2} & 0 \\ \frac{1}{2} & 0 & 0 & \frac{1}{2} \\ \frac{1}{2} & 0 & 0 & \frac{1}{2} \\ 0 & \frac{1}{2} & \frac{1}{2} & 0 \end{pmatrix} \cdot e^{+iH_{IS_{weak}}\boldsymbol{t}} \tag{41}$$

will result in the non-zero elements (SQ coherences) acquiring a phase label according to their energy levels:

$$\begin{aligned}
\hat{I}_+\hat{S}_\alpha &\xrightarrow{t_1(\Omega_I\hat{I}_z+\Omega_S\hat{S}_z+2\pi J\hat{I}_z\hat{S}_z)} exp[-i(\Omega_I + \pi J)t_1]\, \hat{I}_+\hat{S}_\alpha \\
\hat{I}_+\hat{S}_\beta &\xrightarrow{t_1(\Omega_I\hat{I}_z+\Omega_S\hat{S}_z+2\pi J\hat{I}_z\hat{S}_z)} exp[-i(\Omega_I - \pi J)t_1]\, \hat{I}_+\hat{I}_\beta \\
\hat{I}_-\hat{S}_\alpha &\xrightarrow{t_1(\Omega_I\hat{I}_z+\Omega_S\hat{S}_z+2\pi J\hat{I}_z\hat{S}_z)} exp[+i(\Omega_I + \pi J)t_1]\, \hat{I}_-\hat{I}_\alpha \\
\hat{I}_-\hat{S}_\beta &\xrightarrow{t_1(\Omega_I\hat{I}_z+\Omega_S\hat{S}_z+2\pi J\hat{I}_z\hat{S}_z)} exp[+i(\Omega_I - \pi J)t_1]\, \hat{I}_-\hat{I}_\beta \\
\hat{I}_\alpha\hat{S}_+ &\xrightarrow{t_1(\Omega_I\hat{I}_z+\Omega_S\hat{S}_z+2\pi J\hat{I}_z\hat{S}_z)} exp[-i(\Omega_S + \pi J)t_1]\, \hat{I}_\alpha\hat{I}_+ \\
\hat{I}_\beta\hat{S}_+ &\xrightarrow{t_1(\Omega_I\hat{I}_z+\Omega_S\hat{S}_z+2\pi J\hat{I}_z\hat{S}_z)} exp[-i(\Omega_S - \pi J)t_1]\, \hat{I}_\beta\hat{I}_+ \\
\hat{I}_\alpha\hat{S}_- &\xrightarrow{t_1(\Omega_I\hat{I}_z+\Omega_S\hat{S}_z+2\pi J\hat{I}_z\hat{S}_z)} exp[+i(\Omega_S + \pi J)t_1]\, \hat{I}_\alpha\hat{I}_- \\
\hat{I}_\beta\hat{S}_- &\xrightarrow{t_1(\Omega_I\hat{I}_z+\Omega_S\hat{S}_z+2\pi J\hat{I}_z\hat{S}_z)} exp[+i(\Omega_S - \pi J)t_1]\, \hat{I}_\beta\hat{I}_-
\end{aligned} \tag{42}$$

The very important point to make here is that the different elements of the density matrix can be grouped according to the phase they will acquire upon a rotation. This makes it possible to differentiate between these groups during the pulse sequence. This is the base of the coherence selection by phase cycling, gradients or even specially designed algorithms (E-COSY[32]).

F. Amplitude and phase modulation

This assumption that only one of the two coherence orders (-1 or $+1$) - constituting the transverse magnetization and represented in the basis in Eq (37) - is observable, comes from the fact that the magnetization is detected using two orthogonal channels. For each resonance in the spectrum, the two signals so acquired are cosine and sine functions of the offset frequency Ω. They can be thought of as the real and imaginary parts of a complex exponential function describing the time-domain signal. Since both of them are accessible, the "direction" of the rotation of the magnetization is known. This is why there is no need to consider all the eight basis operators, but only the half of them with $p = -1$. A similar logic applies to special experiments such as the *J*-resolved spectroscopy, where no mixing is present and so the information about the direction of the rotation is well preserved.

Most standard two-dimensional experiments require a quadrature detection, equivalent to collecting two orthogonal components of the magnetization. There are several methods to achieve this, the most common being echo-antiecho or States-TPPI procedures. The possibility to collect equal amounts of the orthogonal components of the magnetization is the consequence of preserving the symmetry between the coherences with $p = +n$ and $p = -n$ and plays a central role in the possibility to obtain the frequency discrimination and perfectly absorptive signals after the 2D Fourier Transformation. The symmetry must be preserved during the entire pulse sequence until the last (mixing) pulse, which converts the magnetization of orders $+n$ and $-n$ to the -1 magnetization, just at the moment when the detection starts. If the symmetry cannot be maintained, a phase-twist signals or signals with phase distortion will be present in the two-dimensional spectrum.

G. Mixing and coherence transfer, small flip angle pulses

If a pulse of a flip angle *different than* 180° is applied to the transverse magnetization of at least two coupled spins after they were evolving for some time τ, it plays the role of a mixing

pulse. Mixing pulse causes coherence transfer between coupled spins and generation of coherences of an order higher or lower than ± 1. Again, if we consider the simplified geometrical interpretation of the situation (vector model), these transfers can only be triggered by a pulse, which is *not* parallel to the vector representing the magnetization (because the two operators must not commute). Since the magnetization usually evolves for some time in the transverse plane before the mixing pulse is applied, it acquires a certain phase (the magnetization vector may be pointing to any direction in the transverse plane at the moment of the occurrence of the pulse). There is only a low probability that the two vectors (the magnetization and the phase of the pulse in the rotating frame) will be either perpendicular or parallel to each other. More generally, the magnetization vector will be somewhere in between the parallel and the perpendicular arrangement with the phase of the pulse (understood here as the axis in the rotating frame). This is very often expressed as the ***fixed relative*** amount of the *x* and *y* magnetization (when chemical shift evolution is considered) or as the ***fixed relative*** amount of the so-called in-phase and antiphase magnetization (when the *J*-coupling is considered). The in-phase and antiphase terms represent the decomposition of the magnetization vector into two perpendicular directions.

Even if the two vectors are not perpendicular to each other (but ***importantly*** not parallel neither), the commutator of the corresponding operators is non-zero and the magnetization transfer will occur. Let's designate the magnetization vector as $\left(\hat{I} + \hat{S}\right)_{transverse\_\Phi}$ and the pulse: $\hat{I}_x + \hat{S}_x$. Under the special condition of this pulse being a 90° pulse - and regardless the phase the magnetization has acquired at the moment of the arrival of the pulse - the magnetization vector will be moved to a plane which is perpendicular to the transverse plane. This change of the geometry by the 90° is illustrated in Figure 7.

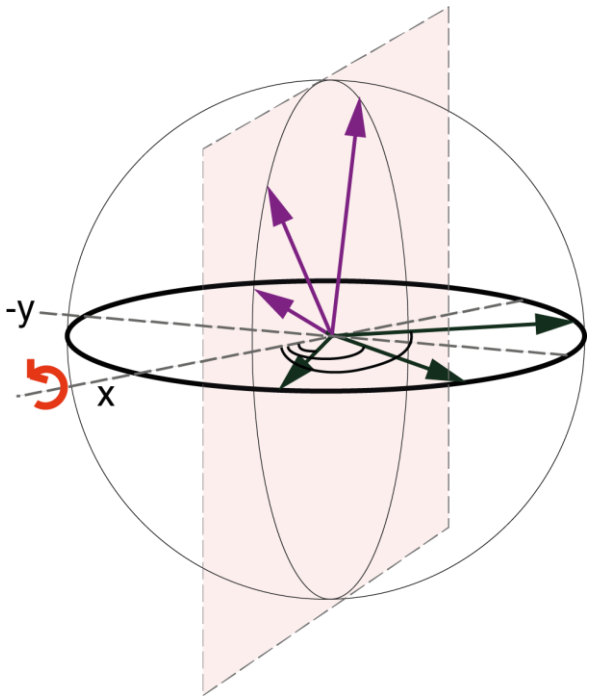

Figure 7. The geometrical representation of the generation of the amplitude-modulated two-dimensional dataset from the phase-modulated dataset by the application of a 90°$_x$ mixing pulse. Three time increments are considered for the simplicity of the demonstration.

The same can be formally calculated through the following propagation (where the matrix exponential is specific for an *x* pulse):

$$(t) = \underbrace{\begin{pmatrix} c^2 & -isc & -isc & -s^2 \\ -isc & c^2 & -s^2 & -isc \\ -isc & -s^2 & c^2 & -isc \\ -s^2 & -isc & -isc & c^2 \end{pmatrix}}_{e^{-i\theta\cdot\hat{I}_x}} \cdot \underbrace{\begin{pmatrix} 0 & +\frac{i}{2}e^{i(-\Omega_S-\pi J)t} & +\frac{i}{2}e^{i(-\Omega_I-\pi J)t} & 0 \\ -\frac{i}{2}e^{i(-\Omega_S-\pi J)t} & 0 & 0 & +\frac{i}{2}e^{i(-\Omega_I+\pi J)t} \\ -\frac{i}{2}e^{i(-\Omega_I-\pi J)t} & 0 & 0 & +\frac{i}{2}e^{i(-\Omega_S+\pi J)t} \\ 0 & -\frac{i}{2}e^{i(-\Omega_I+\pi J)t} & -\frac{i}{2}e^{i(-\Omega_S+\pi J)t} & 0 \end{pmatrix}}_{\text{Matrix representation of the transverse magnetization, equivalent with Eq (42)}} \cdot \underbrace{\begin{pmatrix} c^2 & +isc & +isc & -s^2 \\ +isc & c^2 & -s^2 & +isc \\ +isc & -s^2 & c^2 & +isc \\ -s^2 & +isc & +isc & c^2 \end{pmatrix}}_{e^{+i\theta\cdot\hat{I}_x}} \quad (43)$$

with $\theta = \frac{\pi}{2}$ (flip angle) and $c = \cos\left(\frac{1}{2}\cdot\frac{\pi}{2}\right)$, $s = \sin\left(\frac{1}{2}\cdot\frac{\pi}{2}\right)$.

So that the propagator in this case is just:

$$U = \begin{pmatrix} \frac{1}{2} & \frac{1}{2} & \frac{1}{2} & -\frac{1}{2} \\ \frac{1}{2} & \frac{1}{2} & -\frac{1}{2} & \frac{1}{2} \\ \frac{1}{2} & -\frac{1}{2} & \frac{1}{2} & \frac{1}{2} \\ -\frac{1}{2} & \frac{1}{2} & \frac{1}{2} & \frac{1}{2} \end{pmatrix} \tag{44}$$

However, if a small flip angle *x* pulse (for example 30°) is applied as a mixing pulse, then depending on the phase the magnetization has acquired in the transverse plane up to the moment when the pulse is applied, it will end up with a certain phase with respect to the phase of the detector. In other words, if the two-dimensional dataset acquisition is then considered, the magnetization will not be *purely amplitude modulated*, but an additional phase factor must be taken into account (Figure 8).

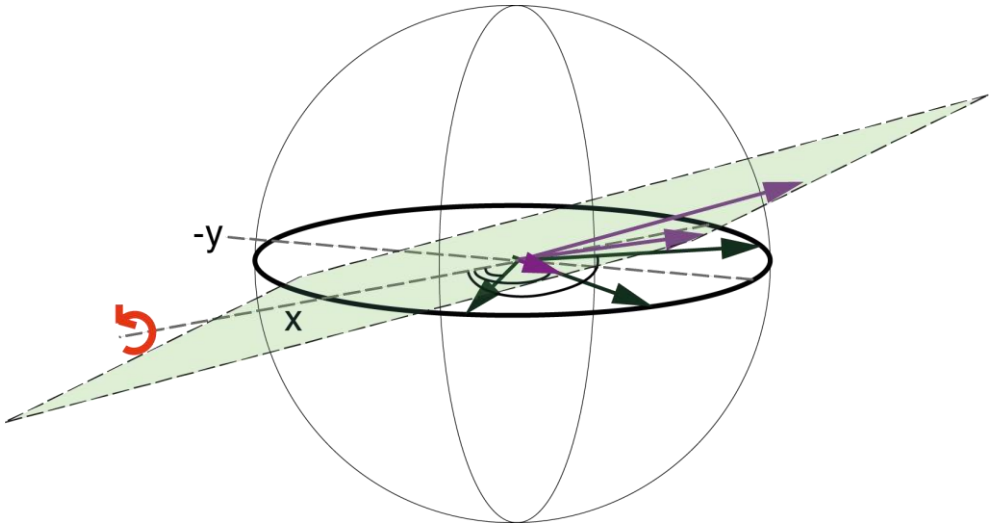

Figure 8. The geometrical representation of the effect of a small flip angle mixing pulse on the transverse magnetization.

The propagator in this case is:

$$U = \begin{pmatrix} \frac{2+\sqrt{3}}{4} & -\frac{1}{4}i & -\frac{1}{4}i & \frac{-2+\sqrt{3}}{4} \\ -\frac{1}{4}i & \frac{2+\sqrt{3}}{4} & \frac{-2+\sqrt{3}}{4} & -\frac{1}{4}i \\ -\frac{1}{4}i & \frac{-2+\sqrt{3}}{4} & \frac{2+\sqrt{3}}{4} & -\frac{1}{4}i \\ \frac{-2+\sqrt{3}}{4} & -\frac{1}{4}i & -\frac{1}{4}i & \frac{2+\sqrt{3}}{4} \end{pmatrix} \tag{45}$$

The important conclusion that can be drawn out of this simple calculations is that in case of the two-dimensional dataset acquisition, even though the arrangement between the magnetization vector and the vector representing the pulse cannot be perpendicular, the 90° flip angle of the pulse may ensure amplitude modulation along one fixed axis in the rotating frame. In other words, if the density matrix representing magnetization in the transverse plane is rotated by a 90° mixing pulse, then the resulting density matrix will be symmetrical with respect to the generated coherences, on the contrary to the small flip angle mixing pulse.

The rotation experienced by a spin I magnetization in the transverse plane by a mixing pulse of any phase ϕ and/or any flip angle θ can be generalized according to trigonometric relationships governing the rotations involved in the propagation of the density matrix[33]:

$$\begin{aligned}
\hat{I}_+ &\xrightarrow{\theta\hat{I}_\phi} cos^2\left(\tfrac{1}{2}\theta\right)\hat{I}_+ + exp[+i2\phi]\cdot sin^2\left(\tfrac{1}{2}\theta\right)\hat{I}_- + \tfrac{1}{2}\, i\, exp[+i\phi]\cdot sin\theta\left(\hat{I}_\alpha - \hat{I}_\beta\right)\\
\hat{I}_- &\xrightarrow{\theta\hat{I}_\phi} cos^2\left(\tfrac{1}{2}\theta\right)\hat{I}_- + exp[-i2\phi]\cdot sin^2\left(\tfrac{1}{2}\theta\right)\hat{I}_+ - \tfrac{1}{2}\, i\, exp[-i\phi]\cdot sin\theta\left(\hat{I}_\alpha - \hat{I}_\beta\right)\\
\hat{I}_\alpha &\xrightarrow{\theta\hat{I}_\phi} cos^2\left(\tfrac{1}{2}\theta\right)\hat{I}_\alpha + sin^2\left(\tfrac{1}{2}\theta\right)\hat{I}_\beta + \tfrac{1}{2} i\, sin\theta\cdot(\hat{I}_+\, exp[-i\phi] - \hat{I}_-\, exp[+i\phi])\\
\hat{I}_\beta &\xrightarrow{\theta\hat{I}_\phi} cos^2\left(\tfrac{1}{2}\theta\right)\hat{I}_\beta + sin^2\left(\tfrac{1}{2}\theta\right)\hat{I}_\alpha - \tfrac{1}{2} i\, sin\theta\cdot(\hat{I}_+\, exp[-i\phi] - \hat{I}_-\, exp[+i\phi])
\end{aligned} \tag{46}$$

The transverse magnetization after a period of free precession, represented by the non-diagonal density matrix with the eight non-zero elements (SQC), each with the corresponding phase label, is rotated by the mixing pulse propagator and ends up as another matrix with all elements being non-zero. In fact, each term representing a single-quantum coherence on a given spin is transferred with a given amplitude (probability) and phase (the proportion of the real and imaginary part of the number expressing the probability) to terms representing single-quantum coherences on the coupled partner and moreover populations, zero-quantum and double-quantum coherences. All these just enumerated terms can be represented by operators involving all possible combinations of products of the $\hat{I}_+$, $\hat{I}_-$, $\hat{I}_\alpha$, $\hat{I}_\beta$ operators.

The sign and amplitude of a transition from each single element of the density matrix representing the ± 1 coherence to all possible observable elements - as calculated by the equations just above - will be manifested as a positive or negative peaks with the corresponding amplitude in the 2D spectrum. This means that the phase label that each of the elements acquires during each incremented period of evolution just prior to the mixing pulse does not need to be taken into account when these transition probabilities are calculated. This is justified by the fact that the phase label acquired in the transverse plane is precisely translated to an amplitude modulation of the 2D dataset. This is *apparently* ensured by the fact that the magnetization vector before the rotation and after the rotation are 90° out of phase with

respect to each other. For the purpose of a demonstration, all possible transfers from just one single transition operator (normally eight are present before mixing) are calculated:

$$\phi_{label}\,\hat{I}_+\hat{S}_\alpha \xrightarrow{90^\circ_x\ mixing\ pulse}$$

$$\begin{gathered}
\phi_{label}\cdot\hat{I}_-\hat{S}_\alpha\cdot sin^2\left(\frac{\pi}{4}\right)\cdot cos^2\left(\frac{\pi}{4}\right)=\phi_{label}\cdot\frac{1}{4}\cdot\hat{I}_-\hat{S}_\alpha\\
\phi_{label}\cdot\hat{I}_-\hat{S}_\beta\cdot sin^2\left(\frac{\pi}{4}\right)\cdot sin^2\left(\frac{\pi}{4}\right)=\phi_{label}\cdot\frac{1}{4}\cdot\hat{I}_-\hat{S}_\beta\\
\\
\phi_{label}\cdot\hat{I}_a\hat{S}_-\cdot\frac{1}{2}i\,sin\left(\frac{\pi}{2}\right)\cdot-\frac{1}{2}i\,sin\left(\frac{\pi}{2}\right)=\phi_{label}\cdot\frac{1}{4}\cdot\hat{I}_a\hat{S}_-\\
\phi_{label}\cdot\hat{I}_\beta\hat{S}_-\cdot-\frac{1}{2}i\,sin\left(\frac{\pi}{2}\right)\cdot-\frac{1}{2}i\,sin\left(\frac{\pi}{2}\right)=\phi_{label}\cdot-\frac{1}{4}\cdot\hat{I}_\beta\hat{S}_-\\
\\
\phi_{label}\cdot\hat{I}_\alpha\hat{S}_\beta\cdot\frac{1}{2}\,i\,sin\left(\frac{\pi}{2}\right)\cdot sin^2\left(\frac{\pi}{4}\right)=\phi_{label}\cdot\frac{1}{4}i\cdot\hat{I}_\alpha\hat{S}_\beta\\
\phi_{label}\cdot\hat{I}_\beta\hat{S}_\alpha\cdot-\frac{1}{2}i\,sin\left(\frac{\pi}{2}\right)\cdot cos^2\left(\frac{\pi}{4}\right)=\phi_{label}\cdot-\frac{1}{4}i\cdot\hat{I}_\beta\hat{S}_\alpha\\
\phi_{label}\cdot\hat{I}_\alpha\hat{S}_\alpha\cdot\frac{1}{2}i\,sin\left(\frac{\pi}{2}\right)\cdot cos^2\left(\frac{\pi}{4}\right)=\phi_{label}\cdot\frac{1}{4}i\cdot\hat{I}_\alpha\hat{S}_\alpha\\
\phi_{label}\cdot\hat{I}_\beta\hat{S}_\beta\cdot-\frac{1}{2}\,i\,sin\left(\frac{\pi}{2}\right)\cdot sin^2\left(\frac{\pi}{4}\right)=\phi_{label}\cdot-\frac{1}{4}i\cdot\hat{I}_\beta\hat{S}_\beta\\
\\
\phi_{label}\cdot\hat{I}_-\hat{S}_-\cdot sin^2\left(\frac{\pi}{4}\right)\cdot-\frac{1}{2}i\,sin\left(\frac{\pi}{2}\right)=\phi_{label}\cdot-\frac{1}{4}i\cdot\hat{I}_-\hat{S}_-\\
\phi_{label}\cdot\hat{I}_+\hat{S}_+\cdot cos^2\left(\frac{\pi}{4}\right)\cdot+\frac{1}{2}i\,sin\left(\frac{\pi}{2}\right)=\phi_{label}\cdot\frac{1}{4}i\cdot\hat{I}_+\hat{S}_+\\
\\
\phi_{label}\cdot\hat{I}_-\hat{S}_+\cdot sin^2\left(\frac{\pi}{4}\right)\cdot+\frac{1}{2}i\,sin\left(\frac{\pi}{2}\right)=\phi_{label}\cdot\frac{1}{4}i\cdot\hat{I}_-\hat{S}_+\\
\phi_{label}\cdot\hat{I}_+\hat{S}_-\cdot cos^2\left(\frac{\pi}{4}\right)\cdot-\frac{1}{2}i\,sin\left(\frac{\pi}{2}\right)=\phi_{label}\cdot-\frac{1}{4}i\cdot\hat{I}_+\hat{S}_-\\
\\
\phi_{label}\cdot\hat{I}_+\hat{S}_\alpha\cdot cos^2\left(\frac{\pi}{4}\right)\cdot cos^2\left(\frac{\pi}{4}\right)=\phi_{label}\cdot\frac{1}{4}\cdot\hat{I}_+\hat{S}_\alpha\\
\phi_{label}\cdot\hat{I}_+\hat{S}_\beta\cdot cos^2\left(\frac{\pi}{4}\right)\cdot sin^2\left(\frac{\pi}{4}\right)=\phi_{label}\cdot\frac{1}{4}\cdot\hat{I}_+\hat{S}_\beta\\
\phi_{label}\cdot\hat{I}_\alpha\hat{S}_+\frac{1}{2}i\,sin\left(\frac{\pi}{2}\right)\cdot\frac{1}{2}i\,sin\left(\frac{\pi}{2}\right)=\phi_{label}\cdot-\frac{1}{4}\cdot\hat{I}_\alpha\hat{S}_+\\
\phi_{label}\cdot\hat{I}_\beta\hat{S}_+-\frac{1}{2}i\,sin\left(\frac{\pi}{2}\right)\cdot-\frac{1}{2}i\,sin\left(\frac{\pi}{2}\right)=\phi_{label}\cdot-\frac{1}{4}\cdot\hat{I}_\beta\hat{S}_+
\end{gathered}\tag{47}$$

where: $\phi_{label}=exp[-i(\Omega_I+\pi J)t_1]$.

For the complementary term $\hat{I}_-\hat{S}_\alpha$, as a simple example, only the transfers to the four directly observable terms are calculated:

$$\phi_{label}\,\hat{I}_-\hat{S}_\alpha \xrightarrow{90^\circ_x\ mixing\ pulse}$$

$$\begin{gathered}
\phi_{label}\cdot\hat{I}_-\hat{S}_\alpha\cdot cos^2\left(\frac{\pi}{4}\right)\cdot cos^2\left(\frac{\pi}{4}\right)=\phi_{label}\cdot\frac{1}{4}\cdot\hat{I}_-\hat{S}_\alpha\\
\phi_{label}\cdot\hat{I}_-\hat{S}_\beta\cdot cos^2\left(\frac{\pi}{4}\right)\cdot sin^2\left(\frac{\pi}{4}\right)=\phi_{label}\cdot\frac{1}{4}\cdot\hat{I}_-\hat{S}_\beta\\
\\
\phi_{label}\cdot\hat{I}_a\hat{S}_-\cdot-\frac{1}{2}i\,sin\left(\frac{\pi}{2}\right)\cdot-\frac{1}{2}i\,sin\left(\frac{\pi}{2}\right)=\phi_{label}\cdot-\frac{1}{4}\cdot\hat{I}_a\hat{S}_-
\end{gathered}\tag{48}$$

$$\phi_{label} \cdot \hat{I}_\beta \hat{S}_- \cdot \frac{1}{2} i \, sin\left(\frac{\pi}{2}\right) \cdot -\frac{1}{2} i \, sin\left(\frac{\pi}{2}\right) = \phi_{label} \cdot \frac{1}{4} \cdot \hat{I}_\beta \hat{S}_-$$

If, in a similar experiment, a small flip angle pulse is used as a mixing, the transfers from any term (out of the eight SQC) to all the other sixteen terms do not have the same amplitude and, moreover, transfers originating from terms representing coherence -1 and +1, respectively, are not symmetrical neither. Thus, the probabilities calculated from the equations do not correspond to the intensities of the signals in the 2D spectrum. These probabilities correspond to intensities in the theoretical P and N spectra, however, the acquired 2D spectrum will have phase-distorted signals. In fact, in this case the phase modulation is not exactly translated to the amplitude modulation, as the two vectors: magnetization before the rotation and after the rotation are *not* 90° phase-shifted with respect to each other. This means that after the mixing, the dataset is not purely amplitude modulated, but there is some phase factor to be taken into account that influences the phase of the signals in the 2D spectrum.

Assuming a small flip angle pulses, typically 10°- 30°,

$$\begin{gathered} cos^2\left(\frac{1}{2}\theta\right) \approx 1 \\ sin^2\left(\frac{1}{2}\theta\right) \approx \frac{1}{4}\theta^2 \\ sin\theta \approx \theta \end{gathered} \tag{49}$$

and the transfer probabilities are:

$$\phi_{label} \, \hat{I}_+ \hat{S}_\alpha \xrightarrow{\theta_x \, mixing \, pulse}$$

$$\begin{gathered} \phi_{label} \cdot \hat{I}_- \hat{S}_\alpha \cdot \frac{1}{4}\theta^2 \cdot 1 = \phi_{label} \cdot \frac{1}{4}\theta^2 \cdot \hat{I}_- \hat{S}_\alpha \\ \phi_{label} \cdot \hat{I}_- \hat{S}_\beta \cdot \frac{1}{4}\theta^2 \cdot \frac{1}{4}\theta^2 = \phi_{label} \cdot \frac{1}{16}\theta^4 \cdot \hat{I}_- \hat{S}_\beta \\ \\ \phi_{label} \cdot \hat{I}_\alpha \hat{S}_- \cdot \frac{1}{2} i\,\theta \cdot -\frac{1}{2} i\,\theta = \phi_{label} \cdot \frac{1}{4}\theta^2 \cdot \hat{I}_\alpha \hat{S}_- \\ \phi_{label} \cdot \hat{I}_\beta \hat{S}_- \cdot -\frac{1}{2} i\,\theta \cdot -\frac{1}{2} i\,\theta = \phi_{label} \cdot -\frac{1}{4}\theta^2 \cdot \hat{I}_\beta \hat{S}_- \\ \\ \phi_{label} \cdot \hat{I}_\alpha \hat{S}_\beta \cdot \frac{1}{2} i\,\theta \cdot \frac{1}{4}\theta^2 = \phi_{label} \cdot \frac{1}{8} i\,\theta^3 \cdot \hat{I}_\alpha \hat{S}_\beta \\ \phi_{label} \cdot \hat{I}_\beta \hat{S}_\alpha - \frac{1}{2} i\,\theta \cdot 1 = \phi_{label} \cdot -\frac{1}{2} i\,\theta \cdot \hat{I}_\beta \hat{S}_\alpha \\ \phi_{label} \cdot \hat{I}_\alpha \hat{S}_\alpha \cdot \frac{1}{2} i\,\theta \cdot 1 = \phi_{label} \cdot \frac{1}{2} i\,\theta \cdot \hat{I}_\alpha \hat{S}_\alpha \\ \phi_{label} \cdot \hat{I}_\beta \hat{S}_\beta \cdot -\frac{1}{2} i\,\theta \cdot \frac{1}{4}\theta^2 = \phi_{label} \cdot -\frac{1}{8} i\,\theta^3 \cdot \hat{I}_\beta \hat{S}_\beta \\ \\ \phi_{label} \cdot \hat{I}_- \hat{S}_- \cdot \frac{1}{4}\theta^2 \cdot -\frac{1}{2} i\,\theta = \phi_{label} \cdot -\frac{1}{8} i\,\theta^3 \cdot \hat{I}_- \hat{S}_- \\ \phi_{label} \cdot \hat{I}_+ \hat{S}_+ \cdot 1 \cdot \frac{1}{2} i\,\theta = \phi_{label} \cdot \frac{1}{2} i\,\theta \cdot \hat{I}_+ \hat{S}_+ \end{gathered} \tag{50}$$

$$\phi_{label} \cdot \hat{I}_{-}\hat{S}_{+} \cdot \frac{1}{4}\theta^2 \cdot \frac{1}{2} i\,\theta = \phi_{label} \cdot \frac{1}{8} i\,\theta^3 \cdot \hat{I}_{-}\hat{S}_{+}$$
$$\phi_{label} \cdot \hat{I}_{+}\hat{S}_{-} \cdot 1 \cdot -\frac{1}{2} i\,\theta = \phi_{label} \cdot -\frac{1}{2} i\,\theta \cdot \hat{I}_{+}\hat{S}_{-}$$

$$\phi_{label} \cdot \hat{I}_{+}\hat{S}_{\alpha} \cdot 1 = \phi_{label} \cdot \hat{I}_{+}\hat{S}_{\alpha}$$
$$\phi_{label} \cdot \hat{I}_{+}\hat{S}_{\beta} \cdot 1 \cdot \frac{1}{4}\theta^2 = \phi_{label} \cdot \frac{1}{4}\theta^2 \cdot \hat{I}_{+}\hat{S}_{\beta}$$
$$\phi_{label} \cdot \hat{I}_{\alpha}\hat{S}_{+} \cdot \frac{1}{2} i\,\theta \cdot \frac{1}{2} i\,\theta = \phi_{label} \cdot -\frac{1}{4}\theta^2 \cdot \hat{I}_{\alpha}\hat{S}_{+}$$
$$\phi_{label} \cdot \hat{I}_{\beta}\hat{S}_{2+} \cdot -\frac{1}{2} i\,\theta \cdot \frac{1}{2} i\,\theta = \phi_{label} \cdot \frac{1}{4}\theta^2 \cdot \hat{I}_{\beta}\hat{S}_{-}$$

where: $\phi_{label} = exp[-i(\Omega_I + \pi J)t_1]$.

For the complementary term $\hat{I}_{-}\hat{S}_{\alpha}$, as an example, only the transfers to the four directly observable terms and the populations are calculated:

$$\phi_{label}\ \hat{I}_{-}\hat{S}_{\alpha} \xrightarrow{\theta_x\ mixing\ pulse}$$

$$\phi_{label} \cdot \hat{I}_{1-}\hat{I}_{2\alpha} \cdot 1 \cdot 1 = \phi_{label} \cdot \hat{I}_{1-}\hat{I}_{2\alpha}$$
$$\phi_{label} \cdot \hat{I}_{1-}\hat{I}_{2\beta} \cdot 1 \cdot \frac{1}{4}\theta^2 = \phi_{label} \cdot \frac{1}{4}\theta^2 \cdot \hat{I}_{1-}\hat{I}_{2\beta}$$

$$\phi_{label} \cdot \hat{I}_{1\alpha}\hat{I}_{2-} \cdot -\frac{1}{2} i\,\theta \cdot -\frac{1}{2} i\,\theta = \phi_{label} \cdot -\frac{1}{4}\theta^2 \cdot \hat{I}_{1\alpha}\hat{I}_{2-}$$
$$\phi_{label} \cdot \hat{I}_{1\beta}\hat{I}_{2-} \cdot -\frac{1}{2} i\,\theta \cdot -\frac{1}{2} i\,\theta = \phi_{label} \cdot -\frac{1}{4}\theta^2 \cdot \hat{I}_{1\beta}\hat{I}_{2-} \qquad (51)$$

$$\phi_{label} \cdot \hat{I}_{1\alpha}\hat{I}_{2\beta} \cdot -\frac{1}{2} i\,\theta \cdot \frac{1}{4}\theta^2 = \phi_{label} \cdot -\frac{1}{8} i\,\theta^3 \cdot \hat{I}_{1\alpha}\hat{I}_{2\beta}$$
$$\phi_{label} \cdot \hat{I}_{1\beta}\hat{I}_{2\alpha} \cdot \frac{1}{2} i\,\theta \cdot 1 = \phi_{label} \cdot \frac{1}{2} i\,\theta \cdot \hat{I}_{1\beta}\hat{I}_{2\alpha}$$
$$\phi_{label} \cdot \hat{I}_{1\alpha}\hat{I}_{2\alpha} \cdot -\frac{1}{2} i\,\theta \cdot 1 = \phi_{label} \cdot -\frac{1}{2} i\,\theta \cdot \hat{I}_{1\alpha}\hat{I}_{2\alpha}$$
$$\phi_{label} \cdot \hat{I}_{1\beta}\hat{I}_{2\beta} \cdot \frac{1}{2} i\,\theta \cdot \frac{1}{4}\theta^2 = \phi_{label} \cdot \frac{1}{8} i\,\theta^3 \cdot \hat{I}_{1\beta}\hat{I}_{2\beta}$$

The fact that the elements representing the single quantum coherences are transferred to other elements with different coherence orders can be thought of (using the vector model) as transferring a magnetization from one plane to another plane. The magnetization still exists but since it is not in the transverse plane, it will not induce current in the receiver coil.

Spectra resulting from 2D experiments using small flip angle mixing pulse are not expected to be in pure absorption because the shift by the 90° of the first pulse (in two consecutive transients for the quadrature detection) will not have the same effect on the magnetization as it has when a 90° mixing pulse is used. In fact, when a 90° mixing pulse is used, the transition probabilities and sign are such that a following property regarding the P and N type spectra can be calculated:

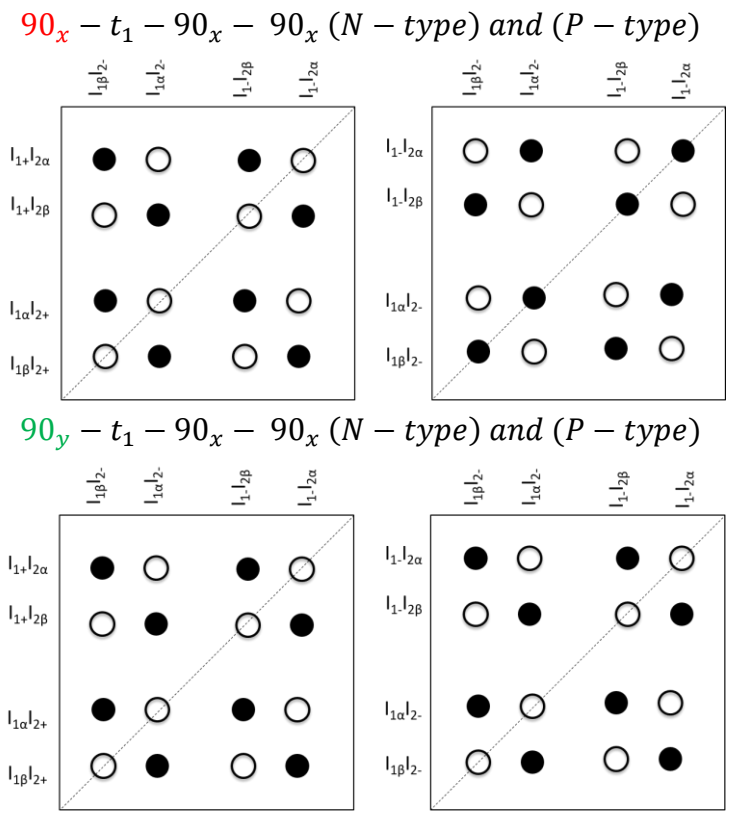

Figure 9. N-type and P-type DQF-COSY spectra of two coupled spins and the effect of changing the phase of the first pulse.

Of course, it should be noted that the sign and amplitude of the absorptive signals in these P and N spectra is theoretical (calculated according to the Eq (46)). In reality, P and N spectra necessarily have the phase-twist lineshapes.

The property shown in Figure 9 is not valid when a small flip angle pulse is used as a mixing[31]. Using phase shift different than 90° in the two steps of the quadrature could probably be considered. Another solution to this problem of phase-distorted signals in experiments based on small flip angle mixing pulses, is to go through a non-direct (requiring more than one step) path, to reach the observable magnetization. In other words, the observable magnetization present just after the small flip angle mixing pulse and having undesirable dependency on the rotations needed for the quadrature detection, can be ignored at first. Instead, a different part of the magnetization may be chosen at this step – the one that is not observable yet, but has the advantageous dependence on rotations (for example the populations part of the magnetization, compare Eq (50) and Eq (51)). Subsequently, additional pulse(s) can be applied to make the magnetization observable. This trick has been employed by Bodenhausen and co-workers[34] in their *z*-filtered COSY experiment in order to improve the phase properties of the small flip angle COSY. Similar selection is used in the PSYCHE element,

as only the population terms should be retained between the small flip angle rotations coming from the two chirped pulses (see Section III.B.2.b).

More generally (apart from the context of small flip angle pulses), the same principle of introducing a multi-step - employing additional pulses and delays - mixing, in order to adjust the trajectory of the magnetization, is used for example in multiple-quantum filtered (MQF) spectroscopy[35, 36].

H. Weak versus strong coupling

In a strongly coupled system, the Zeeman basis states: $|\alpha_I\alpha_S\rangle$, $|\alpha_I\beta_S\rangle$, $|\beta_I\alpha_S\rangle$ and $|\beta_I\beta_S\rangle$ are not anymore the eigenstates of the free precession Hamiltonian, which has the form:

$$\widehat{H}_{IS_{strong}} = \Omega_I\hat{I}_z + \Omega_S\hat{S}_z + 2\pi J \cdot \left(\hat{I}_x\hat{S}_x + \hat{I}_y\hat{S}_y + \hat{I}_z\hat{S}_z\right), \tag{52}$$

where the coupling part of the Hamiltonian is often referred to as secular isotropic Hamiltonian $\widehat{H}_{J_{iso}} = 2\pi J \cdot \left(\hat{I}_x\hat{S}_x + \hat{I}_y\hat{S}_y + \hat{I}_z\hat{S}_z\right)$. However, the eigenstates of this Hamiltonian can be found as a certain combination of the Zeeman basis states. A very convenient and intuitive way to express it is that, for the $\widehat{H}_{IS_{strong}}$ operator, in order to avoid causing any rotation to the Zeeman basis states, or in other words to prevent transforming them in any way - it must be the combination of the rotated Zeeman basis states that will constitute the eigenstates. It may be equivalently expressed the other way round: during the free precession of a strongly coupled spin system, the magnetization experiences not only a *z* rotation, but the trajectory is more complex and the axis of the rotation has all three perpendicular components. Notably, the phase acquired by a given operator as a result of a *z*-rotation is a criterion to assess the coherence order of an operator or products of operators, as discussed in Section II.E. In case of the strong coupling, this definition cannot be applied here directly, or, in other words: "in a strongly coupled spin system coherences can no longer be assigned to individual spins"[25].

What should be highlighted here is that only sometimes the basis states are identical to the eigenstates. The basis states, orthogonal to each other, serve to entirely represent a given spin system, which does not necessarily imply that a Hamiltonian acting on these basis states do not change them. In fact, in NMR, we usually choose Hamiltonians in such a way as to exert a change in a system. It is quite a special case that the basis states are equally the eigenstates of the weak coupling Hamiltonian representing the evolution during free precession and that the system acquires only an additional phase factor (it is like a scaling factor here), which is not the case in the currently discussed system of strongly coupled spins.

The four eigenstates of the $\widehat{H}_{IS_{strong}}$ with the corresponding eigenvalues are:

$$\begin{aligned}
&1.\ |\alpha\alpha> && E_1 = \tfrac{1}{2}(\Omega_I + \Omega_S + \pi J)\\
&2.\ cos\theta|\alpha\beta> - sin\theta|\beta\alpha> && E_2 = \tfrac{1}{2}(\Delta\Omega - \pi J)\\
&3.\ cos\theta|\beta\alpha> + sin\theta|\alpha\beta> && E_3 = \tfrac{1}{2}(-\Delta\Omega - \pi J)\\
&4.\ |\beta\beta> && E_4 = \tfrac{1}{2}(-\Omega_I - \Omega_S + \pi J)
\end{aligned} \tag{53}$$

The strong coupling parameter θ, which indicates the strength of the coupling interaction, is defined as: $\tan 2\theta = \frac{2\pi J}{\Omega_S - \Omega_I}$, and the positive parameter $\Delta\Omega = \sqrt{(\Omega_I - \Omega_S)^2 + 4\pi^2 J^2}$, which is roughly equal to the chemical shift difference, when the coupling is not too strong (otherwise, when $\Omega_I \approx \Omega_S$, the parameter starts to depends only on the coupling constant: $\Delta\Omega = 2\pi J$).

The matrix representation of the strong coupling Hamiltonian is not diagonal, Eq (54), just as for example the matrix representing the *x* pulse: $\omega_1 \hat{I}_x$:

$$\widehat{H}_{IS_{strong}} = \begin{pmatrix} \frac{1}{2}(\Omega_I + \Omega_S) + \frac{1}{2}\pi J & 0 & 0 & 0 \\ 0 & \frac{1}{2}(\Omega_I - \Omega_S) - \frac{1}{2}\pi J & \pi J & 0 \\ 0 & \pi J & -\frac{1}{2}(\Omega_I - \Omega_S) - \frac{1}{2}\pi J & 0 \\ 0 & 0 & 0 & -\frac{1}{2}(\Omega_I + \Omega_S) + \frac{1}{2}\pi J \end{pmatrix} \tag{54}$$

The matrix exponential of non-diagonal matrices will contain some elements with a cos and/or sin modulation that will be "conveyed" to the elements of the matrix being propagated in the form of an amplitude modulation of its elements, unlike the diagonal matrix exponentials that "furnish" just an additional phase label.

In most course books, the effect of the strong coupling is illustrated as the modification of the energy levels and, consequently, the modification of transition probabilities, leading to the "famous" roof effect. It is very useful however, in particular in the context of two-dimensional experiments, to consider the intensity distortions in the 1D spectra of strongly coupled spins as a result of magnetization transfer[21, 37]. When the chemical shift difference between coupled spins becomes small relative to the coupling, the effective secular coupling Hamiltonian ($\widehat{H}_{IS_{strong}}$) resembles the one active during Hartmann-Hahn coherence transfer periods. The Hartmann-Hahn transfer is of a great importance in the context of this thesis, as it underlies the magnetization transfers during the strong coupling[21], the TOCSY mixing[38] and even the special rotation during a biselective pulse[26, 39]. Regarding this magnetization transfer,

an analogy can be drawn between an action of the strong coupling Hamiltonian and a mixing pulse, both represented by a non-diagonal matrices.

The TOCSY experiment uses a period called *spin-locking* to cause a coherence transfer. The spin-locking effect may be achieved by applying a long, strong radiofrequency pulse in the presence of which the individual chemical shifts start to lose their effect on the spin dynamics and it is the Hamiltonian shown in Eq (55) that dominates the evolution of the system (compare with Eq (52)):

$$\hat{H}_{spin-lock} = \omega_1\left(\hat{I}_x + \hat{S}_x\right) + 2\pi J \cdot \left(\hat{I}_x\hat{S}_x + \hat{I}_y\hat{S}_y + \hat{I}_z\hat{S}_z\right). \tag{55}$$

In the strong coupling limit, the Hamiltonian has a very similar form, with the difference that the ω_1 is replaced by $\Omega = \Omega_I \approx \Omega_S$ and $\hat{I}_x + \hat{S}_x$ by $\hat{I}_z + \hat{S}_z$ (see Eq (52)).

$$\hat{H}_{IS_{strong}} = \Omega\left(\hat{I}_z + \hat{S}_z\right) + 2\pi J \cdot \left(\hat{I}_x\hat{S}_x + \hat{I}_y\hat{S}_y + \hat{I}_z\hat{S}_z\right) \tag{56}$$

In both cases (TOCSY and strong coupling), the two spins aim towards equivalency – which is known as the Hartmann-Hahn condition - and it is the *J*-coupling term that will cause the transfer. In such an arrangement, the two spins evolve "together", which, in this simple system, can be accurately described as the evolution of the sums or differences of the single spin operators (or sums/differences of the products of the spin operators)[38]:

$$\begin{aligned} \Sigma_k &= {}^1\!/_2\,\{I_k + S_k\} \\ \Delta_k &= {}^1\!/_2\,\{I_k - S_k\} \\ \Sigma_{kl} &= {}^1\!/_2\,\{I_k S_l + I_l S_k\} \\ \Delta_{kl} &= {}^1\!/_2\,\{I_k S_l - I_l S_k\} \end{aligned} \tag{57}$$

(where *k*, *l* = *x*, *y*, *z),* with the following commutation relations:

$$\begin{aligned} \left[\hat{H}_{J_{iso}}, \Sigma_k\right] &= 0 \\ \left[\hat{H}_{J_{iso}}, \Sigma_{kl}\right] &= 0 \\ \left[\hat{H}_{J_{iso}}, \Delta_k\right] &= i\Delta_{l,m} \\ \left[\hat{H}_{J_{iso}}, \Delta_{lm}\right] &= -i\Delta_k \end{aligned} \tag{58}$$

where *k*, *l*, *m* is a cyclic permutation of (*x*, *y*, *z*).

It is clear that the sum of operators or their products cannot evolve, however, the difference evolves according to the equation:

$$\boldsymbol{A} \xrightarrow{b\boldsymbol{B}t} \boldsymbol{A}\cos bt - \boldsymbol{C}\sin bt, \tag{59}$$

which is a direct consequence of the Liouville-von Neumann equation and is true exclusively if the following commutation relations hold:

$$\begin{aligned}[\boldsymbol{A},\boldsymbol{B}] &= i\,\boldsymbol{C}\\ [\boldsymbol{B},\boldsymbol{C}] &= i\,\boldsymbol{A}.\end{aligned} \tag{60}$$

For example, the populations: $\hat{I}_z + \hat{S}_z = \begin{pmatrix} 1 & 0 & 0 & 0 \\ 0 & 0 & 0 & 0 \\ 0 & 0 & 0 & 0 \\ 0 & 0 & 0 & -1 \end{pmatrix}$ do not evolve under the strong coupling Hamiltonian, unlike the term: $\hat{I}_z - \hat{S}_z = \begin{pmatrix} 0 & 0 & 0 & 0 \\ 0 & 1 & 0 & 0 \\ 0 & 0 & -1 & 0 \\ 0 & 0 & 0 & 0 \end{pmatrix}$.

Similarly, the difference: $\left(\hat{I}_x - \hat{S}_x\right)$ evolves according to:

$$\left(\hat{I}_x - \hat{S}_x\right) \xrightarrow{\hat{H}_{J_{iso}}\cdot\tau} \left(\hat{I}_x - \hat{S}_x\right)\cdot cos(2\pi J_{IS}\tau) + \left(\hat{I}_y\hat{S}_z - \hat{I}_z\hat{S}_y\right)\cdot sin(2\pi J_{IS}\tau) \tag{61}$$

which, after simple calculations becomes:

$$\begin{aligned}\hat{I}_x \xrightarrow{\hat{H}_{J_{iso}}\cdot\tau} \frac{1}{2}\hat{I}_x\cdot(1 + cos(2\pi J_{IS}\tau)) + \frac{1}{2}\hat{S}_x\cdot(1 - cos(2\pi J_{IS}\tau))\\ + \left(\hat{I}_y\hat{S}_z - \hat{I}_z\hat{S}_y\right)\cdot sin(2\pi J_{IS}\tau)\end{aligned} \tag{62}$$

This equation shows that, in the strong coupling approximation, an in-phase magnetization along the *x* axis evolves not only into antiphase magnetization (the usual situation) but moreover into an in-phase and antiphase magnetization on the coupled partner. In the absence of the strong coupling, such transfer is possible *only if* an *rf* mixing pulse is applied.

In a 1D NMR spectrum, such transfers, which involve the evolution of magnetization from x to y axis (being 90° out-of-phase) cannot be resolved (which, on the contrary, *is possible*

in 2D, where the two dimensions are perpendicular) and will result only in the intensity distortion[21], as shown in Figure 10.

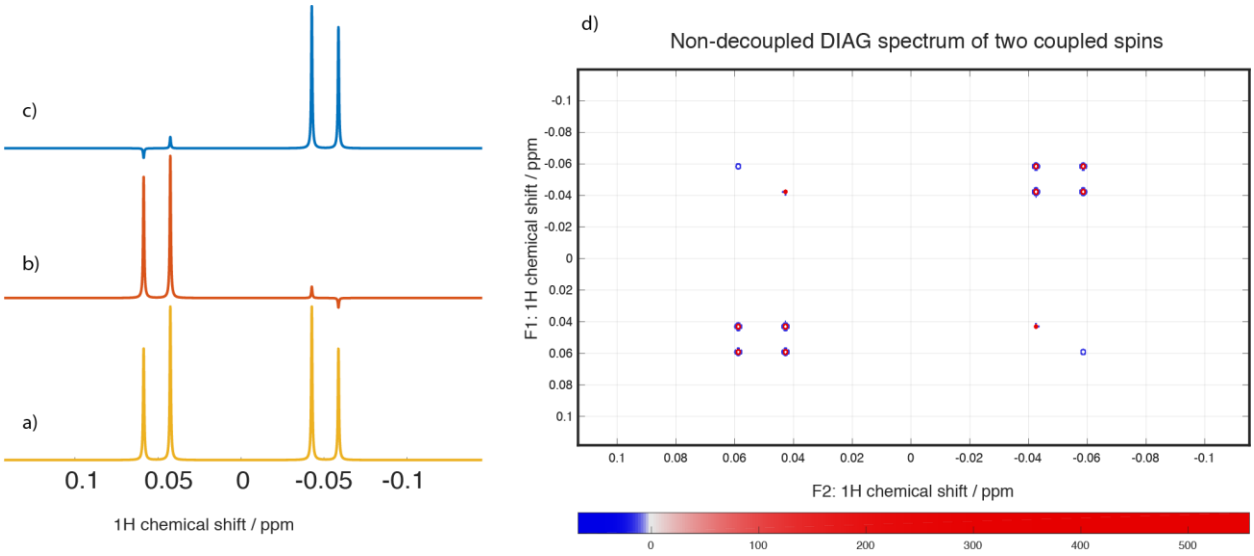

Figure 10. Simulated DIAG spectrum of an AB system: $\delta_1 = 0.05$ ppm, $\delta_2 = -0.05$ and $J_{12} = 8$ Hz. (a) 1D proton spectrum; (b) and (c) 1D proton spectra resulting from excitation of only one of the two spins, by an ideal pulse represented by either $\hat{I}_x$ or $\hat{S}_x$ operator, but not the sum of $\hat{I}_x$ and $\hat{S}_x$; (c) the corresponding non-decoupled DIAG spectrum.

The simulations show the 1D spectrum of two strongly coupled spins with the "roof effect" and the theoretical "decomposition" of this spectrum into spectra of the spins excited independently by an "ideal selective pulse" (excitation effectuated by propagating the density matrix with either $\hat{I}_x$ or $\hat{S}_x$ operator and not $\hat{I}_x + \hat{S}_x$). The spectra illustrate the transfer of magnetization to the strongly coupled partner during the free precession. In a 2D experiment, lacking any mixing pulse or possessing just 90° pulse for the in-phase transfer before detection (as in DIAG), the transfers will give rise to anti-phase signals at the frequency Ω_I and Ω_S in F1, and Ω_S and Ω_I in F2[21], respectively. For example, in a non-decoupled DIAG experiment, the z-filtered magnetization is placed in a transverse plane in the form of $\hat{I}_x$ by the last 90° pulse (one should assume the pulse to be 90_y° in this case) just before the detection. During the acquisition, the mixed states evolve and the antiphase signals, on the anti-diagonal of what would be a standard cross-peak multiplet, will be generated. In other words, this transfer results in forming a special kind of a "reduced multiplet pattern" in the spectrum. This can be thought of as transfers only between connected transitions (See Section III.B.2 and Figure 13) taking place. What is unusual, however, is that the signals resulting from these transfers do not have the same sign (to say the "in-phase" pattern) on the anti-diagonal of a cross-peak multiplet. The exact sign ("plus" or "minus") in the calculations depends on whether the

transfer is considered for a term belonging to the P or the N group (See for example Eq (47) and Eq (48) and Figure 9. In the present case of the strong coupling, the antiphase pattern of the anti-diagonal of a multiplet could be seen as a result of a "mixing" between the P and N paths. The existence of these two distinct paths is dictated by the effect on the detectable magnetization upon the switch of the phase of the (usually) first pulse by 90°. The possibility to intervene in this "mixing" between the P and N datasets (if spins are strongly coupled), when 2D experiments with quadrature are considered, will be explored in a future work. Possible directions to develop this idea may be to separate the processing of the P and N spectra or to use more sophisticated propagation path in order to produce a rotation being a combination of several rotations.

A 2D experiment, where no mixing is present and out-of-diagonal signals are not expected unless spins are strongly coupled, can be seen as a special correlation experiment, connecting exclusively the spins, whose wavefunctions are mixed[21].

In the **F1-decoupled** DIAG, the antiphase signals at the positions that are usual for cross-peaks (in standard correlation experiments), persist, however, since the *J* is refocused in F1, the antiphase multiplet components are spread horizontally. Again, this magnetization is a result of the Hartmann-Hahn condition being fulfilled and manifested during the detection.

All transfers related to strong coupling or coming from weakly-coupled spins which were rendered temporarily equivalent and show more complex behavior during the decoupling in the middle of the t_1 evolution, will result in signals at chemical shifts different than shifts of the individual spins. Very often, the "artifact" will resonate in-between the individual shifts of the spins. However, if the part of the pulse sequence in which the spin echo should take place (but does not) has a duration of tens of milliseconds (very selective 180° refocusing pulses) – the magnetization may acquire an additional phase and amplitude and will result in signals with chemical shift, phase and amplitude different from the ones of the individual spins or their average.

III. Homonuclear decoupling in F1

A. Spin echo

The aim of this chapter is to present the general mechanism underlying the homonuclear decoupling and, subsequently, the specific methods based on this mechanism. One of the main challenges of the project was to understand the fundamental differences between the older methods and the recently introduced PSYCHE method (see Section I) in order to systematically compare their performance and, if possible, to optimize the latter one. Since the analysis of the PSYCHE decoupling as well as the artifacts in the spectra require the use of the polarization operators, the introduction to the quantum mechanical description of NMR was necessary and concepts introduced in the previous chapter will be used to advantage in the present one.

The spin echo element lies at the core of experiments (such as the toolbox ones) allowing to eliminate and/or separate interactions. Generally, the spin echo relies on the inversion of the evolution of interactions in the middle of a given period of time τ and their consequent elimination in the end of this period. However, it should be noted that not in all cases it is possible to eliminate all existing interactions in the same spin echo sequence.

It is very intuitive to understand the spin echo from a demonstration using the Cartesian product operators that conveniently describe the π rotations applied in the middle of a τ period. When a hard π pulse is used, the chemical shift is refocused, but the *J* evolves:

$$\begin{aligned}\hat{I}_z \xrightarrow{90^\circ_x} -\hat{I}_y \xrightarrow{\frac{\tau}{2}(\Omega_I\hat{I}_z+\Omega_S\hat{S}_z+2\pi J\hat{I}_z\hat{S}_z)} & -\hat{I}_y cos(\pi J\tau)cos(\Omega_I\tau) + 2\hat{I}_x\hat{S}_z sin(\pi J\tau)cos(\Omega_I\tau) \\ & + \hat{I}_x cos(\pi J\tau)sin(\Omega_I\tau) + 2\hat{I}_y\hat{S}_z sin(\pi J\tau)sin(\Omega_I\tau) \\ \xrightarrow{\pi(\hat{I}_y+\hat{S}_y)} \xrightarrow{\frac{\tau}{2}(\Omega_I\hat{I}_z+\Omega_S\hat{S}_z+2\pi J\hat{I}_z\hat{S}_z)} & -\hat{I}_y cos(\pi J\tau) + 2\hat{I}_x\hat{S}_z sin(\pi J\tau)\end{aligned} \tag{63}$$

On the other hand, in order to cause a selective *J* coupling refocusing, the hard π pulse must be followed by a selective π pulse applied to one of the spins, here $\hat{I}$, and then only the chemical shift modulates the in-phase terms:

$$\begin{aligned}\hat{I}_z \xrightarrow{90^\circ_x} -\hat{I}_y \xrightarrow{\frac{\tau}{2}(\Omega_I\hat{I}_z+\Omega_S\hat{S}_z+2\pi J\hat{I}_z\hat{S}_z)} & -\hat{I}_y cos(\pi J\tau)cos(\Omega_I\tau) + 2\hat{I}_x\hat{S}_z sin(\pi J\tau)cos(\Omega_I\tau) \\ & + \hat{I}_x cos(\pi J\tau)sin(\Omega_I\tau) + 2\hat{I}_{1y}\hat{I}_{2z} sin(\pi J\tau)sin(\Omega_I\tau)\end{aligned} \tag{64}$$

$$\xrightarrow{\pi(\hat{I}_x+\hat{S}_x)+\pi(\hat{I}_x)} \xrightarrow{\frac{\tau}{2}(\Omega_I\hat{I}_z+\Omega_S\hat{S}_z+2\pi J\hat{I}_z\hat{S}_z)} -\hat{I}_y cos(\Omega_I\tau) + \hat{I}_x sin(\Omega_I\tau)$$

However, for the purpose of in-detail analysis of the spectral artifacts which may be generated during a spin echo and in order to explain the new selective refocusing PSYCHE method, *alternative* to the methods based on π rotations, it is convenient to consider the spin echo in the subset of a single transition operator base, given in Eq (37).

For example, the operator $\hat{I}_+\hat{S}_\beta$ evolves during a period τ acquiring a phase determined by the density matrix transformation upon the propagator involving the free precession Hamiltonian for two weakly coupled spins. If, in the middle of this period, the coherence on the active spin changes sign and the polarization of the passive spin is inverted, the δ chemical shift will be refocused:

$$\begin{aligned}\hat{I}_+\hat{S}_\beta \xrightarrow{\frac{\tau}{2}(\Omega_I\hat{I}_z+\Omega_S\hat{S}_z+2\pi J\hat{I}_z\hat{S}_z)} exp\left[-\frac{1}{2}i(\Omega_I-\pi J)\tau\right]\hat{I}_+\hat{S}_\beta \xrightarrow{\pi(\hat{I}_x+\hat{S}_x)} exp\left[-\frac{1}{2}i(\Omega_I-\pi J)\tau\right]\hat{I}_-\hat{S}_\alpha \\ \xrightarrow{\frac{\tau}{2}(\Omega_I\hat{I}_z+\Omega_S\hat{S}_z+2\pi J\hat{I}_z\hat{S}_z)} exp\left[-\frac{1}{2}i(\Omega_I-\pi J)\tau\right]exp\left[+\frac{1}{2}i(\Omega_I+\pi J)\tau\right]\hat{I}_-\hat{S}_\alpha,\end{aligned} \tag{65}$$

which simplifies to:

$$exp[i\pi J\tau]\hat{I}_-\hat{S}_\alpha. \tag{66}$$

This term in the spectrum will give rise to a single peak at the chemical shift displaced by πJ from the chemical shift $\delta = 0$. In other words, only the frequency related to the *J* coupling can be read in the spectrum.

Similarly, the *J* coupling is refocused if, in the middle of the evolution period τ, the coherence on the active spin remains unchanged but the polarization of the coupling partner (the passive spin) is inverted:

$$\begin{aligned}\hat{I}_-\hat{S}_\beta \xrightarrow{\frac{\tau}{2}(\Omega_I\hat{I}_z+\Omega_S\hat{S}_z+2\pi J\hat{I}_z\hat{S}_z)} exp\left[+\frac{1}{2}i(\Omega_I-\pi J)\tau\right]\hat{I}_-\hat{S}_\beta \xrightarrow{\pi(\hat{I}_x+\hat{S}_x)+\pi(\hat{I}_x)} \\ exp\left[+\frac{1}{2}i(\Omega_I-\pi J)\tau\right]\hat{I}_-\hat{S}_\alpha \\ \xrightarrow{\frac{\tau}{2}(\Omega_I\hat{I}_z+\Omega_S\hat{S}_z+2\pi J\hat{I}_z\hat{S}_z)} exp\left[+\frac{1}{2}i(\Omega_I-\pi J)\tau\right]exp\left[+\frac{1}{2}i(\Omega_I+\pi J)\tau\right]\hat{I}_-\hat{S}_\alpha\end{aligned} \tag{67}$$

which simplifies to:

$$exp[i\Omega_I\tau]\hat{I}_-\hat{S}_\alpha. \tag{68}$$

In the equations above, the spin echo is achieved when a sign preceding the chemical shift frequency or the *J*-coupling frequency under the exponential is inverted. The sign preceding the former depends on the sign of the coherence, whereas the sign preceding the latter term depends on the polarization of the coupled partner. In the same way as the symmetry between the terms with opposite sign in two equal periods of evolution must be retained to induce a spin echo, the symmetry in the positive and negative coherences during $t_1$plays a pivotal role in the possibility to obtain absorption lineshapes in 2D. In an analogical way, in a system of three coupled spins, in order to decouple a spin from its two coupling partners, after they all get treated by a hard 180° pulse, it is only the active spin that should be *selectively* flipped back:

$$\begin{aligned}
&\hat{I}_{-}\hat{S}_{\beta}\hat{K}_{\beta} \xrightarrow{\frac{\tau}{2}\left(\Omega_I\hat{I}_z+\Omega_S\hat{S}_z+\Omega_K\hat{K}_z+2\pi J\cdot\sum\hat{M}_z\hat{N}_z\right)} exp\left[+\frac{1}{2}i(\Omega_I-\pi J_{IS}-\pi J_{IK})\tau\right]\hat{I}_{-}\hat{S}_{\beta}\hat{K}_{\beta} \xrightarrow{\pi(\hat{I}_x+\hat{S}_x+\hat{K}_x)+\pi(\hat{I}_x)} \\
&exp\left[+\frac{1}{2}i(\Omega_I-\pi J_{IS}-\pi J_{IK})\tau\right]\hat{I}_{-}\hat{S}_{\alpha}\hat{K}_{\alpha} \xrightarrow{\frac{\tau}{2}\left(\Omega_I\hat{I}_z+\Omega_S\hat{S}_z+\Omega_K\hat{K}_z+2\pi J\cdot\sum\hat{M}_z\hat{N}_z\right)} \\
&\quad exp\left[+\frac{1}{2}i(\Omega_I-\pi J_{IS}-\pi J_{IK})\tau\right]exp\left[+\frac{1}{2}i(\Omega_I+\pi J_{IS}+\pi J_{IK})\tau\right]\hat{I}_{-}\hat{S}_{\alpha}\hat{K}_{\alpha} = exp[i\Omega_I\tau]\hat{I}_{-}\hat{S}_{\alpha}\hat{K}_{\alpha},
\end{aligned} \tag{69}$$

where *M*, *N* is a cyclic permutation of (*I*, *S*, *K*).

B. Methods for homonuclear decoupling

1. Zangger-Sterk method

In recent years, the most common method to perform the *broadband* homonuclear decoupling was the use of the so called Zangger-Sterk element, introduced for the first time in 1996[17]. It was proposed at that time as an alternative to projecting the sheared *J*-resolved spectra to attain the pure-shift spectrum. This brilliant method combines the use of a hard 180° and a selective refocusing 180° pulse in the presence of a weak field gradient.

As demonstrated in Section III.A, the consequence of applying the overall 2π rotation to the active spin and the selective π rotation to the passive spins, results in unperturbed chemical shift evolution of the active spin and refocusing its *J*-coupling to the passive spins. The principal constraint of this approach for the broadband decoupling is the necessity to repeat the selective experiment for each signal in the spectrum. The Zangger-Sterk method overcomes this limitation in a very neat way: the introduction of a spatial encoding of the frequency shift. This enables the “simultaneous” refocusing of different spins in different positions in the sample by

a single selective refocusing pulse tailored to a single frequency. Selective pulses coupled with gradients are used since decades in MRI (Magnetic Resonance Imaging)[40, 41], where the object to be imaged (often human tissues) is first excited with the *rf* radiation and subsequently emitted with intensity depending on the efficiency of the emission (different in different tissues). In this way, the signal carries the information about the position thanks to the presence of the gradient. It was an ingenious idea of Zangger and Sterk to use the frequency encoding to run a decoupling of individual signals in different positions along the NMR sample tube in a single experiment.

a) Spatial encoding

Spatial encoding relies on applying a magnetic field gradient, usually along the *z* axis, simultaneously with a frequency-selective or frequency-swept pulses. The effective field is thus made regularly inhomogeneous:

$$B_{z\,(eff)} = B_0 + Gz, \tag{70}$$

where G is the magnetic field gradient in units of field per unit length: G cm^{-1} and z is the coordinate along the field direction, measured (in cm). The encoding gradient is usually applied in such way that in the middle (along the gradient direction) of the active volume of the sample the field is unchanged with respect to B_0, whereas the field increases ($B_{z\,(eff)} = B_0 + Gz$) or decreases ($B_{z\,(eff)} = B_0 - Gz$) when going up or down the sample, respectively.

This arrangement makes it possible to manipulate interactions occurring over a range of different magnetic fields in one sample. Then, these interactions are slightly different in each of these fields, since the energy levels are modified - notably, the precession frequency of spins varies between these different fields and consequently each spin acquires a spatially-dependent phase along the sample's length. For example, if one takes a single spin resonating at exactly 500 MHz in one of these fields, the spin may well resonate, if properly adjusted, with any frequency in a range of 500 MHz ± 2.5 kHz, in one of the other fields (different *z* position in the tube), *etc*. A recorded signal of this single spin in this gradient would correspond to one broad signal covering 10 ppm. The spatial variation of the frequency in the presence of a gradient can be employed for several different applications. Some of them will be discussed here, whereas those requiring the chirp pulse applied together with the weak gradient will be presented in Section III.B.2.a).

First of all, the spatially-dependent phase for each given spin in the presence of a field gradient can be used to average out to zero the magnetization with the different phases along the length of the sample. For example, the standard Bruker gradient unit provides the

maximum field gradient of: $G = 58\,{}^{G}/_{cm} = 0.0058\,{}^{T}/_{cm}$. When such a strong gradient – and with sufficient duration - is applied to a sample containing proton spins, the frequency of each individual spin differs so much along the sample that the magnetization is completely dephased, resulting to no signal. Gradients are indeed commonly used to select a desired part of a coherence (the one which does not evolve at all) and dephase the unwanted one (the one that acquires the spatially varying phase). For example:

$$S = \frac{1}{L}\int_0^L exp[+i[(\Omega_I - \pi J) + \Omega_z]\tau]\mathrm{dz} \cdot \hat{I}_-\hat{S}_\beta \to 0, \tag{71}$$

where S is the signal approaching zero intensity if L is properly adjusted to the duration and strength of G.

Secondly, when the gradient strength is much weaker and frequency-selective pulses are applied along, the spatial encoding can be used to the advantage of rendering the frequency (and so the phase) ***equal*** for spins with ***normally different*** chemical environment and thus different chemical shift:

$$\begin{gathered} exp[+i[(\Omega_I - \pi J) + \Omega_{z1}]\tau]\ \hat{I}_-\hat{S}_\beta \\ exp[+i[(\Omega_S - \pi J) + \Omega_{z2}]\tau]\ \hat{I}_\beta\hat{S}_- \\ (\Omega_I - \pi J) + \Omega_{z1} = (\Omega_S - \pi J) + \Omega_{z2} \end{gathered} \tag{72}$$

The possibility to act on a spin system in a way *as if* being able to do it on several different spectrometers (or equivalently *as if* using several selective pulses each with different offset) at the same time, gives a great flexibility and allows to speed-up certain experiments enormously.

Variation of the field that is of interest for the broadband homonuclear decoupling is typically the one which ensures that a single frequency of each spin resonating in assumed spectral range of 0-10 ppm can be spread by the encoding gradient over 10 ppm (typical spectral width in proton spectra), in the sample length of 1.5 cm, so that a spin resonating with no gradient at frequency corresponding to 8 ppm, may now resonate at all frequencies corresponding to the range of 13 ppm and 2 ppm with the encoding gradient applied. In order for the gradient to cover 10 ppm (4981.816 Hz) on a 500 MHz spectrometer, it should have a strength calculated as follows:

$$G = \frac{SW_G}{\gamma \cdot L} = \frac{4981.86\ Hz}{4258\ {}^{Hz}/_{G} \cdot 1.5\ cm} = 0.78\,{}^{G}/_{cm}, \tag{73}$$

which corresponds to 1.3% of the max ($58\,{}^{G}/_{cm}$) provided by our gradient unit.

b) *Multiple-modulated pulse*

The main disadvantage of the use of the Zangger-Sterk element is that the decoupled spectra have a very low sensitivity. The reason is that unlike in the standard experiments, the decoupled signals here come from a narrow "slice" of the sample volume. The thickness of the "slice" is defined by the bandwidth of the selective pulse applied together with the gradient of certain strength. It is this bandwidth that determines what is the range of slightly different spin frequencies (comprised in the volume slice) that are (or almost are) *on-resonance* with the pulse. For example, all frequencies in a range of 0-20 Hz form one slice, if a very selective pulse exerts an effect over this range. This directly implies that the sensitivity problem is especially salient when a high selectivity is required – as the more selective pulse will refocus the magnetization in a narrower slice of the sample volume. This also points to another problem related to the selectivity of the refocusing pulse, as it is impossible to decouple spins that resonate with frequencies differing by less than the bandwidth of the pulse and being within one slice.

A way of overcoming the sensitivity issue is to use a modulated selective pulse, which is a sum of several shapes, each with different offset. For example, a modulated pulse could be a sum of four shapes with offsets: 3 ppm, 5 ppm, 7 ppm and 9 ppm. In such an arrangement, each spin, for instance one with offset 6 ppm without any gradient, would then be selectively refocused when resonating at frequencies corresponding to 3 ppm, 5 ppm, 7 ppm and 9 ppm in four different positions in the sample, respectively The resulting decoupled signals are four times more intense. Since the four offsets differ by the same number of Hz (2 ppm ≈ 1000 Hz), also the four positions differ by the same distance (cm). The number of modulations as high as 40-50 could be used in order to increase the intensity by the same factor. One problem related to increasing the number of positions where a spin is refocused is that the probability of two coupled spins being accidentally refocused in the very same position increases. This situation would prevent them from being properly decoupled. The denser the irradiation sites, the higher the probability of recoupling, since the refocusing takes place in increased number of positions within the finite length of the active volume.

One problem in using multiple-modulated pulses should be addressed. It is important to ensure that all the signals in the spectrum can be affected in the same number of positions in the active volume of the sample. To remedy this issue, the encoding gradient should be increased and several blocks of irradiations should be used, in order to homogenously cover the observed spectral window. Figure 1 shows a situation in which the spins resonating on the borders of the observed *SW* (with frequency higher than 8 ppm and lower than 2 ppm) will be excited only in one position, in contrast to spins from the central region of the *SW*. On the contrary, Figure 12 in the following section, shows two blocks of 50 irradiations applied with a

gradient covering 20 ppm in order to ensure homogenous coverage of the entire observed region *SW* = 10 ppm.

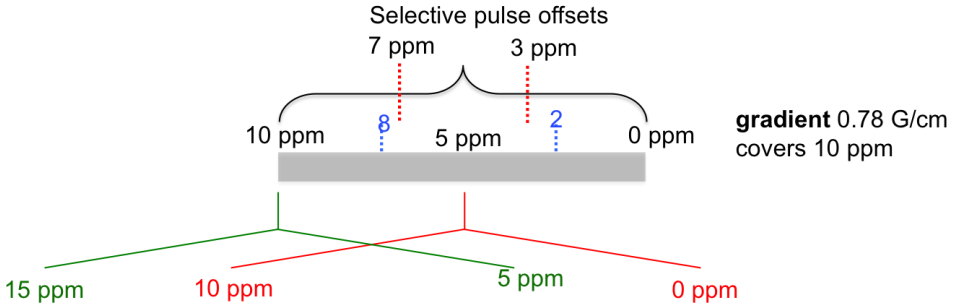

Figure 11. Scheme showing a doubly modulated pulse (exciting at 3 ppm and 7 ppm) applied with the G_s covering 10 ppm. The green and red "shoulders" show the spread of the chemical shift due to the gradient for spins that without any gradient would resonate at 5 ppm and 10 ppm. In the region outside the 2-8 ppm, indicated in blue, spins are non-homogenously refocused.

c) nemoZS

An interesting improvement of the multiple-modulation of the selective pulse was proposed in Cotte *et al*. [10]. A novel way to add the individual pulse shapes into the composite shape was designed to account for the increased number of recoupling artifacts coming as a price for the increased sensitivity due to multiple positions at which magnetization at the same frequency is selectively refocused. The modification relies on a non-equidistant separation of the irradiation sites in a way so that the artifacts resulting from the casual refocusing of coupled spins in the same position are averaged out. In the *nemoZS* element, an effort is put to ensure the homogenous refocusing of all observed signals. The scheme of the multiple modulation should be optimized with respect to the characteristics of a given isotope, as it was demonstrated and published for the case of ^{13}C-^{13}C homonuclear decoupling in ^{13}C-enriched cholesterol[42].

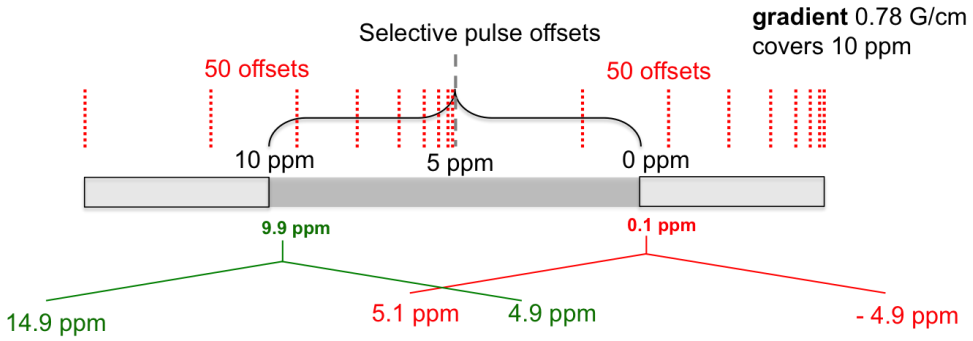

Figure 12. Scheme showing a selective pulse with two blocks of 50 irradiation sites with the G_s covering 20 ppm in order to homogenously refocus all spins resonating in the range 0-10 ppm. The green and red "shoulders" show the spread of the chemical shift due to the gradient for spins that without any gradient would resonate at 0.1 ppm and 9.9 ppm.

2. Small flip angle pulses

The effects of the implementation of a small flip angle (typically 20°) mixing pulses were intensely studied in the mid-80s[32, 34, 43]. Such pulses have an interesting impact on the magnetization, as they restrict the coherence transfers to take place ***primarily*** between connected transitions in the energy level diagram.

For the sake of the demonstration of the mechanism, the graphical representation of the Hamiltonian eigenstates and coherences in an energy level diagram is discussed for a system of three weakly coupled spins. In such system, the important concept of the passive coupling can be introduced. As shown in Figure 13(a), the energy levels of this system form a three-dimensional cube-like diagram.

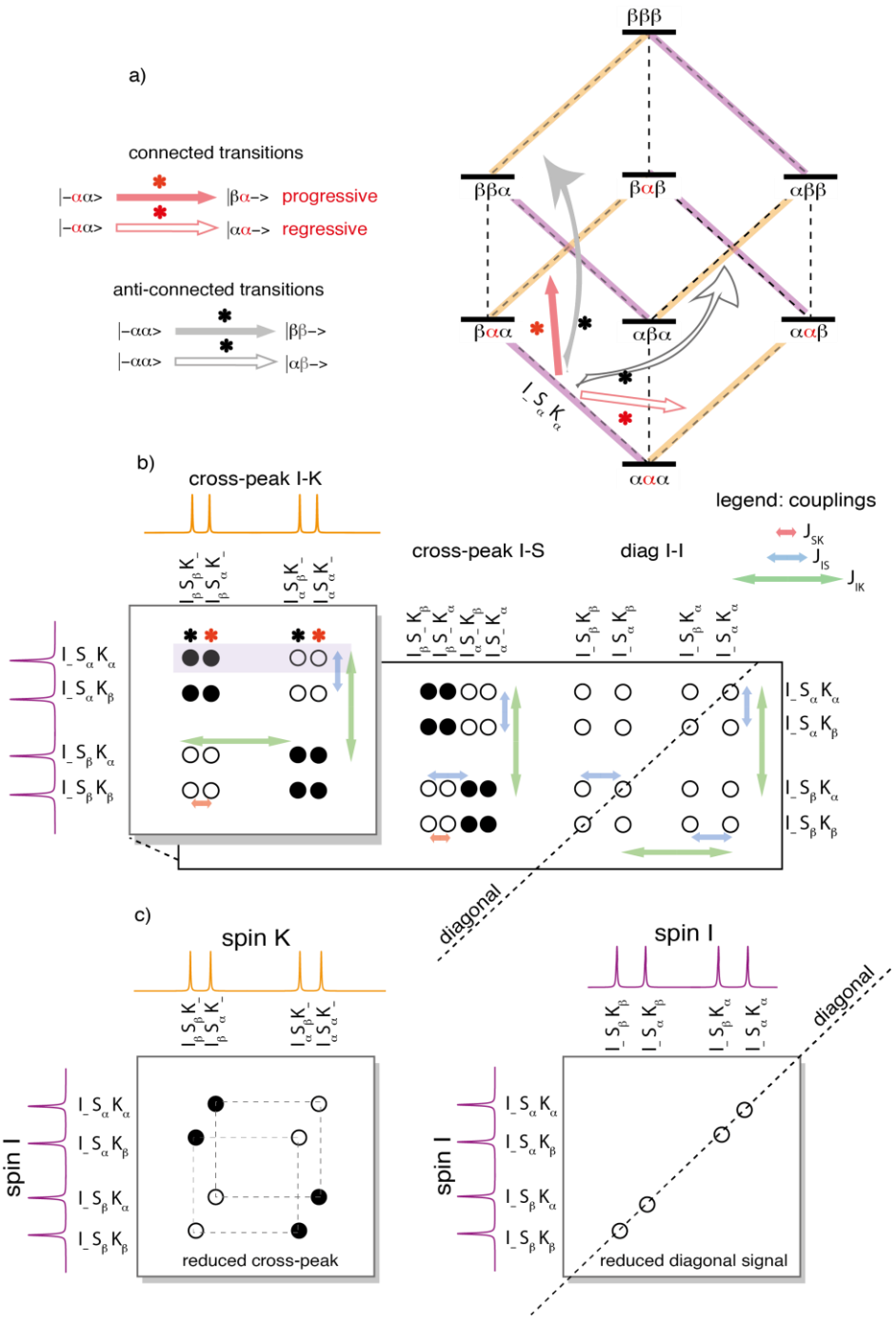

Figure 13. (a) Energy level diagram for three coupled spins I, S and K with connected and anti-connected transitions from coherence on the I spin to different coherences on the K spin. (b) A fragment of a schematic COSY spectrum of the ISK spin system, showing the diagonal and cross-peaks centered at frequency Ω_I in the F1 dimension. The dashed line indicates the part of the diagonal that passes through this section of the spectrum. The phase shift between the diagonal and cross-peak signals has been ignored for the simplicity of the demonstration and thus all signals are represented in absorption. The red, blue and green arrows indicate the splitting due to the J_{SK}, J_{IS} and J_{IK}, respectively. The red and black asterisks pinpoint the connected and anti-connected transitions, respectively. (c) The reduced I-I diagonal and I-K cross-peak signal patterns when transitions between only the connected transitions take place.

In this cubic representation of the energy levels, three sets of parallel lines can be distinguished (purple, orange and uncolored dashed, respectively), each set corresponding to one of the three coupled spins. The three sets are perpendicular to each other. The parallel lines in each of the set correspond to the four lines of a doublet of doublet pattern. It can be noticed that each individual single quantum coherence of a given spin can be transferred to the four lines of its coupling partner upon application of a mixing pulse and be observed as a separate signal in a 2D spectrum. In Figure 13a, for example, the coherence $\hat{I}_{-}\hat{S}_{\alpha}\hat{K}_{\alpha}$ is transferred to the four lines of the spin K and represented by four arrows. Importantly, in two of the four transitions, the polarization of the passive spin S does not change and in the remaining two, the polarization of the passive spin S gets inverted. The two classes of transitions are easily distinguished in the diagram, as the former pair of transitions "belongs" to the same plane as the original coherence and the latter pair "belongs" to a plane, which is "*shifted up"* by the polarization difference on the passive spin. The ones where the polarization of passive spin remains unchanged are called: *connected transitions* and the ones where the polarization of all passive spins change (in this example there is only one passive spin S), are called *anti-connected* transitions. The order of connectivity of the connected transitions in this example is *r* = 0 (as none of the passive spins changes its polarization) and of the anti-connected transitions it is *r* = 1 (as one passive spin changes its polarization). The transition: $\hat{I}_{-}\hat{S}_{\alpha}\hat{K}_{\alpha} \rightarrow \hat{I}_{\beta}\hat{S}_{\alpha}\hat{K}_{-}$ is classified as ***progressive***, as the two levels that embrace the transition: $\alpha\alpha\alpha \rightarrow \beta\alpha\beta$ differ in the magnetic quantum number by: $\Delta\left(M_{\beta\alpha\beta} - M_{\alpha\alpha\alpha}\right) = -2$. The complementary transition: $\hat{I}_{-}\hat{S}_{\alpha}\hat{K}_{\alpha} \rightarrow \hat{I}_{\alpha}\hat{S}_{\alpha}\hat{K}_{-}$ is called ***regressive*** with the $\Delta\left(M_{\alpha\beta\beta} - M_{\beta\beta\alpha}\right) = 0$. The manner in which the single mixing pulse propagator rotates the density matrix in order to provoke *coherence transfer* is determined by the solution of the *Liouville-von Neumann* equation (Eq (7)) and directly given by the Eq (46). It is clear that peaks representing correlations between the progressively and regressively connected transitions have opposite phase (the antiphase arrangement). Since such dependence on the rotation by a single mixing pulse is intrinsic to the spin dynamics, it is impossible to overcome this phase feature. It will be shown in Section IV.B that in order to achieve the in-phase pattern of signals originating from the progressive and regressive transitions it is necessary to use more sophisticated mixing sequence to modify the phase and amplitude properties of the transitions. It was also mentioned in Section II.H that when strong coupling interaction takes place, the regressive (progressive) transitions that normally have the same sign for all spins contributing to a multiplet pattern, may appear in the antiphase arrangement instead (Figure 10).

What is essential for this section is that the small flip angle pulses discriminate in favor of terms in which the spin states of the passive spins are preserved.

If, on the other hand, ***one*** or ***two*** hard small flip angle pulses are combined with a hard 180° pulse, the transfers of coherence occur mainly between the anti-connected transitions. In this case, the spin states (polarizations) of the passive spins are changed while the active spin's coherence remains unaffected. Notably, this effect was discussed above (Section III.A, Eq (67)), where the $180°_{hard}$ + $180°_{sel}$ pulse element was presented. In other words, there is an inherent selectivity in the action of the small flip angle pulse as it discriminates the spins during the coherence transfers according to their polarization.

It was clear already in the mid-80s[43] that such a restriction of transitions induced in the middle of the t_1 results in the time-reversal of the evolution under scalarinteractions[32] and hence the broadband F1-homodecoupling. There is however one fundamental difference between the small flip angle pulse that could be used for selective refocusing of the *J*-couplings and a selective refocusing 180° pulse, in that the former still induces the mixing of the spin states and thus generates the cross-peaks, even though in a reduced form (Figure 13 (c)). Hence, it is important to highlight that, when inserted in the middle of t_1, the small flip angle pulse generates the magnetization that would normally lead to diagonal signals and the one that would lead to the cross-peaks with the anti-phase pattern - if the element was used to separate spectral dimensions, which is not the case in this particular application for homodecoupling.

The presence of the reduced cross-peaks is used to a great advantage in some important two-dimensional correlation experiments[32, 34], however, in the context of the homonuclear decoupling it is a limitation, as the responses are undesirable. That is probably one of the main reasons why the property of the small flip angle pulses was not really exploited as a homodecoupling method for decades.

The recent work of James Keeler[25, 44, 45] remarkably contributed to the revival of these ideas.

a) Keeler's one-shot dephasing of unwanted coherences

This subsection does not relate only to small flip angle pulses, it is more general, however it fits well as an introduction to the PSYCHE element, which owes its functionality not only to the special property of the small flip angle pulses but equally to the spatiotemporal averaging provided by simultaneous use of chirped pulses and weak pulsed-field gradient.

Hence, it is worthwhile to assemble and reconsider the most important solutions brought by Keeler and co-workers[18, 25, 44, 45] to enable the manipulation of coherences in a way not accessible by more standard methods (phase cycling, gradients). The logic they rely on is absolutely crucial to understand the mechanism of the PSYCHE decoupling. The several

methods discussed here were introduced for different applications, however, they are based on the same principle. The one-shot zero-quantum filter had major repercussions for the NMR methodology of small organic molecules. It achieves the differentiation between the ZQ coherences and the *z*-magnetization and elimination of the former in a single pulse sequence element. The separation of the two types of magnetization, both having the coherence order: $p = 0$, was a problematic issue for decades. The Keeler's filter is based on the simultaneous use of a weak gradient and a frequency-swept pulse[46]. This arrangement allows for a *spatiotemporal* encoding of interactions as spins of a given frequency can be affected by an action of a pulse at different times in different positions in the sample. The characteristics of the chirp excitation were discussed in Section II.C.3 and the description of the spatial encoding was given in Section III.B.1.a). The addition of the time parameter to the spatial distribution of the frequency of a given spin offers an increased flexibility for an independent treatment of different coherences. In other words, the magnetization can be selectively excited not only with regard to the *resonance frequency* but also with *respect to time*.

Generally, the ZQ terms do not acquire a spatially dependent phase in the presence of the gradient Eq (74), because the *difference* of two offsets in different positions in the sample along which the gradient is applied has the same value, even though the offsets themselves vary along the sample length.

$$\begin{aligned} exp[i[(+\Omega_I + \Omega_{z1} - \Omega_S - \Omega_{z1})]\tau]\ \hat{I}_-\hat{S}_+ &= exp[i[(+\Omega_I - \Omega_S)]\tau]\ \hat{I}_-\hat{S}_+ \\ exp[i[(+\Omega_I + \Omega_{z2} - \Omega_S - \Omega_{z2})]\tau]\ \hat{I}_-\hat{S}_+ &= exp[i[(+\Omega_I - \Omega_S)]\tau]\ \hat{I}_-\hat{S}_+ \end{aligned} \quad (74)$$

However, in Keeler's sequence element, the ZQ terms are dephased due to the fact that in different positions in the sample, a different fraction of its evolution is refocused by spin-echo. The spin-echo occurring at different moments going from the top to the bottom of the sample is ensured by the chirped 180° pulse (Figure 14 and Eqs (75) - (78)).

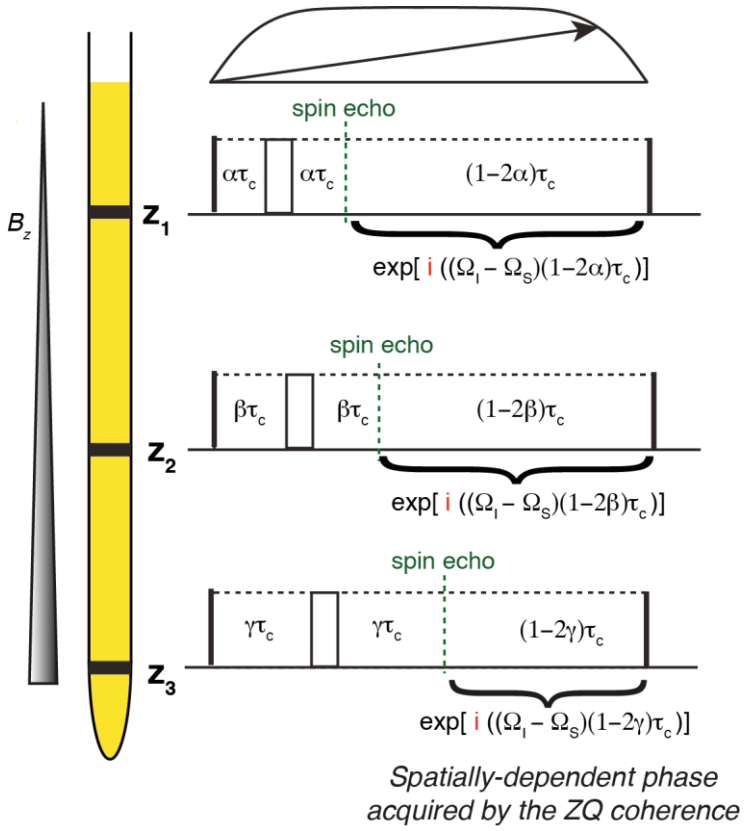

Figure 14. Schematic representation of the action of a 180° chirp pulse in the presence of an encoding gradient.

In the position 1 along the tube the chirp causes a spin echo at the moment τ_{z1}:

$$\begin{aligned} & exp[i[(+\Omega_I + \Omega_{z1} - \Omega_S - \Omega_{z1})](\alpha t_c)]\ \hat{I}_-\hat{S}_+ \\ \xrightarrow{180^\circ_c(\hat{I}_{\phi z1}+\hat{S}_{\phi z1})(\tau_{z1})} & exp[i[(+\Omega_I + \Omega_{z1} - \Omega_S - \Omega_{z1})](\alpha t_c)] \\ & \cdot exp[i[(-\Omega_I - \Omega_{z1} + \Omega_S + \Omega_{z1})](\alpha t_c)]\ \hat{I}_+\hat{S}_- , \end{aligned} \tag{75}$$

which gives:

$$\hat{I}_+\hat{S}_-$$

(no position-dependent phase),

which then evolves during the remaining part of the chirp pulse:

$$\begin{aligned} \hat{I}_+\hat{S}_- \xrightarrow{(1-2\alpha)t_c} & exp[i[(-\Omega_I - \Omega_{z1} + \Omega_S + \Omega_{z1})]((1-2\alpha)t_c)]\ \hat{I}_+\hat{S}_- \\ = & exp[i[(-\Omega_I + \Omega_S)]((1-2\alpha)t_c)]\ \hat{I}_+\hat{S}_- \end{aligned} \tag{76}$$

(position-dependent phase)

And similarly in the position 2, the spin echo occurs at the moment τ_{z2}:

$$\begin{aligned} & exp[i[(+\Omega_I + \Omega_{z2} - \Omega_S - \Omega_{z2})](\beta t_c)]\ \hat{I}_-\hat{S}_+ \\ \xrightarrow{180^\circ_c(\hat{I}_{\phi z2}+\hat{S}_{\phi z2})(\tau_{z2})} & exp[i[(+\Omega_I + \Omega_{z2} - \Omega_S - \Omega_{z2})](\beta t_c)] \\ & \cdot exp[i[(-\Omega_I - \Omega_{z2} + \Omega_S + \Omega_{z2})](\beta t_c)]\ \hat{I}_+\hat{S}_- \end{aligned} \tag{77}$$

which gives: $\hat{I}_+\hat{S}_-$. Then:

$$\begin{aligned} \hat{I}_+\hat{S}_- \xrightarrow{(1-2\beta)t_c} & exp[i[(-\Omega_I - \Omega_{z2} + \Omega_S + \Omega_{z2})](1-2\beta)t_c]\ \hat{I}_+\hat{S}_- \\ = & exp[i[(-\Omega_I + \Omega_S)](1-2\beta)t_c]\ \hat{I}_+\hat{S}_- \end{aligned} \tag{78}$$

It can be noted that even though the spins I and S are not affected by the chirp pulse at the same instant of time, what matters in the present application is the possibility to invert both spins in an interval of time much shorter than the overall evolution (before and after 180°_c) of the ZQ.

One other important point to note here is that the ZQ coherence to be dephased during the filter is generated by the 90° hard pulse at the beginning of the filter from the antiphase magnetization present at that time in the transverse plane. So the amount and phase of the ZQ coherence is well-defined at the beginning of this filter. Moreover, it is easy to calculate the fraction of the ZQ coherence that can be dephased within the filter, conditional to the filter parameters. Firstly, it is only the cos part of the entire ZQ coherence: $exp[i[(-\Omega_I + \Omega_S)]((1-2\alpha)t_c)]\ \hat{I}_-\hat{S}_+$ that will contribute to the observable signal:

$$ZQ_{obs}(\alpha) = \cos\left(\Omega_{ZQ}(1-2\alpha)t_c\right) \tag{79}$$

where $\alpha = z/L$, if the sample is enclosed between $z = 0$ and $z = L$ and the chirp pulse sweeps over the frequencies of all spins between $z = 0$ and $z = L$ in time t_c. The attenuation factor, *A*, is then obtained by integrating $ZQ_{obs}(\alpha)$ over the whole sample[18]:

$$A = \frac{1}{L}\int_0^L \cos\left[\Omega_{ZQ}\left(1-2\frac{z}{L}\right)t_c\right]dz = \frac{\sin\Omega_{ZQ}t_c}{\Omega_{ZQ}t_c}. \tag{80}$$

A very similar trick, also based on a "moving spin echo" along the sample length was used for the suppression of strong coupling artifacts in *J*-resolved spectra[25]. This application is

quite impressive, as the strong coupling artifacts are intrinsic to the spin system and arise from the way the basis states superpose in this system. However, as already mentioned, the density matrix describing a particular state of the system and the matrices representing the propagators can be seen as entities expressing a certain geometry, e.g. $\hat{I}_x$, $\hat{I}_z$, $\hat{I}_y \cdot \cos(\theta)$, *etc*. Broadly speaking, the strong coupling can be seen as differing from the weak one in terms of geometry. The deliberate choice of the combination of propagators with respect to a given form of a density matrix may lead to minimization of certain elements of the former which may correspond to minimization of signals coming from the strong coupling interaction. In the case where spins are strongly coupled, a 180° pulse can cause a coherence transfer (mixing) between coupled spins, which is normally not allowed. In Keeler's version of the *J*-spectroscopy (Figure 15), the magnetization resulting from this transfer acquires a spatially dependent phase in a variable delay αt_c ensured by the chirp pulse. This magnetization cannot be refocused by spin echo (unlike the desired one that is indeed refocused) because the frequency of its evolution is different on both sides of the central 180° pulse: Ω_I and Ω_S, respectively (or Ω_S and Ω_I, respectively).

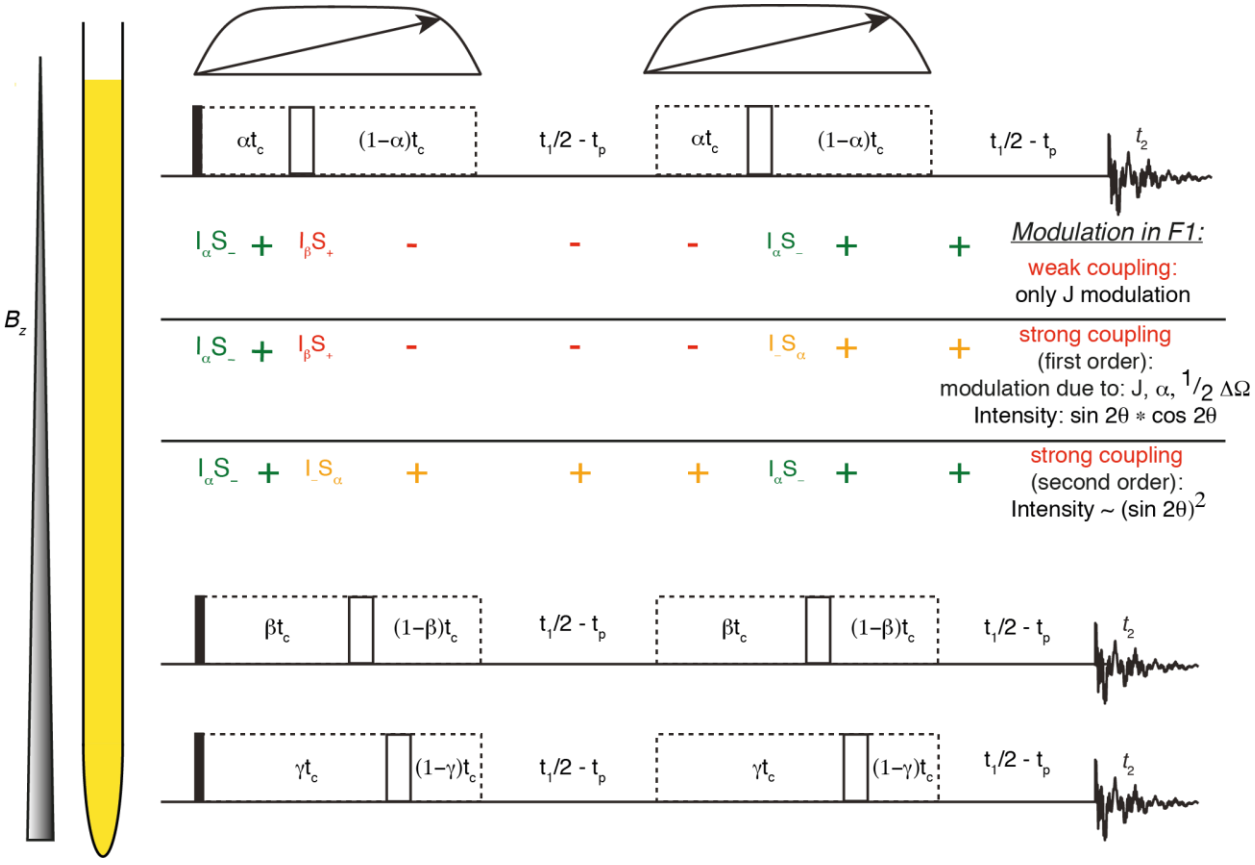

Figure 15. Schematic representation of the action of the two 180° chirp pulses in the presence of a weak gradient allowing the spatiotemporal averaging of the strong coupling artifacts during the J-spectroscopy sequence.

An equivalent reasoning underlies the design of the sequence proposed by Keeler[45] to retain only the diagonal responses in his *anti-z*-COSY experiment (designed specifically for broadband homonuclear decoupling) and remove all the correlation signals. Again, any magnetization that is transferred to the coupling partner by a mixing pulse cannot undergo a spin echo, as the evolution on both sides of the pulse occurs with different frequencies. Thus, the evolution of the diagonal magnetization during δ is refocused by spin echo arranged by two rotations of pulses of small flip angle and the cross-peaks are dephased during this variable delay, as shown in In such an arrangement, the combined effect of the two small flip angle pulses becomes equivalent to the effect of a rotation provided by a 180° pulse. The novelty in this experiment, with respect to those described previously[18, 25], relies on the fact that it is the excitation and not the spin echo that is time-dependent in the consecutive experiments in the series where δ is varied (Figure 16a).

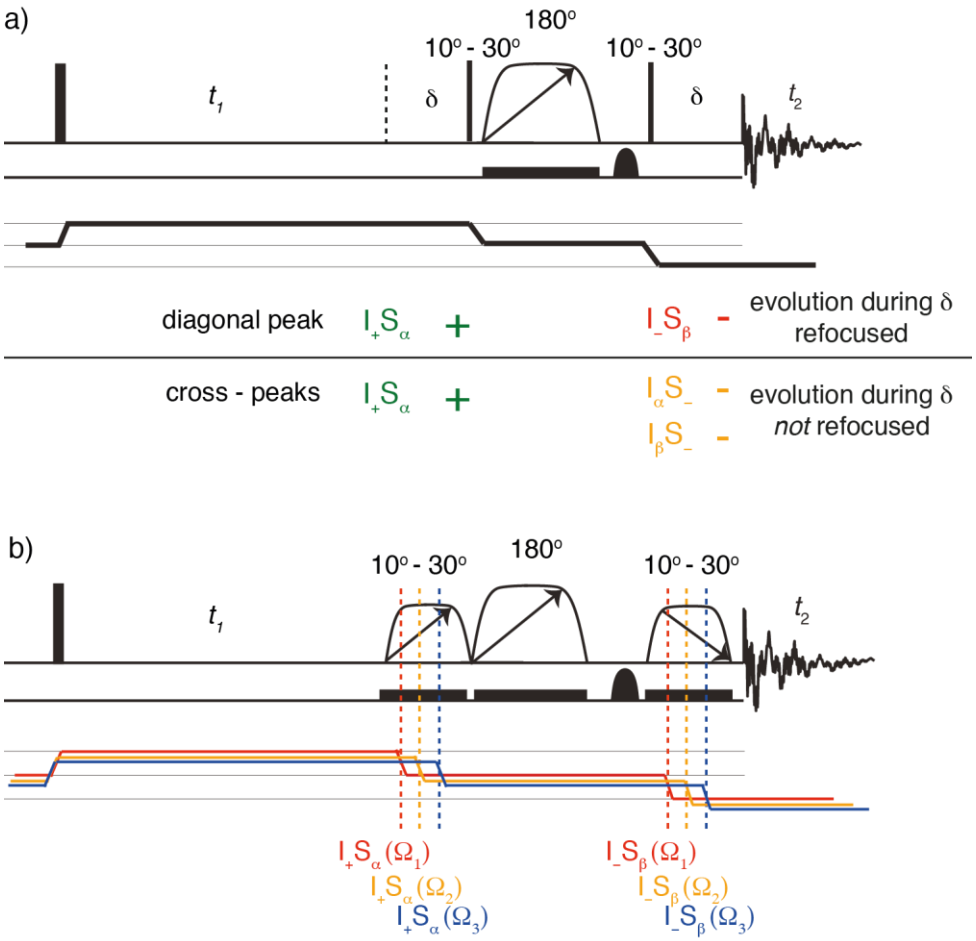

Figure 16. (a) The N-type spectrum of the anti-z-COSY incorporating the multi-scan cross-peak suppression scheme proposed by Pell and Keeler where the δ is varied at each scan. (b) Conceptual one-shot version of the sequence in (a), never reported.

b) PSYCHE

(1) Mechanism

The PSYCHE element, introduced recently by Mohammadali Foroozandeh[9], combines the ideas introduced above (Section III.B.2.a)) in a truly genuine way. Most importantly, it takes advantage of the method of Pell and Keeler to ***imitate*** the deprivation of the small flip angle "mixing pulses" from its "mixing ability". Of course, in reality, the mixing still occurs but the "mixed magnetization" tends to be eliminated. PSYCHE adds time-dependent excitation to the "selectivity" provided by the small flip angle rotation and successfully exploits the small flip angle property for homodecoupling when inserted in the middle of t_1, being a much older idea in itself[43]. The PSYCHE element quickly gained a significant popularity. The main reasons for the enthusiastic reception of the method in the community are: the significantly improved sensitivity of the decoupled spectra (with respect to most of other broadband homonuclear decoupling approaches) and the relative ease of the implementation. However, the theoretical bases of the mechanism underlying the PSYCHE decoupling were not thoroughly discussed yet in the literature. Indeed, as mentioned by the author of the technique himself: "Paradoxically, PSYCHE is one of the trickiest of pure shift NMR techniques to understand, but one of the easiest to use[47]." It is worth mentioning, that PSYCHE may not only be used as a homodecoupling element, but can be implemented in any experiment requiring separate treatment of the *subsets* of spins of the same nuclei, as already demonstrated[30] *e.g.* for the phase-sensitive *J*-resolved spectroscopy.

The element consists in two chirped pulses (either phase- or amplitude-modulated) calibrated in a way as to exert a rotation of magnetization by a small angle (typically 10° - 30°) applied simultaneously with the encoding gradient of 1 - 3%. In this way, the interactions are spatiotemporally encoded.

A common set of parameters used for the PSYCHE homodecoupling in the proton spectra is:

- Gradient: $G = \frac{SW_G}{\gamma \cdot L} = \frac{12\ ppm}{4258\ {}^{Hz}/_{G} \cdot 1.5\ cm} = 0.94\ {}^{G}/_{cm} \approx 1.6\%$ of the max.
- Chirp duration: $t_c = 15\ ms$ (thus the duration of the entire element is $30\ ms$)
- Total Sweep-Width: $\Delta F = 10000\ Hz$. Assuming the total 2 x 20% smoothing, the amplitude of the chirp is constant over $\Delta F = 6000\ Hz$.
- The rate of the chirp: $R = \frac{\Delta F}{t_c} = \frac{10000\ Hz}{15\ ms} = \frac{20\ ppm}{15\ ms} = \frac{12\ ppm}{9\ ms}$.

For example, if the chemical shift difference between two coupled spins is: $\Delta\delta = 1\ ppm$, the two spins will be affected by the chirp with the delay of $\Delta(\tau_{I\_z} - \tau_{S\_z}) = 0.75\ ms$

and the distance between positions in the tube where the respective spins are resonant with the irradiation is: $\Delta(I\_z - S\_z) = 0.125\ cm$.

Similarly to the discussed Keeler's method[45] for dephasing cross-peaks in his *z*-cosy experiment, also the PSYCHE benefits from the time-dependent excitation (time-dependent generation of coherences).

The discrimination between the "diagonal" and the "mixed" magnetization (both observable with the coherence order $p = 1$) generated within the PSYCHE element, is based on the fact that the phase label acquired by the "diagonal" during the duration of the chirps plus the gradient period is independent on the moment in which it is generated by the chirp, on the contrary to the "cross-peak" magnetization. Due to the fact that a weak gradient is applied together with the chirped pulses, the chirp affects a spin with a given offset at different times in different positions in the sample and thus the term that would contribute to the same cross-peak but originates from different positions in the sample is labeled by a spatially-dependent phase and consequently can be dephased to, ideally, avoid contributing to the spectrum.

It is very convenient to analyze the PSYCHE element by modeling a two-spin system (weak coupling is assumed) under the influence of the chirp and in the presence of the encoding gradient, as it illustrates the relevant features of the method.

One may consider what happens in a sample containing two coupled spins I and S with offsets Ω_I and Ω_S, respectively; (for a demonstration, only the term $\hat{I}_{1-}\hat{I}_{2\alpha}$ is traced here). The calculations are done according to the simplified pulse sequence in Figure 17b, which is equivalent to the actual one in Figure 17a, requiring an additional 180° pulse and a few more delays for technical reasons.

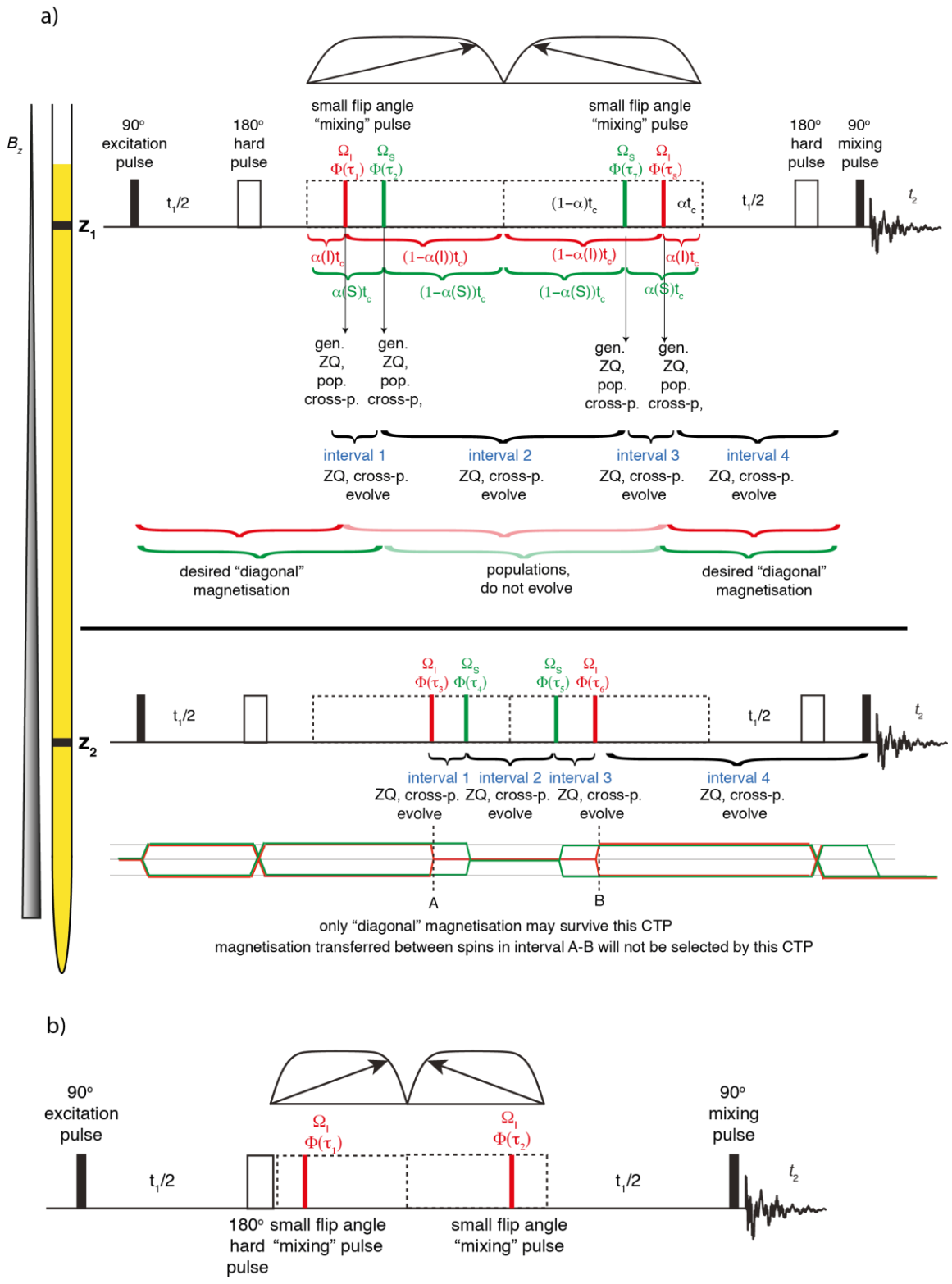

Figure 17. (a) Pulse sequence of the F1-decoupled DIAG experiment and (b) the simplified, but theoretically equivalent version of it.

First, all the spins are instantaneously excited from the equilibrium to the transverse plane, where they acquire a phase label during the first half of the t_1 evolution and then are rotated by a hard 180° pulse. Then, each spin evolves during an additional $\alpha_{zn}t_c$ delay, where α_{zn} is the fraction of the duration of the chirp pulse before a given spin is affected by the pulse according to its chemical shift in position z_n.

$$\hat{I}_{-}\hat{S}_{\alpha} \xrightarrow{evol.\ \left(\frac{t_1}{2}\right)} exp\left[+\frac{1}{2}i(\Omega_I + \pi J)t_1\right] \hat{I}_{-}\hat{S}_{\alpha} \xrightarrow{180^{\circ}(\hat{I}_x+\hat{S}_x)} \xrightarrow{evol.\ \alpha_{zn}t_c} exp\left[+\frac{1}{2}i(\Omega_I + \pi J)t_1\right] \cdot exp\left[-i(\Omega_I - \pi J)\alpha_{I\_zn}t_c\right] \hat{I}_{+}\hat{S}_{\beta} \tag{81}$$

Subsequently, the term $\hat{I}_{+}\hat{S}_{\beta}$ with its phase label is then transferred to all possible terms according to Eq (46). In this demonstration it is assumed that the small flip angle chirp is resonant with a spin I in the position z_1 at the moment τ_{z1} (after the time $\alpha_{I\_z1}t_c$ of free evolution from the beginning of the chirp) and that the magnetization is rotated along the *x* axis in the rotating frame of reference. However, as explained in detail in Section II.C.3, in the case of a phase-modulated chirp, the instantaneous phase of a chirp at a given time is expressed by the integral of its instantaneous frequency at this moment.

A comment is needed regarding the possible situations when the spatiotemporal excitation is considered. Coupled spins *I* and *S* cannot have the same frequency in one single position (*e.g.* z_1), so it will not happen that they are both affected in this very position. There will be certain positions in which some spins I and S have the same resonance frequency (the same offset) and they will be affected at the same moment (*e.g.* $\alpha_{I\_z2,S\_z3}t_c$) by the sweeping chirp, for example, positions z_2 and z_3 (see Figure 18). In most of the other positions, the spins I and S have different offset frequencies and will be affected one after the other, for example: spin I at the time τ_1 at the position z_1 and spin S at the time τ_4 at position z_4, and: $\alpha_{I\_z3}t_c \neq \alpha_{S\_z4}t_c$ (see Figure 18). Importantly, the population terms (and ZQ, DQ) that are of interest in the PSYCHE, can be generated from the SQ terms when the two spins are affected by the pulse but also when either I or S spin is "touched" alone, e.g. transfers of the type: $\hat{I}_{+}\hat{S}_{\beta} \rightarrow \hat{I}_{+}\hat{S}_{+}$ (DQ) or $\hat{I}_{+}\hat{S}_{-}$ (ZQ) or $\hat{I}_{\alpha}\hat{S}_{\beta}$ (populations).

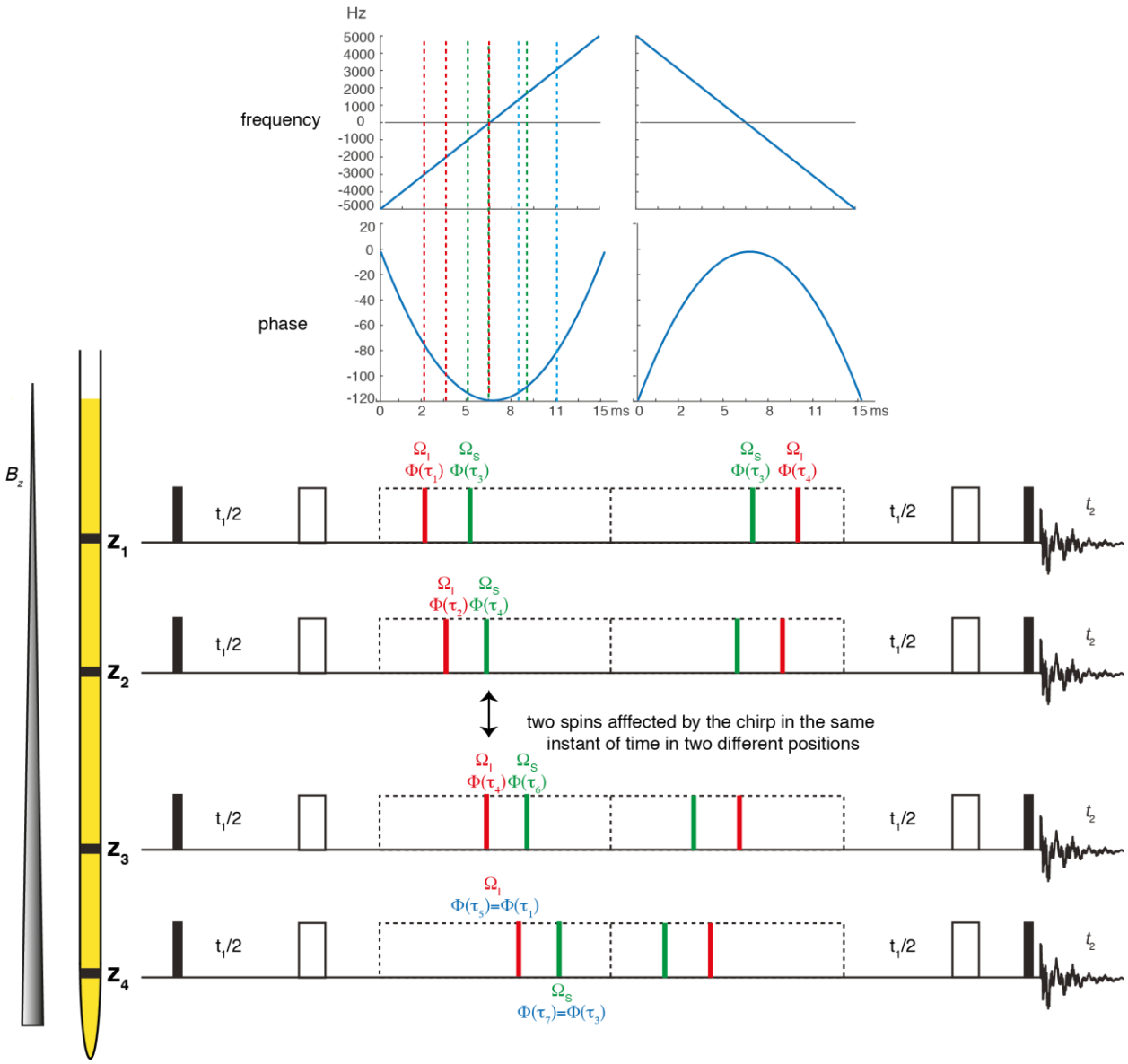

Figure 18. A schematic model of the PSYCHE element showing situations that can occur in different positions in the sample, for example the simultaneous excitation of two coupled spins I and S in two different positions (here z_1 and z_2) or the phase of the pulse being equal at the top and the bottom (blue dashed line) of the sample, due to the symmetry of the parabola representing the phase of the chirp.

Coming back to the outcome of the equation Eq (81) as said above, the term $\hat{I}_{+}\hat{S}_{\beta}$ with its phase label is transferred, upon the rotation by the first chirp, to all possible terms according to Eq (46). It is worth to note that, using only the single rotation by the small flip angle pulse, we would already be in a position to produce a spectrum with decoupled signals (among other coherences), as mainly the term $\hat{I}_{-}\hat{S}_{\beta}$ would be generated, but not the $\hat{I}_{-}\hat{S}_{\alpha}$ (thanks to the "selectivity" characteristic for the small flip angle rotation). The decoupling using a one chirped small flip angle pulse was tested and indeed led to decoupling. No phase distortions were observed,

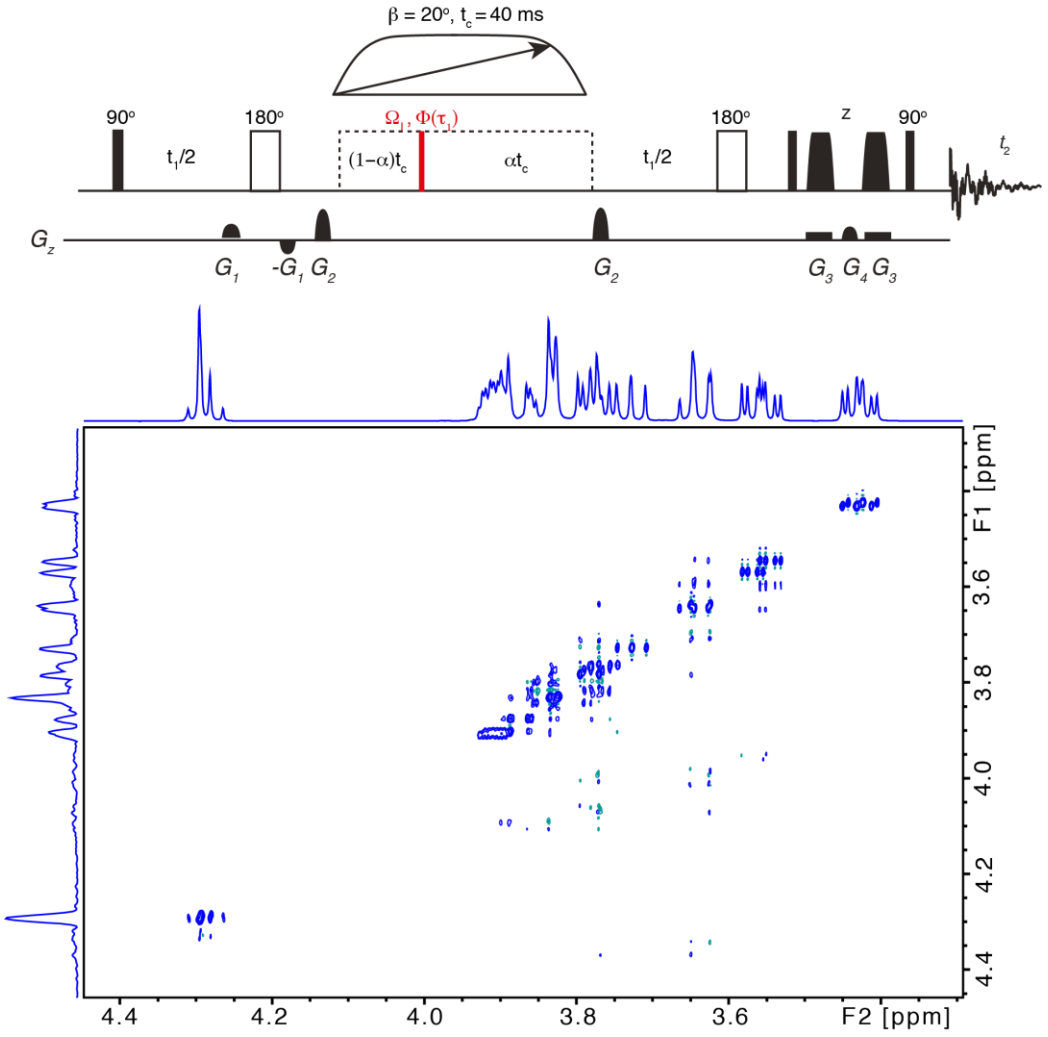

Figure 19. DIAG spectrum of melezitose decoupled with a single 20°, 40 ms chirped pulse.

It should be considered whether and - if yes - why, going through populations is advantageous in PSYCHE. As a reminder from Section II.G, in experiments employing small flip angle pulses, it is beneficial to go through populations (two-step *versus* one-step process) as they are subsequently transferred to SQC with a symmetry regarding the P/N terms which is not the case when the SQC are used directly. This is of importance when the two small flip angle pulses play the role of the mixing, unlike in the present application.

In the PSYCHE method, the terms of interest after the first small flip angle rotation are the populations, for example: $\hat{I}_\beta \hat{S}_\beta$, that come out with certain amplitude, given by the Eq (46). Thus, continuing the analysis from Eq (81) we proceed to Eq (82):

$$\begin{aligned} exp\left[+\frac{1}{2}i(\Omega_I + \pi J)t_1\right] \cdot exp\left[-i(\Omega_I - \pi J)\alpha_{I_{z1}} t_c\right] \hat{I}_+ \hat{S}_\beta \xrightarrow{20^\circ_c \hat{I}_{\phi_c(t)}(\tau_{z1})} \\ -\frac{1}{2}i\theta \cdot exp\left[+\frac{1}{2}i(\Omega_I + \pi J)t_1\right] \cdot exp\left[-i(\Omega_I - \pi J)\alpha_{I_{z1}} t_c\right] \hat{I}_\beta \hat{S}_\beta . \end{aligned} \tag{82}$$

This term will *not* evolve between the two small flip angle pulses $\left(2 * \left(1 - \alpha_{I\_z1} t_c\right)\right)$ – unless we approach the strong coupling situation - but it will be rotated by the second small flip angle pulse. After the second rotation, the terms of interest are those representing the magnetization of coherence order $p = 1$ (SQ coherences). Among them, there is the part of the magnetization where the coherence stays on the first spin Eq (83) and Eq (84) and the one where it is transferred to the second spin (Eq (85) and Eq (86)). Then, both terms evolve during the remaining $\alpha_{I\_z1} t_c$ delay of the second chirp. The diagonal term:

$$\begin{aligned} -\frac{1}{2}i\theta \cdot exp\left[+\frac{1}{2}i(\Omega_I + \pi J)t_1\right] \cdot exp\left[-i(\Omega_I - \pi J)\alpha_{I_{z1}} t_c\right] \hat{I}_\beta \hat{S}_\beta \xrightarrow{20^\circ_c \hat{I}_{\phi_c(t)}(\tau_{z1})} \\ -\frac{1}{2}i\theta \cdot \frac{1}{2}i\theta \cdot exp\left[+\frac{1}{2}i(\Omega_I + \pi J)t_1\right] \cdot exp\left[-i(\Omega_I - \pi J)\alpha_{I_{z1}} t_c\right] \\ \cdot exp\left[+i(\Omega_I - \pi J)\alpha_{I_{z1}} t_c\right] \hat{I}\_ \hat{S}_\beta \end{aligned} \tag{83}$$

simplifies to:

$$exp\left[+\frac{1}{2}i(\Omega_I + \pi J)t_1\right] \hat{I}\_ \hat{S}_\beta \tag{84}$$

and the "cross-peak" term:

$$-\frac{1}{2}i\theta \cdot exp\left[+\frac{1}{2}i(\Omega_I + \pi J)t_1\right] \cdot exp\left[-i(\Omega_I - \pi J)\alpha_{I_{z1}} t_c\right] \hat{I}_\beta \hat{S}_\beta \xrightarrow{20^\circ_c \hat{I}_{\phi_c(t)}(\tau_{z1})} \tag{85}$$

$$-\frac{1}{2}i\theta\cdot\frac{1}{2}i\theta\cdot exp\left[+\frac{1}{2}i(\Omega_I+\pi J)t_1\right]\cdot exp\left[-i(\Omega_I-\pi J)\alpha_{I\_z1}t_c\right]$$
$$\cdot exp\left[+i(\Omega_S-\pi J)\alpha_{I\_z1}t_c\right]\hat{I}_\beta\hat{S}_-$$

simplifies to:

$$exp\left[+\frac{1}{2}i(\Omega_I+\pi J)t_1\right]\cdot exp\left[-i(\Omega_I-\Omega_S)\alpha_{I_{z1}}t_c\right]\hat{I}_\beta\hat{S}_-. \quad (86)$$

The cross-peak terms, on the contrary to the diagonal ones, are modulated according to $\alpha_{I\_z1}t_c$ and therefore may be dephased.

Note that the rotating pulse is called: $20^\circ_c\,\hat{I}_{\phi_c(t)}(\tau_{z1})$ to account for the instantaneous phase of the pulse at a given time τ_{z1}, but the calculations were done for an *x* pulse: $20^\circ_c\,\hat{I}_{x(t)}(\tau_{z1})$ as a demonstration.

The term representing the "diagonal" signal is labeled only by the phase corresponding to the evolution during t_1 and the modulation does not involve the *J* coupling:

$$exp[+i\Omega_I t_1]\,\hat{I}_\beta\hat{S}_-. \quad (87)$$

Note that in order to ensure the decoupling, the sign of the coherence on both sides of the PSYCHE element must be opposite and it is ensured by the symmetric strong gradients surrounding the decoupling element.

The simulated distortions in phase and amplitude of the signals in the presence of strong coupling when decoupling is done with small flip angle hard pulses are shown in Figure 20.

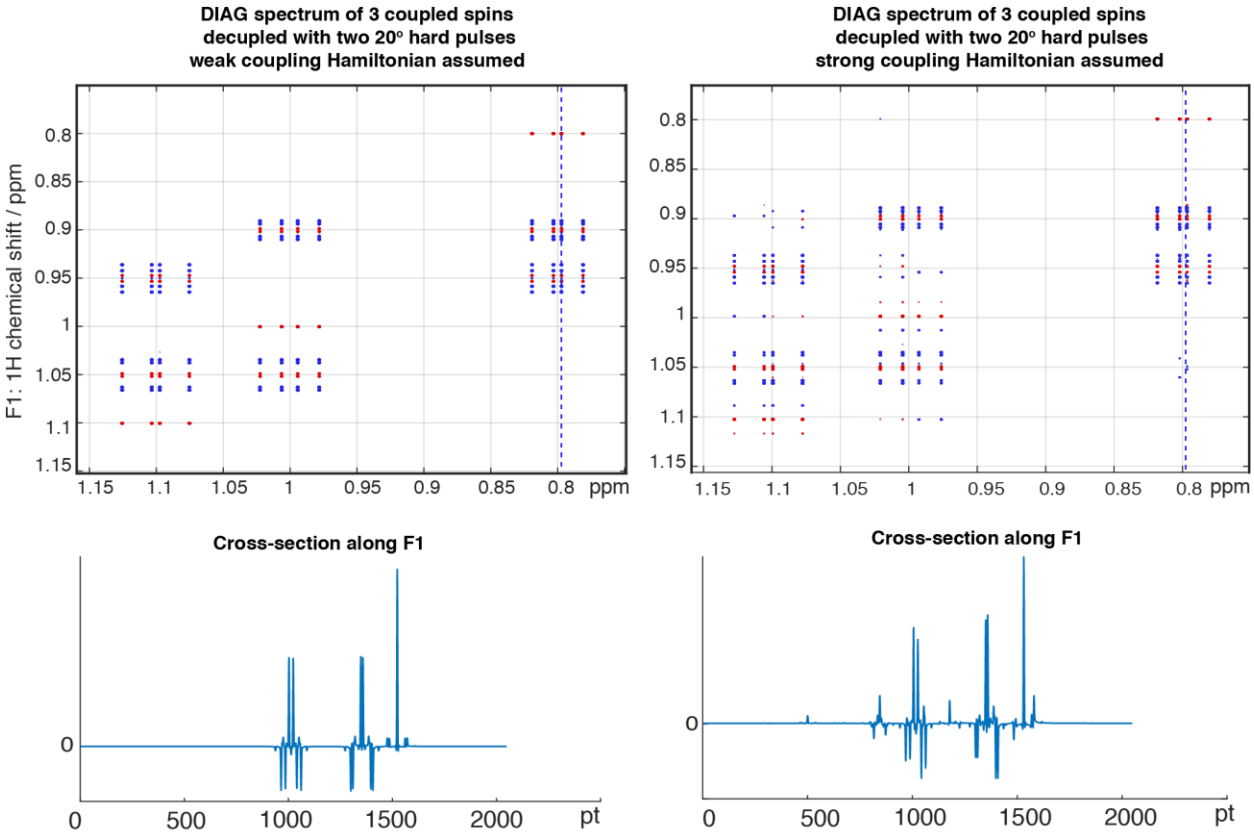

Figure 20. Simulated DIAG spectra of three coupled spins $\delta_1 = 0.8$ ppm, $\delta_2 = 1.0$ ppm, $\delta_3 = 1.1$ ppm decoupled with two 20° hard pulses applied along the x axis. The simulation was run assuming weak coupling Hamiltonian (left) and strong coupling Hamiltonian (right). The cross-sections were taken along F1, as marked by the dark blue dashed line in the 2D spectra.

Regarding the efficiency of the dephasing of the unwanted terms, it should be considered that if the gradient covers around 10 ppm and the chirp sweeps over the 10 ppm (usually it sweeps over more than that, so the sweep over the 10 ppm is well controlled), then the magnetization can be imagined to be excited in infinitely narrow "slices". In this case, the frequency difference (and so the phase difference) between such "slices" is so small, that it would not be sufficient for dephasing. A criterium stating what is the phase variation in a given length that would ensure sufficient dephasing should be evaluated. It will depend on the gradient and the rate of the chirp.

It is interesting to highlight at this point the difference between the ZQ-filter of Keeler[18] and the ZQ dephasing in the PSYCHE element. Keeler's filter is designed to dephase the ZQ coherences generated by a hard pulse of either a small (10° - 30°) or 90° flip angle (or a mixing, like in the TOCSY experiment). The filter itself consists in a weak gradient and a chirped pulse calibrated to 180° as to induce the spin-echo in the evolution of the ZQ at different times in

different *z* positions (Section III.B.2.a)). In such a way, the ZQ coherences acquire a spatially-dependent phase and are averaged out. In the PSYCHE element, the terms seem to be dephased in a similar way as the cross-peaks: as a consequence of the time delay between the moments at which the ZQ terms are generated in different *z* positions along the tube.

(2) Sensitivity and spectral quality

The PSYCHE got the fame of a method that is "much more sensitive than most other broadband homonuclear decoupling approaches"[48]. Indeed, from our experience, the sensitivity of the spectra decoupled with PSYCHE competes fairly with those decoupled with densely modulated selective pulse (comparison data published for ^{13}C-^{13}C decoupling[42] and unpublished for the ^{1}H-^{1}H decoupling). The *nemo*ZS was reported to provide sensitivity of 15-45 times[10] higher than when a non-modulated selective pulse of the same duration is used (original ZS experiment).

Regarding the spectral quality, it has been observed that PSYCHE produces strong signals approximately at the mean of chemical shifts of coupled spins in F1, as discussed in more detail in Section V. The intensity of these disturbing responses does not seem to be proportional to the strength of the coupling. The trends in the appearance of these signals were studied using Spinach simulations. Some work with the simulations is still required in order to present systematic comparisons and draw unambiguous conclusions. One difficulty in this study was to reliably estimate the accuracy of the spatial discretization when simulating spatially encoded experiments.

The appearance of these signals is closely related to the fact that the PSYCHE element is not strictly an optimized refocusing element such as the selective shaped 180° pulses like Rsnob, Reburp, etc. The performance of the PSYCHE depends on the efficiency of the dephasing of the undesired coherences that it produced *itself*. Thus, the quality of the spectra may be quite sensitive to the proper adjustment of the mutually related parameters: chirps rate, the strength of the encoding gradient and the spin system. Moreover, a small amount of magnetization represented by terms in which the polarization of the coupling partner changes is also inherently produced by the small flip angle pulses. The amount of this magnetization – which obviously affects the quality of the decoupled spectrum, scales with the flip angle.

3. The BIRD element

The BIRD (BIlinear Rotation Decoupling) element is one of the oldest sequences invented to produce homonuclear decoupling[3]. However, since then, it was never really used

for this purpose. It has been brought back to the modern pure shift methodology quite recently by Morris and co-workers[6] and it is also ubiquitously used in the real-time decoupling, where the BIRD blocks are inserted in-between the chunks of the detected signal[49].

It was Alex Pines and his co-worker who had the ingenious idea to exploit the sparse ^{13}C nuclei as an auxiliary local field having the ability to induce a rotation of a proton spin without any interference with the state of its coupled partner. In fact, the BIRD element consists in two 180° pulses applied simultaneously to ^{13}C and ^{1}H, "sandwiched" between a pair of 90° pulses acting on ^{1}H only. The net effect of this sequence is to invert only those protons that are directly *J*-bonded to the ^{13}C isotope. Since the inversion is applied to the magnetization in the transverse plane and combined with an additional 180° hard pulse, the chemical shift of the satellites is correctly preserved, while the *J*-coupling splitting is eliminated. Interestingly, it has been also reported in the original publication[3] that a series of such bilinear rotations with appropriate phase shifts of the *rf* irradiation can be used in order to decouple strongly coupled spins. As discussed in Section II.H, the rotation occurring when strongly coupled spins freely precess, must be described by operators acting along *three* orthogonal directions. Thus, in order to decouple strongly coupled spins, it would be necessary to combine several rotations to account for the three-dimensionality of the coupling interactions in a way to average them to zero[3].

The efficiency of the decoupling and - at the same time - the sensitivity penalty to be paid for the selective treatment of a subset of spins, lies in the sparsity of the ^{13}C, dictated by the 1% natural abundance of this isotope. Molecules differening by isotopic substitutionare called isotopomers.

4. Comparison and complementarity

Neither PSYCHE nor *nemoZS* can assure impeccable decoupling of signals arising from strongly coupled spins. In *nemoZS*, the problem is related not only to the modification of the energy levels and more complex magnetization trajectory during the spin echo, but also to the intrinsic limitation of the selective pulse which cannot be illimitably long. When two spins are affected together by the selective pulse, the decoupling cannot be successful. (Notably, in case of broader multiplets, if only part of transitions belonging to a given multiplet is affected by the selective pulse, a partial decoupling occurs; this issue is interesting from the point of view of the spin physics and the quality of decoupling and will be studied with the help of Spinach in the future work).

In the PSYCHE method, since even hard small flip angle pulses (when the spins are touched together) lead to decoupling, the problem seems to be mainly related to the "mixing"

of the basis states of strongly coupled spins, which impairs the small flip angle pulses to discriminate between the passive spins according to their polarization.

The use of the BIRD filter for decoupling offers the possibility to restrict the observation only to protons attached to the ^{13}C isotope. This means that the spin dynamics during the BIRD-based homodecoupling of a given proton spectrum concerns different spin systems than those present when using methods ignoring the ^{13}C isotope. Furthermore, regarding 2D experiments, the refocusing of the *J* coupling interaction in the F1 indirect dimension takes place in a different spin system network than the one present during the detection, if the standard broadband decoupling of ^{13}C isotope is used during the detection. The symmetry of the spin system network between t_1 and t_2 is restored when the decoupler during acquisition is switched off. Depending on the situation, it may or may not be advantageous to preserve the ^{13}C in the detected dimension.

The interest of introducing a distinct isotope to a given spin system lies in the flexibility of causing *different splitting patterns* which may be complementary in cases where spins are strongly coupled. If one of two signals with very similar chemical shift is split by a coupling large enough as to separate the transitions, the strong coupling condition is not fulfilled anymore, (Figure 21).

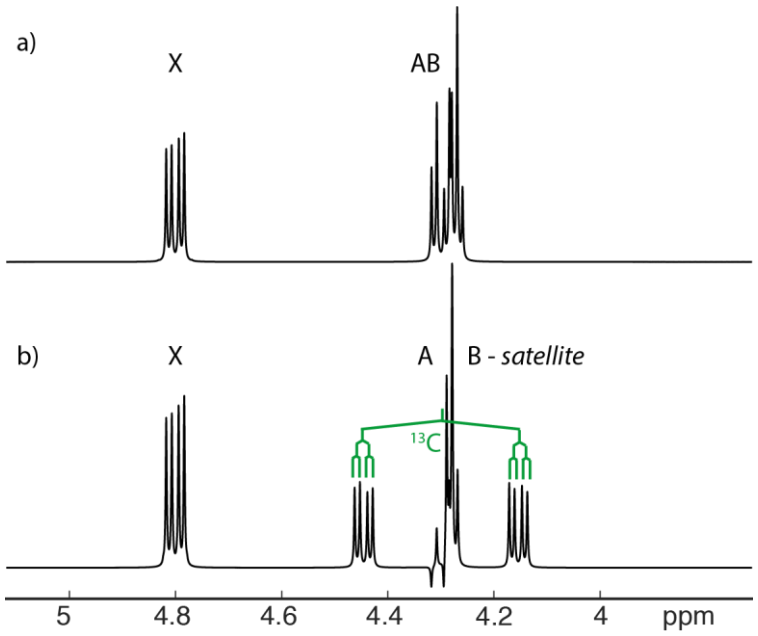

Figure 21. Simulated 1D ^1H NMR spectra of an ABX system: δ_A = 4.3 ppm, δ_B = 4.27 ppm, δ_X = 4.8 ppm, J_{AB} = 5 Hz, J_{AX} = 12 Hz, J_{BX} = 4.9 Hz. a) The spins A and B are very strongly coupled, their corresponding signals severely overlap and the intensities of the individual transitions are distorted. b) ^{13}C spin was added as a fourth spin into the spin system and it is $^1J_{C,H}$ - bonded to the B spin; B is the ^{13}C satellite here. The J_{AB} is revealed when the B multiplet is additionally splitted by the large heteronuclear coupling. The signal A remains distorted due to similar chemical shifts of A and B. The antiphase magnetization transferred between A and B is visible because transitions of B were moved away.

IV. Toolbox of F1-homodecoupled 2D experiments

A. The DIAG experiment

The DIAG[10], issued as an improved version of the δ-resolved[19] experiment, has been designed to address the need to rapidly asses the chemical shift and multiplicity of signals by separating them in an aliased top-resolution 2D spectrum. The experiment takes an enormous advantage of the F1-decoupling and the spectral aliasing, which can be applied by any user, by simply adjusting the acquisition parameters. The simplicity of the experiment is its big asset – it can be easily implemented and the desired information is directly available without any need of "unusual" spectral processing. The DIAG pulse sequence can be thought of as NOESY/TOCSY sequence, out of which the mixing period has been removed, however, the two one-shot Keeler's filters are preserved in order to ensure the most efficient filtration of the in-phase decoupled magnetization from unwanted contributions. The DIAG, in principle generating signals only along the diagonal, turns out to be an excellent *model* experiment to study the effectiveness of the *J*-refocusing in a much more informative way than 1D (like the *se*-SPFGE[15], *selective* - single pulse field gradient echo), since all the non-refocused magnetization will show up as out-of-diagonal artifacts.

1. Aliasing

Spectral aliasing occurs when the detected signal is not sampled with a sufficient rate. It is particularly easy to cause the aliasing of a NMR spectrum on a spectrometer. The only thing which needs to be done is the reduction of the spectral window (in the F1 indirect dimension) in the acquisition parameters. For example, the typical SW = 10 ppm in a proton spectrum can be changed to 0.1 ppm, or if ^{13}C dimension is considered, SW may be reduced from 200 ppm to 10 ppm.

The lowpass sampling theorem (or Nyquist condition) states that we must sample at a rate at least twice that of the highest frequency that we want to detect. For example, if a proton spectrum of the spectral width of 10 ppm (corresponding to 5000 Hz in the 500 MHz spectrometer) is to be acquired, the sampling rate f_s should be at least 10000 Hz. This determines the short time intervals at which oscillating signal should be sampled (called the Dwell time): $\Delta t = DW = \frac{1}{10000} Hz.$ The number of samples (points) - TD - multiplied by the dwell time gives the so-called acquisition time AQ (not experimental time), which determines

for how long the magnetization is acquired. For example, if 512 points (corresponding to increments in F1) are acquired to obtain COSY spectrum with SW = 10 ppm, the acquisition time (AQ) is 51.2 ms (Eq (88)), whereas if the SW is reduced to 0.1 ppm, the acquisition time increases 100 times (Eq (89)).

$$AQ_{(SW=10\ ppm)} = TD \cdot DW = 512 \cdot \left(\frac{1}{2 \cdot 5000}\right) = 51.2\ ms \tag{88}$$

$$AQ_{(SW=0.1\ ppm)} = TD \cdot DW = 512 \cdot \left(\frac{1}{2 \cdot 50}\right) = 5120\ ms \tag{89}$$

In terms of resolution, if the TD is fixed, it is advantageous to detect the magnetization for longer time; the experimental time remains almost exactly the same, but two spins precessing with similar frequency, for example differing by 20 Hz, during a short detection do not have enough time to distinguish themselves – that results in non-resolved signals. The longer the acquisition time, the higher the resolution. In fact, the spectral resolution increases by the factor equal to the reduction of the spectral width.

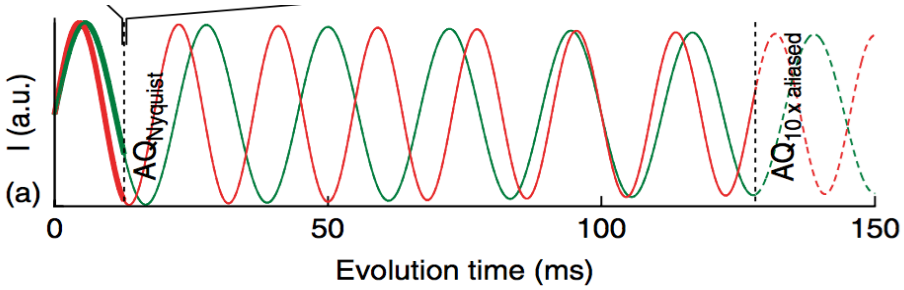

Figure 22. Graph showing the dependence of the duration of the acquisition time and the possibility to distinguish between two spins precessing with similar frequencies. In this example, two carbons resonating at 45 (green) and 55 Hz (red) in a 20 kHz window (200 ppm at 100 MHz) are considered. The dashed lines indicate the acquisition time of 12.8 ms and 128 ms, respectively and in both cases 512 points are acquired.

The immediate consequence of using such atypically short spectral width when acquiring a NMR spectrum, besides the very high resolution, is the so-called “spectral aliasing”, which causes ambiguities in frequencies. It can be understood even in a very intuitive way that with so few points taken when detecting the signal in such a relatively long acquisition time, it is impossible to represent correctly the frequencies in the NMR signal. The actual frequency of precession could be very high, but with poor sampling, it would look like a very low frequency, which is shown in Figure 23.

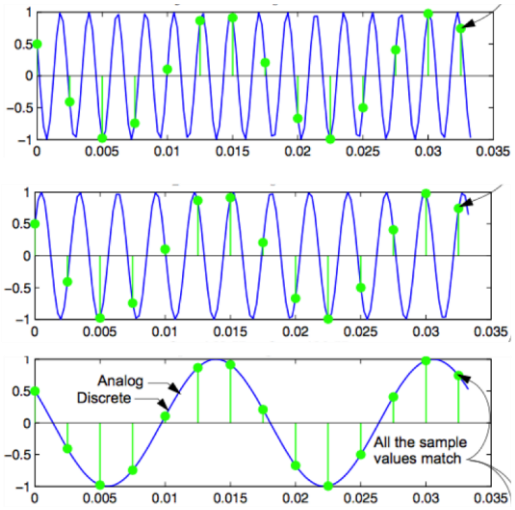

Figure 23. The undersampling is illustrated by the green points. All the three different frequencies illustrated in these three subplots alias to the low frequency shown in green.

When aliasing for example a DIAG spectrum, the diagonal of the original spectrum appears in the aliased one as if it was cut in pieces, but with high-resolution signals attached to it, Figure 24. In this special experiment - the fact that the chemical shifts in F1 are not in their usual positions, but all fall in the range of SW_{alias} = 0.1 ppm - is not problematic, since obviously the chemical shifts of diagonal signals are the same in F1 and F2 and can be read easily from the direct dimension.

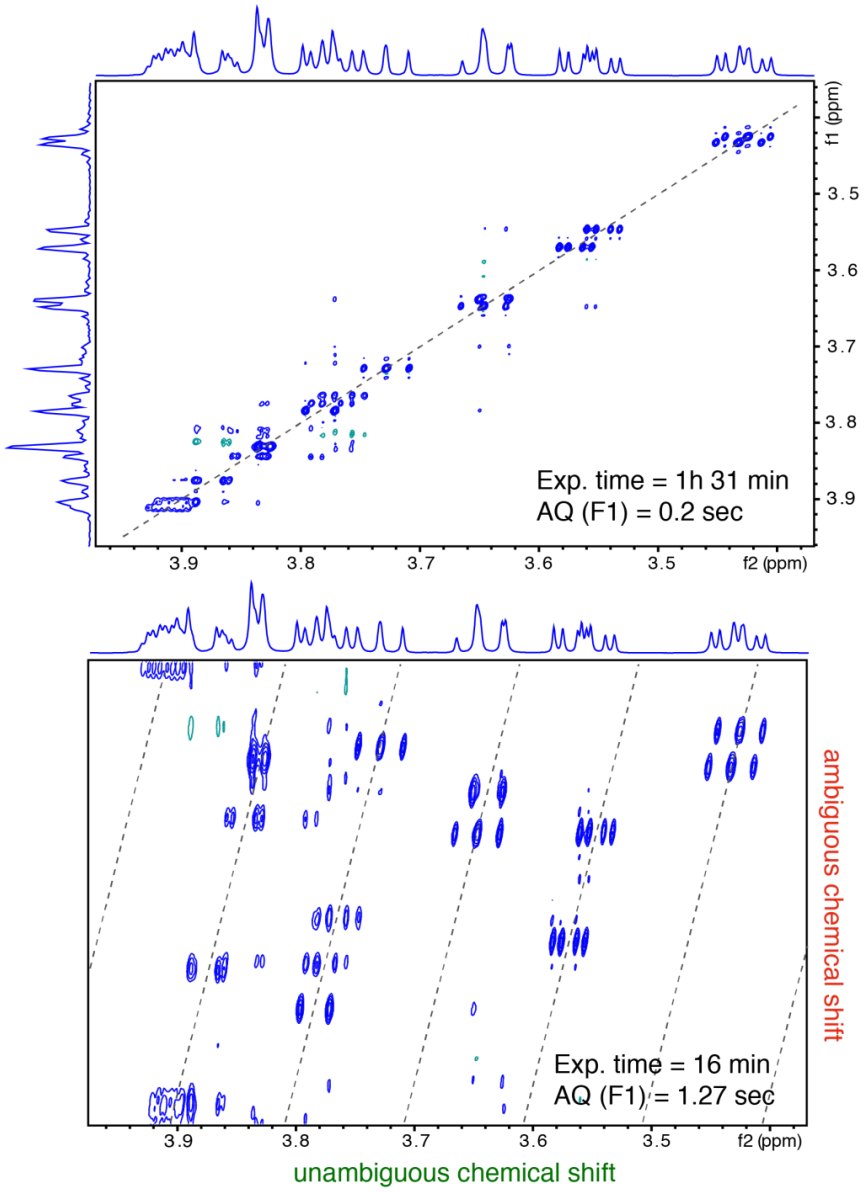

Figure 24. The non-aliased (top) and aliased (bottom) DIAG spectra of melezitose.

In the aliased spectrum, the signals appear at frequencies given by the modulo function:

$$v_a = mod\left(v_0 + \frac{SW_a}{2} - CF, SW_a\right) - \frac{SW_a}{2} + CF \tag{90}$$

where v_0 is the true frequency, SW_a the width of the spectrum and CF the position of the carrier frequency.

2. Comparison of the DIAG and *J*-resolved spectroscopy

a) Separation of interactions

The acquisition parameters, when aliasing the DIAG, become well comparable with those used in the *J*-resolved spectroscopy. In the latter, the spectral width in F1 is typically 50 Hz, since the F1 is the *J*-only dimension. Such a frequency range is covered by several co-occurring scalar couplings. Thus, the ratio SW_1/TD(F1) in the *J* experiment determines the resolution of a multiplet - separation of the individual transitions. It is in opposition to the DIAG, where the F1 is the δ-only dimension and thus the maximal t_1 in this dimension sets the limit in the possibility to detect two spins as individual signals. The DIAG experiment has proven to provide signals separated by as little as 2-3 Hz. On the other hand, the resolution in the F2 direct dimension, which normally is limited only by relaxation (but not the precious experimental time), defines the chemical shift separation between different spins in *J*-res and multiplet resolution in DIAG.

From our experience, the multiplets extracted from both experiments are of very similar quality. A more in-depth analysis of the signals lineshapes could probably reveal some subtle differences as a consequence of these two experiments being radically different yet used for the same purpose - measurement of *J*-coupling constants after separation from the chemical shift evolution.

b) Lineshapes and strong coupling

The *J*-resolved experiment is fundamentally *not* a pure shift experiment. Lacking any mixing, it generates, what could be called – reduced diagonal multiplets with active transitions on the anti-diagonal of what would be a standard 2D multiplet.

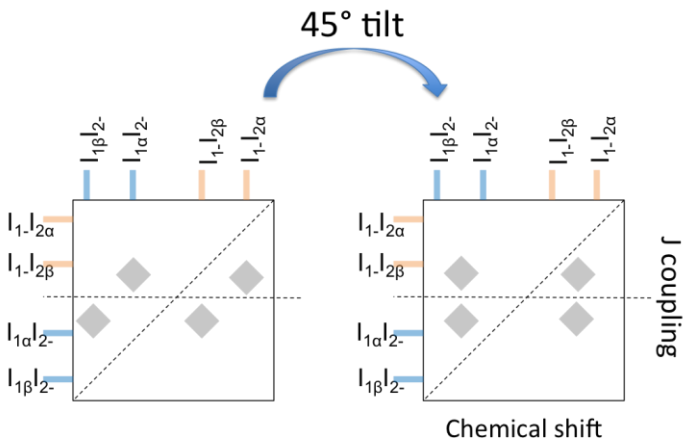

Figure 25. Original form of a J-res spectrum (left) and a spectrum sheared by 45° out of which a pure-shift spectrum is easily obtained by projection along the F1 dimension.

However, when shared by 45°, the projection along the indirect dimension results in a singlet for each chemical shift. Moreover, since no mixing is present in the sequence, the *J*-res is a phase modulated experiment, which means that after the FT, the signals have the phase-twist lineshape. The 45° projection of the phase-twist lineshape in the frequency space is zero, thus, before the shearing, an absolute mode processing is necessary, which prevents this experiment to be applicable to solve problems requiring a top-resolution.

The main reason to compare the DIAG experiment to the *J*-res and cognate experiments[26, 30, 50, 51] is the long-standing interest in this family of methods resulting in quite a rich choice of publications from the last decades, reporting on many different aspects of the technique. Many improvements to the original sequence have been proposed. On the contrary, the δ-resolved family of experiments is a much younger competitor in the NMR methodology and thus the research performed in the field of the *J*-res was quite inspiring in the present study.

There are some methodological issues that allow drawing a parallel between these two families and learning in a reciprocal way. For example, the selectively inverting/refocusing element is as essential for broadband homonuclear decoupling as it is to invert the direction of evolution of the magnetization and have an access to *J* and anti-*J* spectra[44] to combine them and produce the absorption lineshapes. These two areas (quadrature and spin-echo) interfuse and consequently, methods invented for one of them, may be useful for the other.

Besides the absorption lineshapes[44], one other very important advancement in increasing the quality of the *J*-spectra was Keeler's method to eliminate the strong coupling artifacts by spatiotemporal averaging[25].

c) DIAG vs. TSE-PSYCHE 2D J spectroscopy

The most recent version of the *J*-resolved spectroscopy is the so-called TSE-PSYCHE (for triple-spin echo PSYCHE) 2D *J*-spectroscopy, where the central refocusing 180° hard pulse is replaced by a 180° chirped pulse with gradient and, in order to ensure the absorption lineshapes, inversion of the evolution of the magnetization is provided by PSYCHE. For the evolution during the chirp to be compensated, a symmetrical 180° chirped pulse is added in the sequence. The experiment is said to provide "virtually artefact-free 2D *J* spectra with excellent sensitivity, absorption mode lineshapes and no need for any special or non-linear post-processing."[51] The experiment still requires however the shearing by 45°. The high quality of the spectra is attributed to the replacement of all pulses by chirp pulses with weak gradients, making the sequence to be entirely deprived from hard pulses.

The DIAG experiment equally provides multiplets with absorption lineshapes and sensitivity comparable to TSE-PSYCHE 2D *J*. However - if decoupled with the PSYCHE decoupling element - very intense artifacts are present between (strongly) coupled spins (see Section V), even though two Keeler's *z*-filters are kept in the end of the sequence to enhance the filtration of magnetization after applying the PSYCHE-based homodecoupling.

First, after learning that 180° hard pulses may lead to manifestation of the mixing effects when spins are strongly coupled, we were tempted to apply Keeler's trick to the DIAG sequence. Tests with the modified sequence, where all 180° hard pulses are substituted by chirps have been performed and indeed, it seemed that the appearance of these signals is somewhat less random and they are less pronounced. However, in some spectra resulting from experiments using the *nemoZS* decoupling and traditionally the 180° hard pulses, those artifacts were less intense. This was the first indication for us that the responses may be related to the decoupling method itself and that additional filtration is needed to improve the performance of PSYCHE with respect to the nemoZS. It was striking however that such an intense artifacts were never reported in the first articles on PSYCHE[9, 30], available in 2016, when the research of the author of this thesis started.

The second indication that the PSYCHE performance in DIAG and *J*-res may be related to the presence of the mixing pulse(s) came during the very first simulation of the DIAG experiment using the Spinach simulation package, where the original code "psyche_1d" offered by Mohammadali Foroozandeh, was used as a starting point. It became clear that, in order to reproduce properly the coherence selection and the quadrature in the F1-decouled DIAG experiment, it is necessary to retain symmetrical coherence transfer pathways during the t_1 evolution. That prompted us to hypothesize that some magnetization transfers related to the use of the PSYCHE element can be made observable only if a mixing is present. In fact, the

original pseudo-2D PSYCHE sequence as well as the TSE-PSYCHE 2D *J* spectroscopy are based on sequences requiring only one of the paths (+1 or -1) to be retained.

The only truly 2D experiment acquired and published by 2016, exploiting the PSYCHE decoupling, was F1-decoupled TOCSY[4], however, the problem of artifacts was not discussed. Moreover, knowing that transfers of magnetization not symmetrical with respect to spin-echo may occur in the presence of strong coupling, it made me to wonder wheatear the P and N datasets, which could be separated from the Bruker-acquired full dataset, are symmetrical in this case and if there is a potential to examine/process this datasets separately or, alternatively, to introduce a non-standard scheme for phase incrementation for the quadrature. These issues will be explored in the future work. .

To summarize, the DIAG experiment, though excellent to acquire highly resolved multiplets in a minimum experimental time, does not provide any information about the connectivity between spins (unless they are strongly coupled). Thus, a mixing allowing the restration of the COSY-type correlations is highly desired.

B. The CLIP-COSY experiment

1. The pulse sequence

As it was already noted, often, it is not a single pulse which marks the borderline between the t_1 and t_2, but it is rather a combination of several pulses and delays that constitute the "mixing period". Such mixing can be seen as an adjustment of the trajectory of the magnetization in order to prepare it in a desired way for the start of the t_2 evolution.

The CLIP-COSY experiment[16] (Figure 26) employs the *perfect echo*[22] sequence as the mixing period. The sequence consists in five pulses with carefully chosen phases and can be considered as two sequential spin-echoes that refocus the offsets but not the *J*-couplings. The mixing is flanked by two one-shot Keeler's *z*-filters.

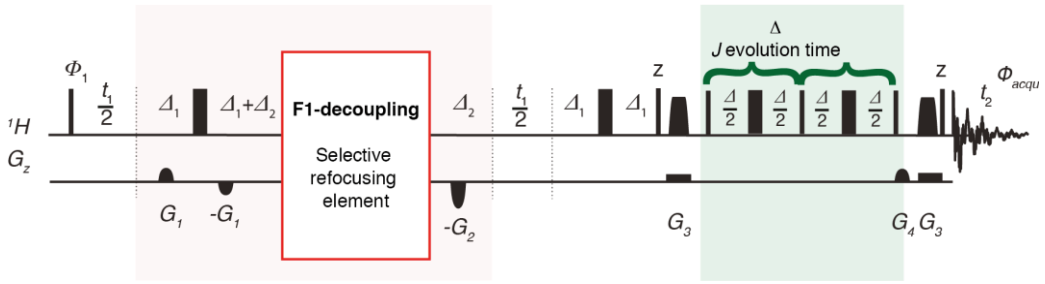

Figure 26. The sequence of the CLIP-COSY experiment with the optional homodecoupling in F1.

The product operator description of the CLIP-COSY experiment shows the fate of the magnetization from the moment of excitation.

$$I_z \xrightarrow{90^\circ_x} -I_y \xrightarrow{t_1} \begin{matrix} -I_y \cdot cos(\Omega_I t_1) \cdot cos(\pi J t_1) \\ +I_x \cdot sin(\Omega_I t_1) \cdot cos(\pi J t_1) \\ -2I_x S_z \cdot cos(\Omega_I t_1) \cdot sin(\pi J t_1) \\ -2I_y S_z \cdot sin(\Omega_I t_1) \cdot sin(\pi J t_1) \end{matrix} \xrightarrow{90^\circ_x} \begin{matrix} -I_z \cdot cos(\Omega_I t_1) \cdot cos(\pi J t_1) \\ +I_x \cdot sin(\Omega_I t_1) \cdot cos(\pi J t_1) \\ -2I_x S_y \cdot cos(\Omega_I t_1) \cdot sin(\pi J t_1) \\ -2I_z S_y \cdot sin(\Omega_I t_1) \cdot sin(\pi J t_1) \end{matrix}$$

In the first stage the magnetization evolves exactly as in the simplest COSY experiment, however, the observable magnetization generated by the first 90° hard pulse at this point is ignored here and only the $-I_z$ term (marked in blue above) is selected by the Keeler's *z*-filter. The product $cos(\Omega_I t_1) \cdot cos(\pi J t_1)$ expresses the modulation of the signals in t_1 (both diagonal and cross-peaks, since both arise from this one term). In the calculations of the trajectory of the magnetization during the mixing, this product will be carried passively and, for simplification, is labeled by $cc(t_1) = cos(\Omega_I t_1) \cdot cos(\pi J t_1)$ in the following:

$$\xrightarrow{z-filter} I_z \cdot cc(t_1) \xrightarrow{90^\circ_x} -I_y \cdot cc(t_1) \xrightarrow{\frac{\Delta}{2},\, 180^\circ_x,\, \frac{\Delta}{2}} \begin{matrix} -I_y \cdot cc(t_1) cos(\pi J \Delta) \\ -2I_x S_z \cdot cc(t_1) sin(\pi J \Delta) \end{matrix} \xrightarrow{90^\circ_y} \begin{matrix} -I_y \cdot cc(t_1) cos(\pi J \Delta) \\ -2I_z S_x \cdot cc(t_1) sin(\pi J \Delta) \end{matrix}$$

$$\xrightarrow{\frac{\Delta}{2},\, 180^\circ_x,\, \frac{\Delta}{2}} \begin{matrix} -I_y \cdot cc(t_1) cos(\pi J \Delta) cos(\pi J \Delta) \\ +2I_x S_z \cdot cc(t_1) cos(\pi J \Delta) sin(\pi J \Delta) \\ -2I_z S_x \cdot cc(t_1) sin(\pi J \Delta) cos(\pi J \Delta) \\ -S_y \cdot cc(t_1) sin(\pi J \Delta) sin(\pi J \Delta) \end{matrix} \xrightarrow{90^\circ_x} \begin{matrix} -I_z \cdot cc(t_1) cos(\pi J \Delta) cos(\pi J \Delta) \\ +2I_x S_y \cdot cc(t_1) cos(\pi J \Delta) sin(\pi J \Delta) \\ +2I_y S_x \cdot cc(t_1) sin(\pi J \Delta) cos(\pi J \Delta) \\ -S_z \cdot cc(t_1) sin(\pi J \Delta) sin(\pi J \Delta) \end{matrix}$$

$$\xrightarrow{z-filter} \begin{matrix} +I_z \cdot cc(t_1) cos^2(\pi J \Delta) \\ +S_z \cdot cc(t_1) sin^2(\pi J \Delta) \end{matrix} \xrightarrow{90^\circ_x} \begin{matrix} -I_y \cdot cc(t_1) cos^2(\pi J \Delta) \\ -S_y \cdot cc(t_1) sin^2(\pi J \Delta) \end{matrix}$$

During the *first* of the two echoes, the antiphase terms are generated, for the coherence transfer to occur upon the subsequent application of the central 90°$_y$ pulse. The *second* echo serves principally to interconvert the antiphase magnetization (now on the second spin) along the *x*-axis to the in-phase magnetization along the *y*-axis. This magnetization will give rise to the cross-peaks (as it was evolving with frequency Ω_I in t_1 and will evolve with frequency Ω_S in t_2. On the other hand, the initial in-phase magnetization along the *y*-axis, generated at the very beginning of the *perfect echo*, remains unaffected by the entire mixing sequence. It will lead to the diagonal signals, provided that the trigonometric term multiplying the product operator is not zero: $cos^2(\pi J \Delta) \neq 0$. The final (fifth) 90°$_x$ pulse of the *perfect echo* drags the two in-phase terms representing the forthcoming diagonal and the cross-peak magnetization away from the

transverse plane and align it with the *z* direction, where it is filtered out from any other (not *z*) magnetization. Thus prepared, the clean in-phase magnetization is eventually made observable by the very last $90°_x$ pulse of the entire sequence.

It is easy to note that the pulses transfer the magnetization between coupled protons in the same way as the well-known refocused INEPT sequence transfers the coherence from proton spins to the coupled ^{13}C spins, where the antiphase proton magnetization is prepared and transferred to the ^{13}C. During the following second delay, the anti-phase on carbon interconverts into the in-phase magnetization. During the entire period, the carbon and proton chemical shift evolutions are refocused in spin-echoes.

As the coherence between coupled spins is usually transferred through the antiphase terms, which are always perpendicular to the anterior in-phase terms, the single rotation provided by an individual mixing pulse will preserve the phase discrepancy between the terms that will eventually lead to diagonal and cross-peaks, respectively. The combination of pulses with deliberately chosen phases and delays adjusted for the interconversion and manipulation of the in-phase and antiphase states can lead to the fine-tuning of the modulation of these two kinds of terms (future diagonal and cross-peak terms). This is what is achieved in the CLIP-COSY experiment – both the diagonal and the cross-peaks arise from in-phase terms described by operators aligned with the same axis in the vector model (*y* in this example). Thus, all the resulting signals can be phased to absorption and moreover, very importantly, all the individual multiplet components will have the same phase.

There is one additional advantage of the fact that the cross-peak signal is modulated just as the diagonal by $cos(\Omega_I t_1) \cdot cos(\pi J t_1)$ in t_1. In most of other COSY-type experiments, the cross-peaks come from antiphase magnetization, which must be then necessarily *sine* modulated, e.g. $sin(\Omega_I t_1) \cdot sin(\pi J t_1)$. A *sine*-modulated FID starts from zero and thus a time is required for the build-up of the signal. With this respect, the advantage of the CLIP-COSY is that there is no minimal limit of points to be acquired to avoid serious drop in signals intensity.

It is noteworthy that even if the very first version of the COSY experiment was introduced in NMR as early as in 1976[52] the CLIP-COSY experiment, taking advantage of the extended mixing sequence of the *perfect echo*, was proposed only very recently (2016)[16]. It adds to the long-lasting trend of searching for ways to improve the phase behavior of the COSY spectra. It was clear that a COSY experiment based solely on in-phase magnetization, besides other advantages, would be compatible with the recently fast-developing homonuclear decoupling. A homodecoupled COSY experiment would be invaluable in assigning spectra where a limit in resolution is difficult to overcome by standard methods (complex multi-component mixtures, mixtures of chemically cognate species, etc.).

However, all the advantages of the CLIP-COSY come with one major disadvantage, which is the variable intensity of signals in the spectra, which depends on coupling constants in a

given spin system and the Δ delay in the perfect echo element. Sometimes, the intensity of signals may be lower than the noise level and thus rendering the spectrum not reliable in indicating the through-bond correlations between the spins. This issue is discussed in detail in the following section.

2. Signals intensity vs. clip delta delay

One of the features that sets the CLIP-COSY apart from many other variants of the COSY experiment, is that the magnetization at the very beginning of the detection period (beginning of the t_2), is modulated not only by the chemical shift and – if *not* F1-decoupled – the *J*-scalar coupling in t_1, but moreover by the *J*-scalar coupling evolving during the four delays $\frac{\Delta}{2}$ of the *perfect echo* sequence. (See the modulation of the final terms in the product operator description of the experiment above, marked in orange). These additional terms multiplying the operators (or their products) carry an information about the amount of the in-phase magnetization corresponding to the "source" spin and its coupled partner, respectively, at the time of the last pulse before detection and therefore translates to the intensity of the signals. It is noteworthy that in most of the standard experiments where the operators before the detection are modulated exclusively during t_1, it is only the *rf* mixing pulse (its flip angle, phase, offset) which will influence the intensity of the generated or transferred magnetization with a specific geometry. Here, in addition to a pulse, the extra modulation must be taken into account.

Each active coupling contributes with a $cos^2(\pi J_{act}\Delta)$ coefficient to the modulation of the "diagonal" term (each of the two spin echoes comes up with the factor $cos(\pi J_{act}\Delta)$) and each passive coupling contributes an additional: $cos^2(\pi J_{pass}\Delta)$. The "cross-peak" term on the other hand is additionally modulated by $sin^2(\pi J_{act}\Delta)$ and each passive coupling adds $cos(\pi J_{pass}\Delta)$. This can be easily summarized in Eq (91) and Eq (92), respectively.

$$I_{diagonal\_12} = cos^2(\pi J_{12}\Delta) \cdot \prod_{i\neq 1,2}^{n} cos^2(\pi J_{1i}\Delta) \tag{91}$$

$$I_{cross-peak\_12} = sin^2(\pi J_{12}\Delta) \cdot \prod_{i\neq 1,2}^{n} cos(\pi J_{1i}\Delta) \cdot \prod_{j\neq 1,2}^{m} cos(\pi J_{2j}\Delta) \tag{92}$$

where *n* and *m* are the number of coupling partners of spins 1 and 2 respectively. Thus, the intensity of signals in the two-dimensional spectrum is a function of the *J*-coupling values and the chosen Δ delay. Moreover, while the diagonal signals will be always positive (modulated by products of functions to a power of two), the cross-peaks may also be negative (due to the product with $cos(\pi J_{pass}\Delta)$). What is essential however, the multiplet components of either diagonal or cross-peaks will all have the same sign. Hence, even in case of low resolution CLIP-COSY spectra, where the active coupling is not resolved, the signals will not cancel out as in antiphase-based experiments. What can however happen, is the cancellation of the positive and negative signals (where the sign results from the dependency on Δ), if they happen to overlap.

Note that the intensity of signals generated in standard experiments depends only on the part of the magnetization selected out of all magnetization to contribute to the spectrum and the flip angle of the pulses. Thus for example, the DQF-COSY has half the intensity of the original COSY experiment, as only the DQ terms (which are in two times smaller quantity than the SQ) contribute to the spectrum, but then, all the signals are made observable by the same $90°_x$ mixing pulse and get from it the same intensity coefficient.

It may seem that the intensity dependence in the CLIP-COSY experiment, strictly linked to individual signals and difficult to guess for complex systems without the necessity of actually doing the calculations, may pose some troubles when analyzing the spectra. For example, it may happen that the intensity of certain cross-peaks reaches zero due to an unfortunate combination of the coupling constants present in the spin system and the CLIP delay. On the other hand however, the possibility to precisely relate the intensity of a given signal to the *J* couplings while deliberately choosing the delay may be exploited to some advantage. In order to maximize the signals intensity, a suitable CLIP delay should be chosen so that the product of functions that underpins the intensity of a given signal reaches its maximum.

As an example, the intensity of chosen cross-peaks expected in the CLIP-COSY spectrum of androstene were calculated on the basis of measured *J* couplings for a range of the CLIP delays (Figure 27). Generally, short delays (up to 25 ms) are somewhat preferred - as the behavior of the functions is well predictable in this interval of arguments – however, often far from optimal for certain signals. It can be clearly seen from the graphs that in order to significantly maximize certain signals, a complementary experiment should be run with a longer delay.

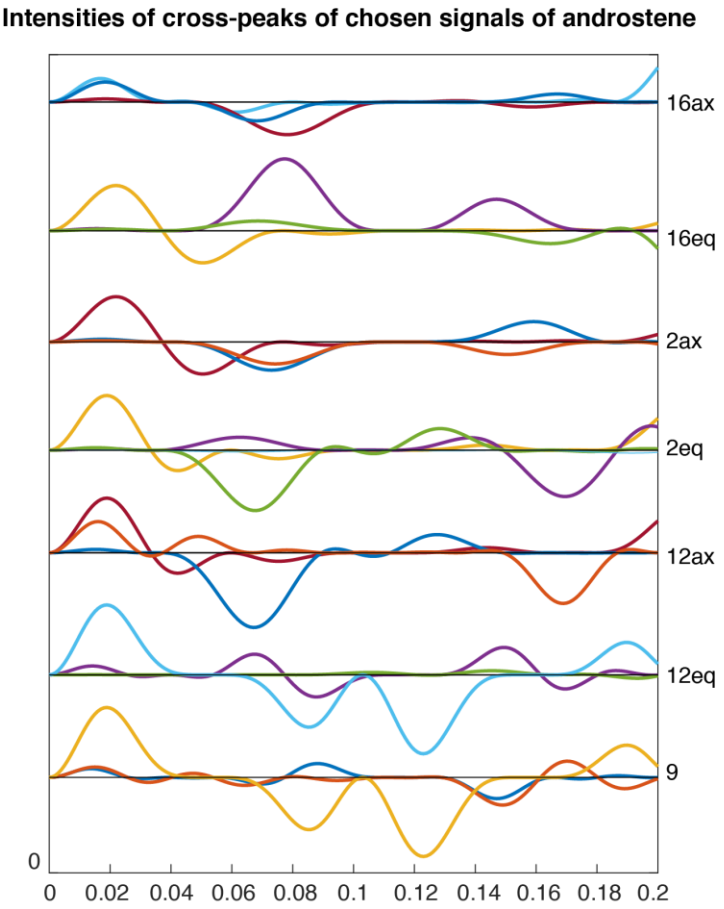

Figure 27. Calculated intensities of cross-peaks of chosen signals of androstene in CLIP-COSY experiment as a function of a CLIP delta delay Δ [sec].

3. Three-dimensional CLIP-COSY experiment

In order to emphasize all cross-peaks, it would be necessary to run several CLIP-COSY experiments, each optimized for a given combination of active and passive couplings. In order to completely remove the intensity variation of the signals, the $\frac{\Delta}{2}$ delays could be incremented so to obtain a dataset that is suitable to be Fourier transformed. In fact, we turned this conceptual experiment into reality. In this 3D CLIP-COSY, each diagonal and cross-peak evolves into a characteristic pattern in the frequency domain of the third, *J*-only dimension, dictated by the same equations that modulate the intensity in the time domain as shown before (Eq (91)

and Eq (92)). The sum of the absolute values of all the multiplet components would provide a CLIP-COSY experiment, without the intensity dependence.

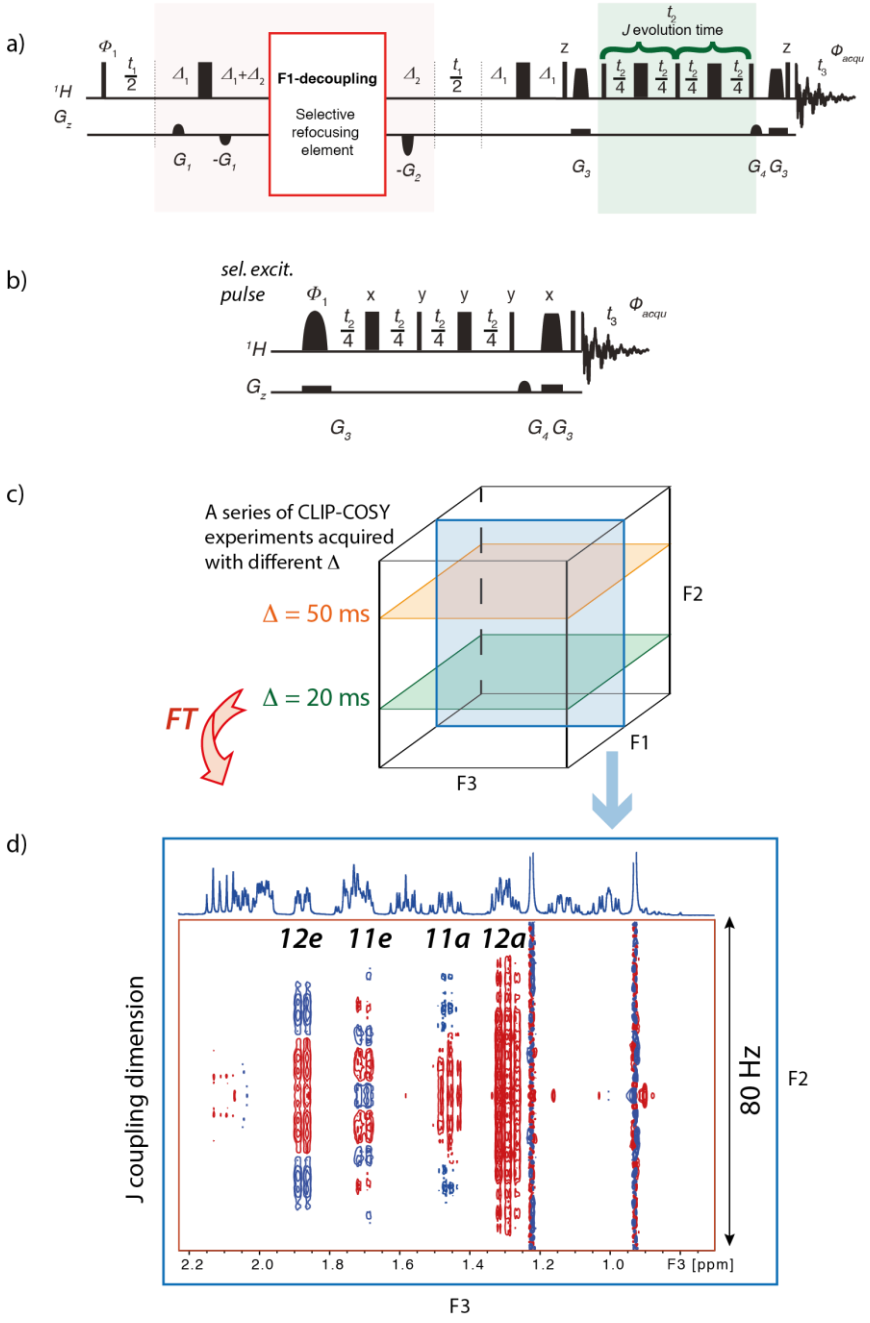

Figure 28. (a) Pulse sequence of the 3D CLIP-COSY. (b) Pulse sequence of a selective 2D experiment allowing the acquisition of spectra of the selectively excited proton and its J-bonded partners. (c) Schematic representation of the 3D CLIP-COSY experiment. The F3 is the directly detected dimension, the F1 is the homodecoupled indirect dimension and F2 is a dimension resulting from the incrementation of the CLIP delta delay Δ and Fourier Transformation. (d) An example of a 2D spectrum, acquired with a pulse sequence shown in (b) and equivalent to

the cross-section of the 3D spectrum taken along the F2 and at δ12a = 1.27 ppm in F1. The diagonal signal 12a is positive and its cross-peaks have antiphase patterns.

The experiment, not thoroughly explored yet, is very interesting conceptually, since the introduction of the third dimension, perpendicular to the other two, may enable the disclosure of the magnetization (including possible artifacts), generated during the mixing. This advantage of replacing a constant delay by an incremented delay in the context of artifacts has been already used[53] to reveal coherence transfer pathways associated with PSYCHE, not detected previously.

4. Comparison with other pure-shift COSY experiments

Several versions of COSY experiments with decoupling in the indirect dimension have already been published[5, 54]. The first of them is *not* based on in-phase magnetization, but achieves the *J*-coupling suppression thanks to the constant time acquisition and was proposed by Gareth Morris – this is the constant time multiple quantum-filtered COSY (CT-MQF-COSY). It should be reminded, for the fair comparison with the CLIP-COSY experiment, that the signals in constant time COSY experiments are represented by equations of the type:

$$\begin{aligned} &-sin(\Omega_I t_1) \cdot cos(\pi JT) \cdot I_x \\ &+sin(\Omega_I t_1) \cdot sin(\pi JT) \cdot 2I_z S_y. \end{aligned} \tag{93}$$

They represent the diagonal and the cross-peaks, respectively and the *T* stands for the *constant time* period. Note that in the particular example, the mixing consisted in a single 90° pulse, which is not the case in DQF/MQF. Nevertheless, the equations serve to demonstrate that there is only one modulation frequency in t_1 (no splitting due to the *J*-coupling). The additional term multiplying the operators (or their products) carry an information about the amount of the in-phase and antiphase magnetization at the time of the last pulse before detection and therefore translates to the intensity of the signals in the 2D spectrum.

The CT-MQF-COSY experiment would not be compatible with any of the homodecoupling elements based on selective refocusing as the experiment exploits the antiphase terms and decoupling would make the signal intensity to collapse to zero. However, since the technique does not require the selective treatment of different spin subsets (with the active spins being usually a much smaller subset than the passive ones), the main advantage of this approach is the relatively high sensitivity of the pure-shift spectrum. However, the relaxation losses in this experiment can be significant because for every t_1 increment, the period between the excitation and detection is constant. The higher the resolution needed, the

longer should be the *T* period. In most of other COSY experiments, the relaxation losses are much smaller when the increments are shorter and increase steadily with t_1.

Another experiment – the PSYCOSY[54], published very recently (2018), is an in-phase experiment and the first COSY-like to use the PSYCHE decoupling element to eliminate the *J*-coupling splitting from the F1-indirect dimension. This experiment, just as the F1-decoupled CLIP-COSY, separates the chemical shift evolution from the *J*-coupling evolution and the coherence transfer. Those two evolutions take place in separate periods in the sequence, before the detection starts. Whereas in the CLIP-COSY the coherence transfer occurs during the *perfect echo* sequence, in the PSYCOSY it is just a delay during which the *J*-couplings evolve. In such a way, the t_1 period can be made very long in order to greatly increase the digital resolution, but without the need to take care of the results of long *J* evolution. The latter would result in appearance of cross-peaks coming from spins coupled through several bonds (up to five or six), which would rather hinder than facilitate the spectral interpretation.

5. BIRD-decoupled CLIP-COSY experiment

The BIRD-based decoupling inserted in the middle of the t_1 evolution of a 2D homonuclear experiment ensures that each ***diagonal*** signal in the spectrum comes from a proton attached to ^{13}C in a different isotopomer. During the mixing, the magnetization is then transferred to the proton coupling partners that are not attached to the ^{13}C isotope, but are still coupled to it through heteronculear couplings of a longer range. Thus, each 1D spectrum extracted from a BIRD-decoupled 2D homonuclear spectrum along the F2 direct dimension is a *fingerprint of a given isotopomer*.

The pulse sequence of the BIRD-decoupled CLIP-COSY experiment is shown in Figure 29. The only modification with respect to the other toolbox experiments using *nemoZS* or PSYCHE decoupling is the additional initial loop with the 180° pulse on the ^{13}C channel being applied in every second scan in order to ensure the best possible elimination of the residual passive magnetization (proton spins attached to ^{12}C). As mentioned in Section III.B.4, the broadband ^{13}C decoupling during acquisition may be optionally switched on/off.

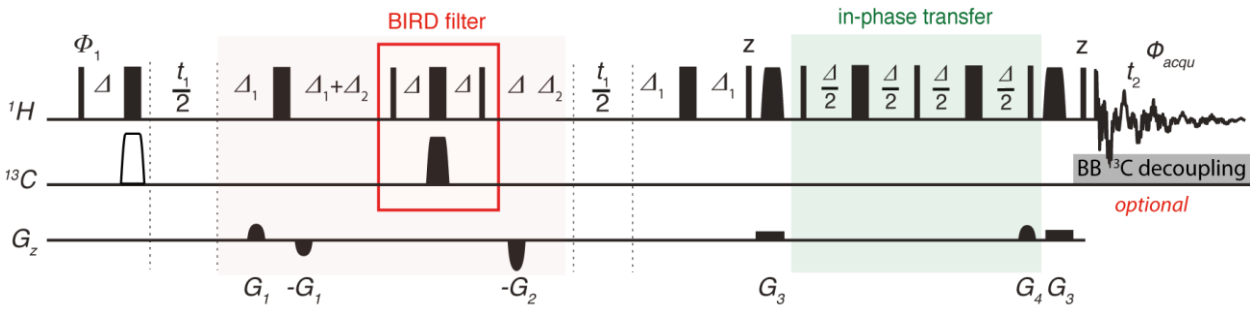

Figure 29. The BIRD-F1-decoupled CLIP-COSY sequence with optional broadband decoupling of the ^{13}C during acquisition.

V. Spectral artifacts

As James Keeler stated, "scientists prefer to interpret the NMR spectra as if they are weakly coupled – each multiplet corresponds to single nuclear environment and each line within the multiplet represents a set of spin states associated with the coupling partners. In practice, the effects of strong coupling are usually evident and these assumptions no longer hold."[25] He actually proved, an in-detail analysis of the source, that the modulation and propagation of the signals coming from second-order effects can lead to finding a method to suppress them, contrarily to what was believed for a long time – that the strong coupling artifacts are unavoidable. The term "artifacts" in the context of strong coupling is often used in the literature and this thesis, however, it is somewhat imprecise, because the signals that originate from the special interaction when spins are strongly coupled are, fundamentally, not artifacts, but naturally occurring responses. It is however their different dependence on the propagation during the pulse sequence - with respect to the weakly coupled spins - that makes them usually appear with different *phase*, *amplitude* and *frequency* than the majority of the signals and hence these strong coupling responses are undesired in the spectrum. The *manipulation* of strong coupling artifacts may however differ for different experiments, as the way how the magnetization is propagated always depends on the propagation pathway used in a specific pulse sequence.

In this thesis, the difficulty to systematically study the artifacts was due to the necessity to first distinguish between different types of artifacts. This required quite a long-term studying of the NMR methodology in general and the strong coupling artifacts in particular. Some of the artifacts observed in the spectra may be related rather to experimental issues than special spin interactions. For example, the proper adjustment of gradients (their strength, length and position) and suitable phase cycling may be essential to improve the quality of the spectrum. The artifacts in our experiments are not ultimately classified and described yet but the aim of this work was to tread the ground to their systematic detection, simulation, explanation and, tentatively – elimination.

The presence of artifacts in DIAG spectra, originating from different sources, have been for the first time signalized in the work published in 2015[10].

The most convenient experiment to start with is the DIAG experiment, as there is no mixing sequence in it. The ideal experimental output of this sequence is shown in Figure 31 where all signals overlapping in 1D are spread with high resolution in the second indirect dimension and the projection along F2 provides a pure shift spectrum.

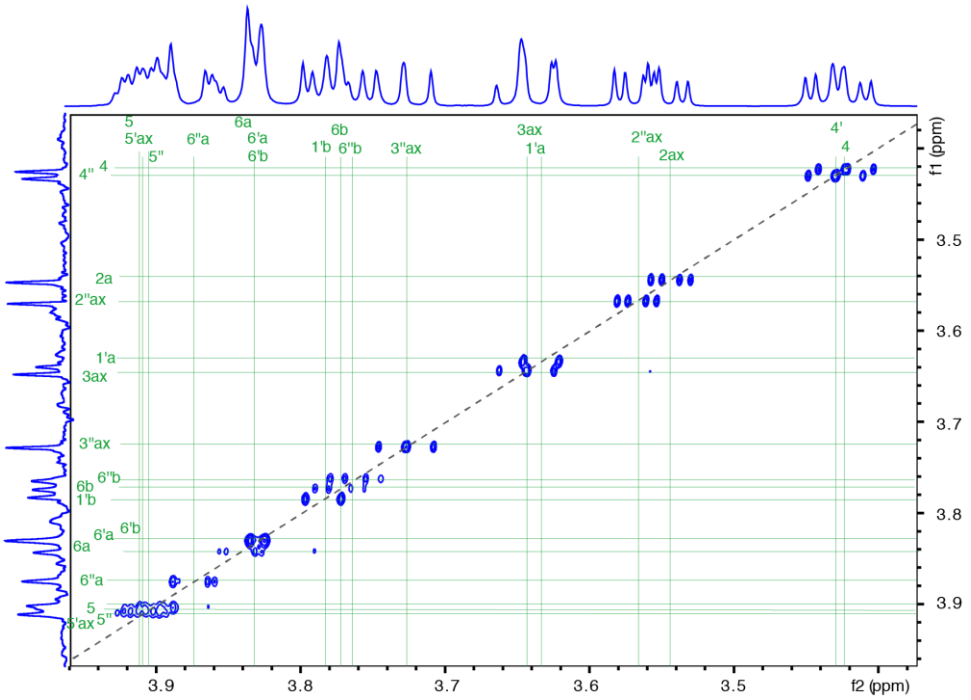

Figure 30. Region of interest of a F1-nemoZS-homodecoupled DIAG spectrum of melezitose, where the out-of-diagonal artifacts are below the chosen signal intensity threshold. This spectrum is equivalent with an "ideal" DIAG spectrum.

A. Comparison of the spectral quality of– decoupled DIAG spectra employing nemoZS, PSYCHE and BIRD elements.

The "true" appearance of non-aliased full spectra of melezitose is shown in Figure 31. The PSYCHE and *nemoZS*-decoupled spectra show non-absorptive artifacts along the half-diagonal, marked with a red dashed line. Some of these artifacts are also spread in the form of several intense, dispersive signals along the F1 dimension. The BIRD-decoupled spectrum is devoid of such artifacts. One should note that for a fair comparison, the BIRD-decoupled spectrum is shown with intensity increased four times with respect to other spectra. Those spurious signals may be somewhat reduced by using a very long homospoil pulse (100 ms) placed between the two final *z*-filters in the sequence. However, this comes at the cost of an increased amount of artifact signals looking like a kind of "noise" along the F1, Figure 32.

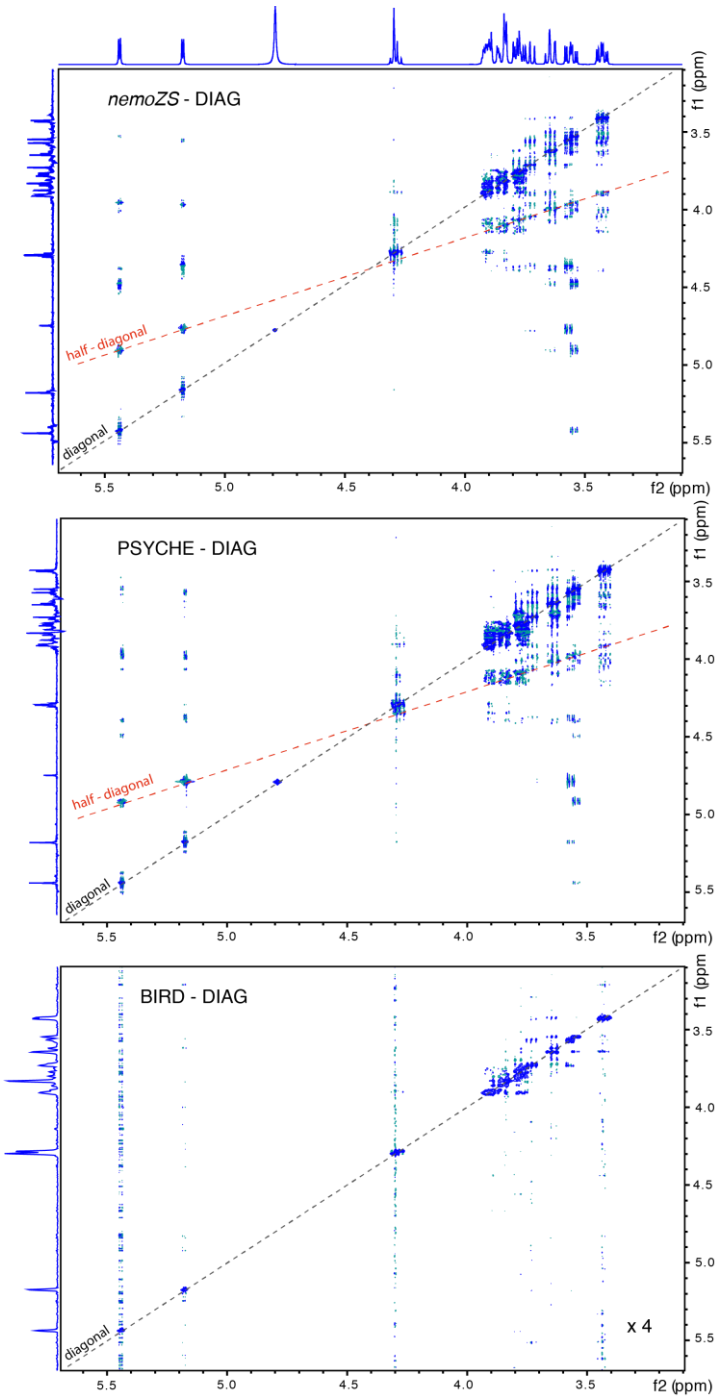

Figure 31. The comparison of DIAG spectra decoupled in F1 with nemoZS, PSYCHE and BIRD elements showing some of the out-of-diagonal artifacts. Spectra were acquired with TD (F2, F1) = (8k, 512), NS = 2 and processed with SINE window function.

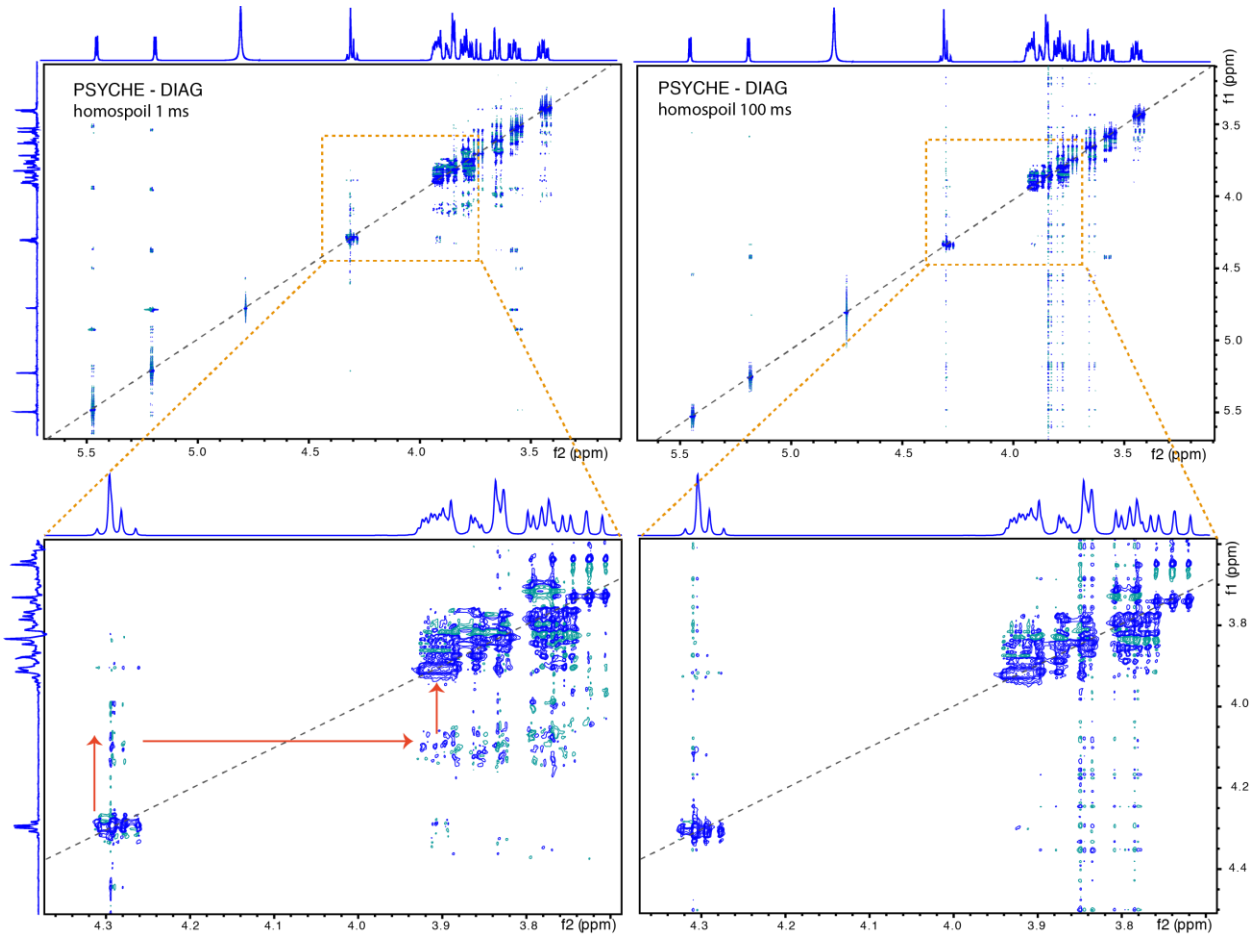

Figure 32. The comparison of PSYCHE-DIAG spectra acquired with homospoil with duration 1 ms and 100 ms, respectively. Spectra were acquired with TD (F2, F1) = (4k, 512), NS = 2. The full spectra are processed without any window function, the enlargements are processed with a SINE window function.

The artifacts resistant to the long homospoil gradient are signalized in Figure 33 and shown in the enlarged regions in Figure 34. Rectangular patterns in color show the positions of these out-of-diagonal artifacts. The right-up and left-down angles of the rectangles drawn with dashed lines indicate the diagonal signals of a pair of coupled spins, whereas the right-down and left-up angles – the positions of cross-peaks. The half-transparent filled rectangles laying at the center of the vertical sides of the dashed rectangles highlight the antiphase artifacts resonating at half the frequency difference between frequencies of the two coupled spins in F1. These artifacts correspond well with the signals expected on account of the calculations presented in the theoretical sections. For example, the rectangle marked with the green dashed line points at the signals of protons 3ax and 4. The numbers are written with a green font. The signal 3ax is additionally involved in a coupling with 2ax and thus the symbol is bicolored (yellow and green).

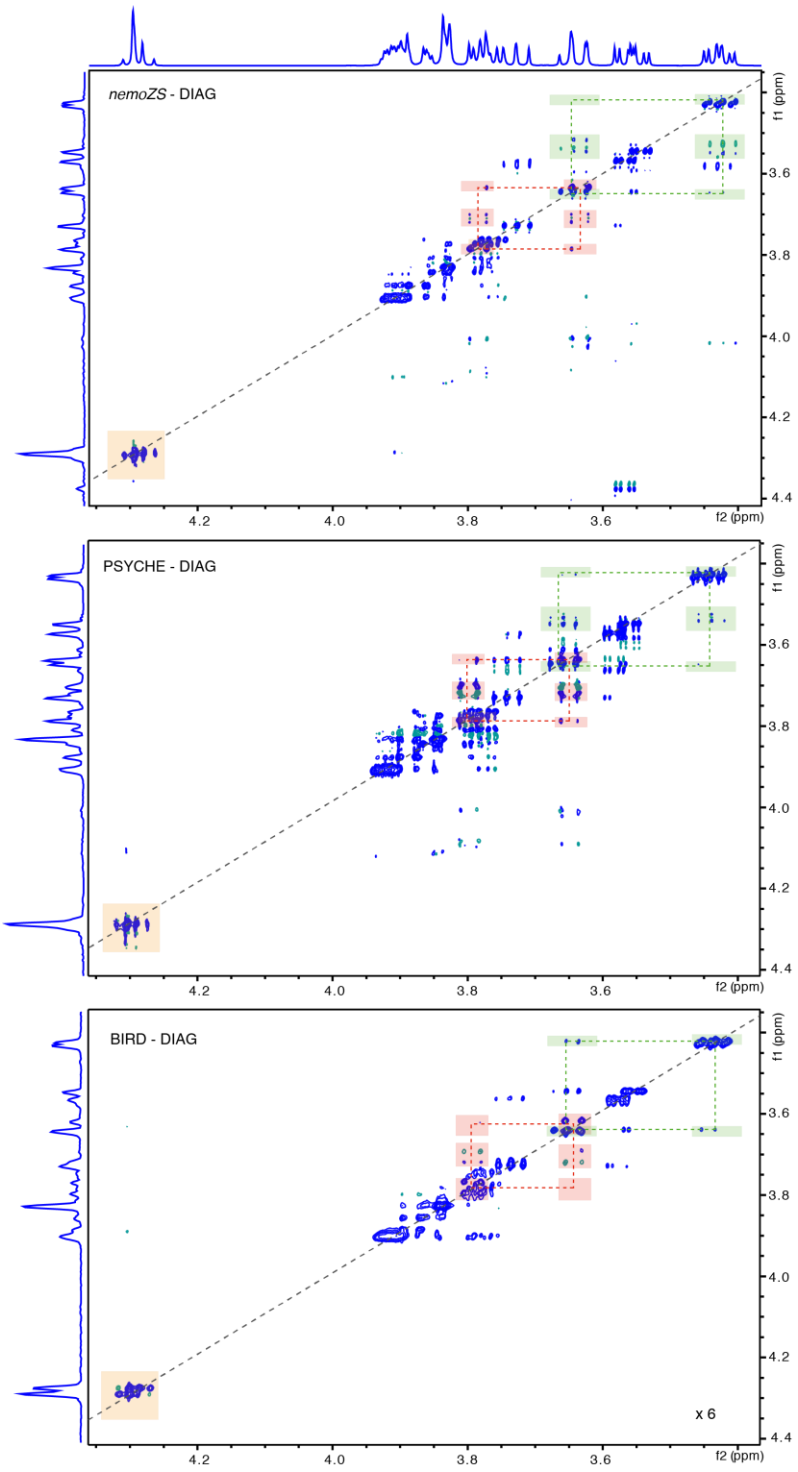

Figure 33. The comparison of DIAG spectra decoupled in F1 with nemoZS, PSYCHE and BIRD element showing some of the out-of-diagonal artifacts (the green and red squares) and a signal with irregular multiplet pattern (orange square).

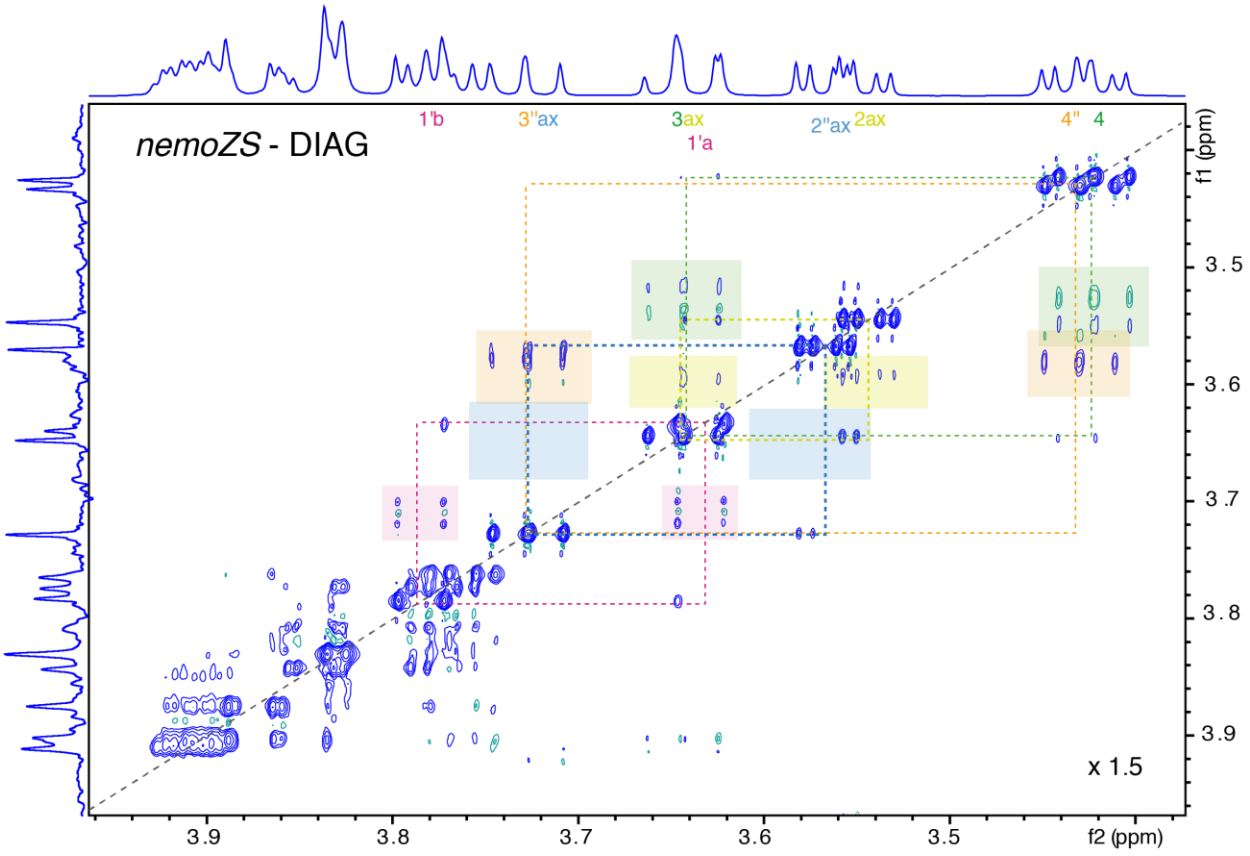
nemoZS - DIAG
1'b
3''ax
3ax
1'a
2''ax
2ax
4''
4
f1 (ppm)
3.5
3.6
3.7
3.8
3.9
x 1.5
3.9
3.8
3.7
3.6
3.5
f2 (ppm)

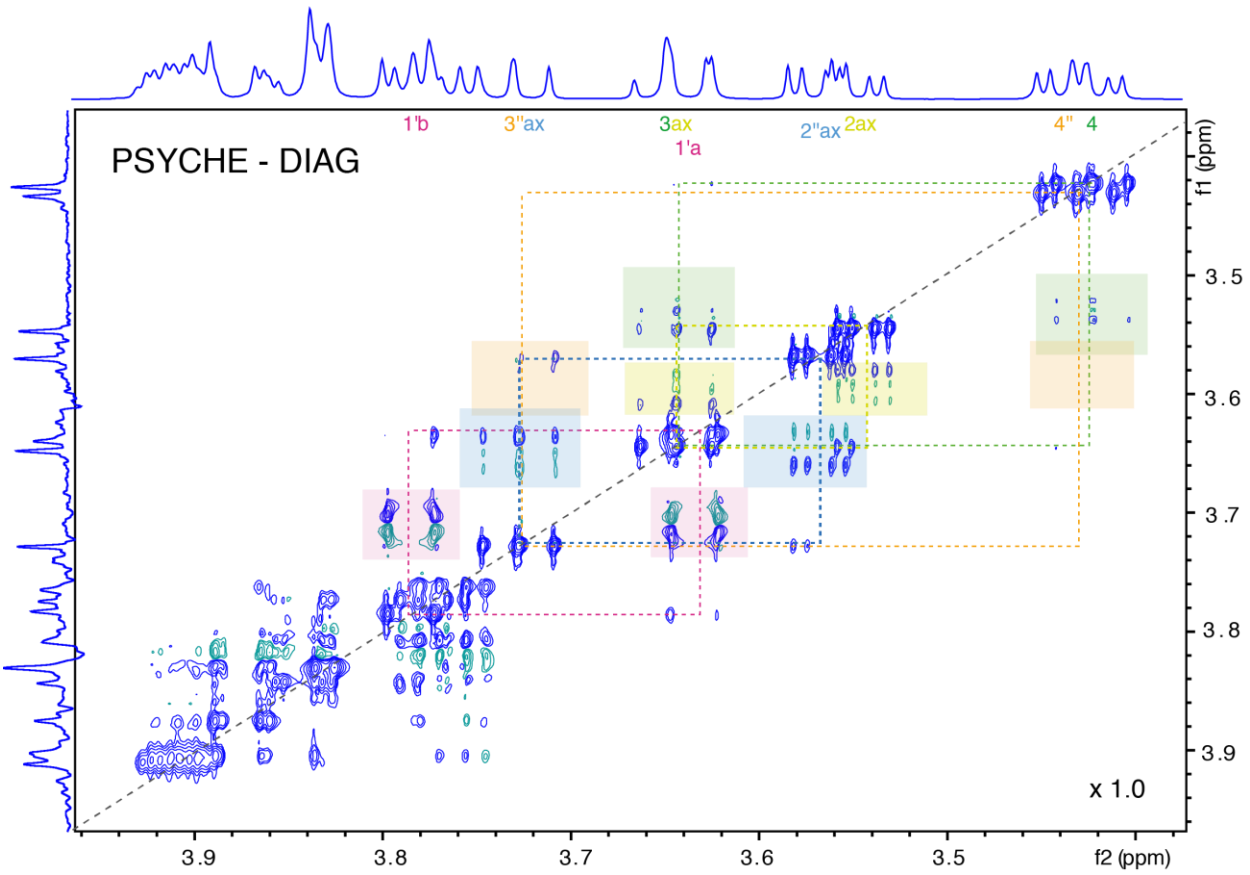
PSYCHE - DIAG
1'b
3''ax
3ax
1'a
2''ax
2ax
4''
4
f1 (ppm)
3.5
3.6
3.7
3.8
3.9
x 1.0
3.9
3.8
3.7
3.6
3.5
f2 (ppm)

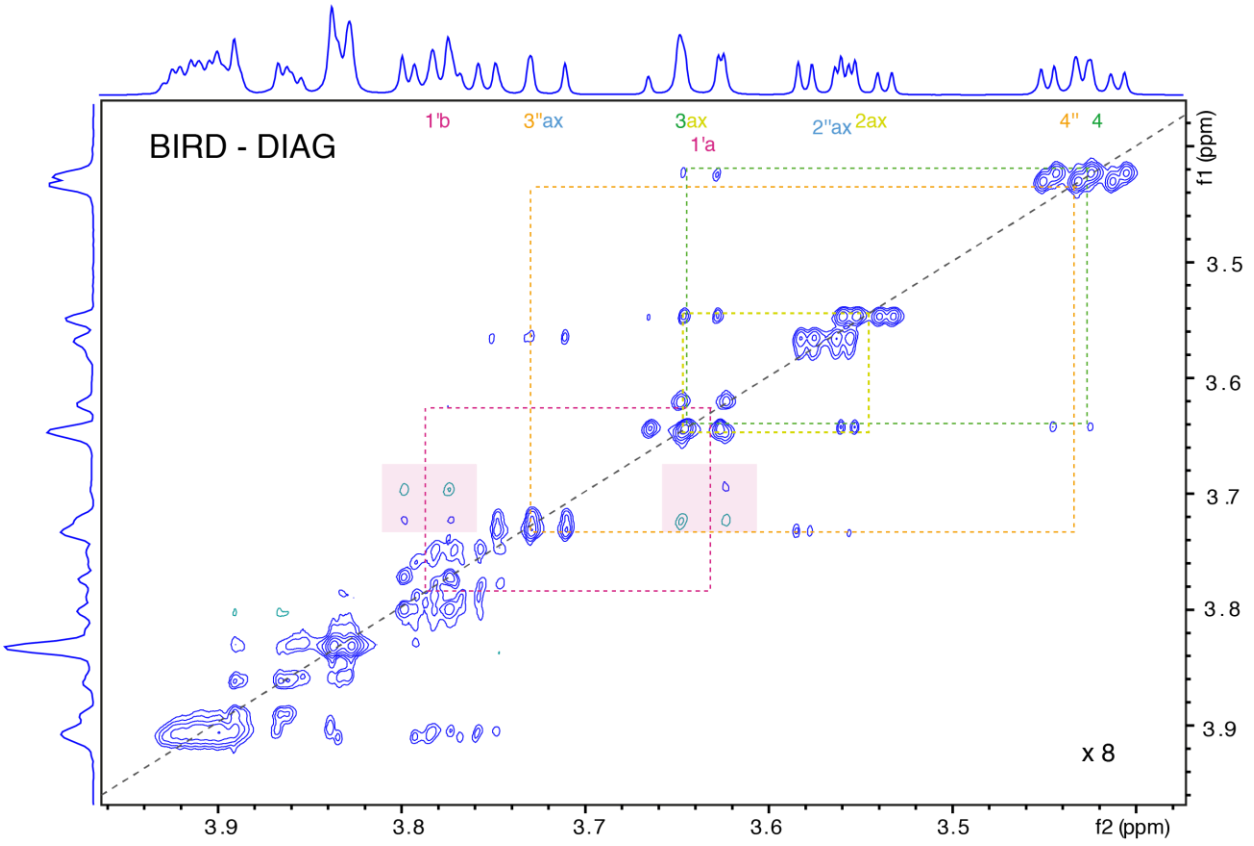

Figure 34. The comparison of DIAG spectra decoupled in F1 with nemoZS, PSYCHE and BIRD elements showing some of the out-of-diagonal artifacts (enlargements).

What can be seen from the figures is that some artifacts are present at the positions of cross-peaks (the left-up and right-down angles of the dashed rectangles). Their multiplicity is preserved only in F2 and the signals have antiphase pattern. In F1 they are singlets. The full pattern is not very well visible in the Figures above as the intensity of the signals is quite low (the strength of the coupling is not very high); most often, it is the positive part of the antiphase pattern that is visible, in fact the intensities of the positive and negative parts are not the same. The origin of these signals was discussed in Section II.H. In 2D, they are generated during acquisition; this is why they are decoupled in F1.

Similar transfer of magnetization, if strong coupling is present, is expected to happen in the period between the preparation and detection, notably, during the sequence element responsible for a spin echo (Section III.B.2.a) in the middle of t_1. This magnetization will not be refocused, as it evolves with different frequencies on both sides of the element. (It should be noted that expressing the phenomenon as “magnetization transfer” or “mixing of the basis states” depends on the basis in which the spin system is considered; if we describe the process in the Hilbert space, we speak about transfer of magnetization during, for example, the 180°

hard pulse). Such a magnetization is expected to be detected in the spectrum approximately at the mean value of their chemical shifts in F1 and indeed it is observed experimentally as intense signals with unpredictable phase.

If those artifacts were originating from just the *mixing* of the basis states, as described by Eq (53) and manifested by rotation induced by the hard 180° and/or "theoretical" selective 180° pulse with no duration (as used in simulations) – their characteristics could be easily calculated. In this case they would be equivalent with the artifacts that Keeler described and suppressed in his *J*-resolved experiment[25]. The multiplicity patterns of these artifacts in DIAG could be rationalized from Eq (57) and Eq (62). Also, their intensity would be comparable with the intensity of signals appearing at the "cross-peaks positions". Such artifacts, with the [+ +] pattern (in the upper row) and [- -](in the lower row) are visible in BIRD-decoupled spectra where strong coupling occurs, Figure 34, highlighted by a half-transparent pink rectangles.

However, in DIAG experiment, where either the very long selective pulses (non-equidistantly modulated) or the PSYCHE element is used, there are different sources of magnetization, which can result in signals just at the middle between the frequencies of coupled spins in F1. As was shown by Nuzillard[26] in the context of the SERF experiment, when the evolution during biselective pulses are used and the Hamiltonian describing the spin dynamics depends on time through the shaped envelope, a condition similar to the one in the Hartmann-Hahn transfer is fulfilled. The consequence of it is that magnetization can be transferred between spins even when they are weakly coupled. Such a magnetization also contributes to the signals at the average of chemical shifts in F1.

The PSYCHE element is the most problematic with this respect, as it is inherent to pulses of a small flip angle to generate cross-peak responses (Sections II.G and III.B.2). This is why they usually play a role of mixing pulses[32, 34].Moreover, a considerable amount of ZQ coherences is also produced within the PSYCHE element. Even if, in principle, those two classes of terms should be dephased as a result of spatiotemporal averaging, their presence may be very sensitive to experimental parameters, above all the duration of the chirped pulses. As demonstrated by Eq (80), it is clear that the attenuation of unwanted coherences depends on the duration of the chirp and its rate, which is related to the range of frequencies that should be covered by the sweeping pulse. One should note that this equation *does not* describe strictly the attenuation of unwanted coherences in the PSYCHE element, since here, the generation of these terms is time-dependent (see Section III.B.2.b)), unlike in the Keeler's *z*-filter.

When the content of the colorful boxes in Figure 35 are examined for spectra decoupled with *nemoZS* and PSYCHE, respectively, it appears that in some cases the methods seem to be complementary, as the very intense artifacts observed in PSYCHE, are not so intense in *nemoZS* and *vice versa*. This complementarity may however not be systematic. Simulations that could establish precisely the criteria for this complementarity will be the objective of future work.

In the BIRD-decoupled DIAG and CLIP-COSY spectra, quite intense artifacts *looking like* t_1 noise appear where spins are strongly coupled (for example Figure 39 and Figure 42). These artifacts change position and intensity, depending whether the broadband decoupler is active or not during the acquisition. This comes as no surprise as the spin system changes in either case. Those artifacts were initially attributed to the low sensitivity of the experiment, t_1 noise or experimental artifacts due to. The Spinach simulations were useful to confirm that these signals result from the spin system itself.

B. Artifacts versus duration of PSYCHE

Regarding the PSYCHE element and its overlooked disposition to dephase unwanted coherences and its dependence on the duration of the decoupling element, this parameter was tested. It was observed that, indeed, the phase and amplitude of the signals at the average of chemical shifts of coupled spins in F1 change upon variation of the length of the PSYCHE element, as shown in Figure 35. It should be noted that the intensity of the spectra was adjusted to expose the artifacts in the semi-transparent rectangular colored frames and so that some recoupling artifacts are additionally visible at the distance of *J*/2 along F1 up and down from the diagonal decoupled signals.

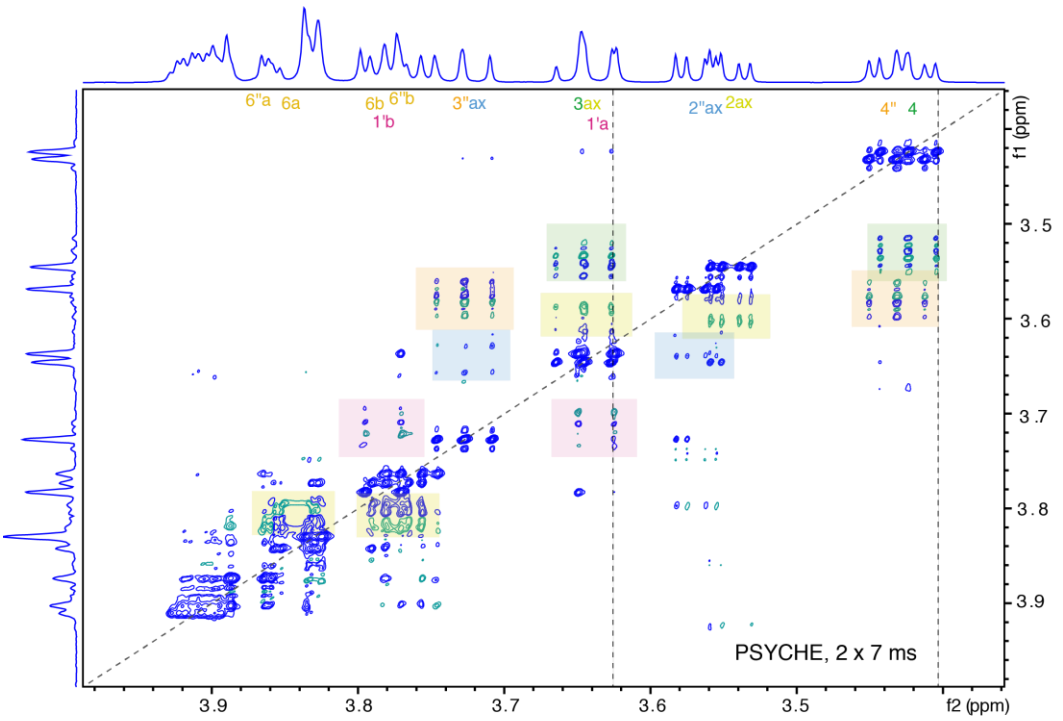
6"a 6a
6b 6"b
1'b
3"ax
3ax
1'a
2"ax 2ax
4" 4
f1 (ppm)
3.5
3.6
3.7
3.8
3.9
PSYCHE, 2 x 7 ms
3.9
3.8
3.7
3.6
3.5
f2 (ppm)

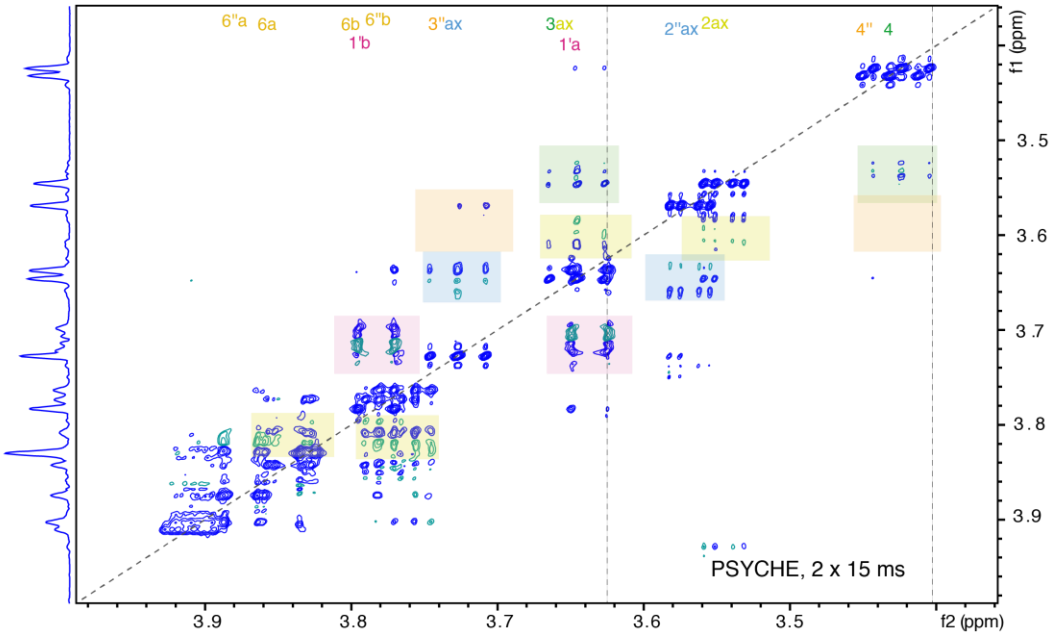
6"a 6a
6b 6"b
1'b
3"ax
3ax
1'a
2"ax 2ax
4" 4
f1 (ppm)
3.5
3.6
3.7
3.8
3.9
PSYCHE, 2 x 15 ms
3.9
3.8
3.7
3.6
3.5
f2 (ppm)

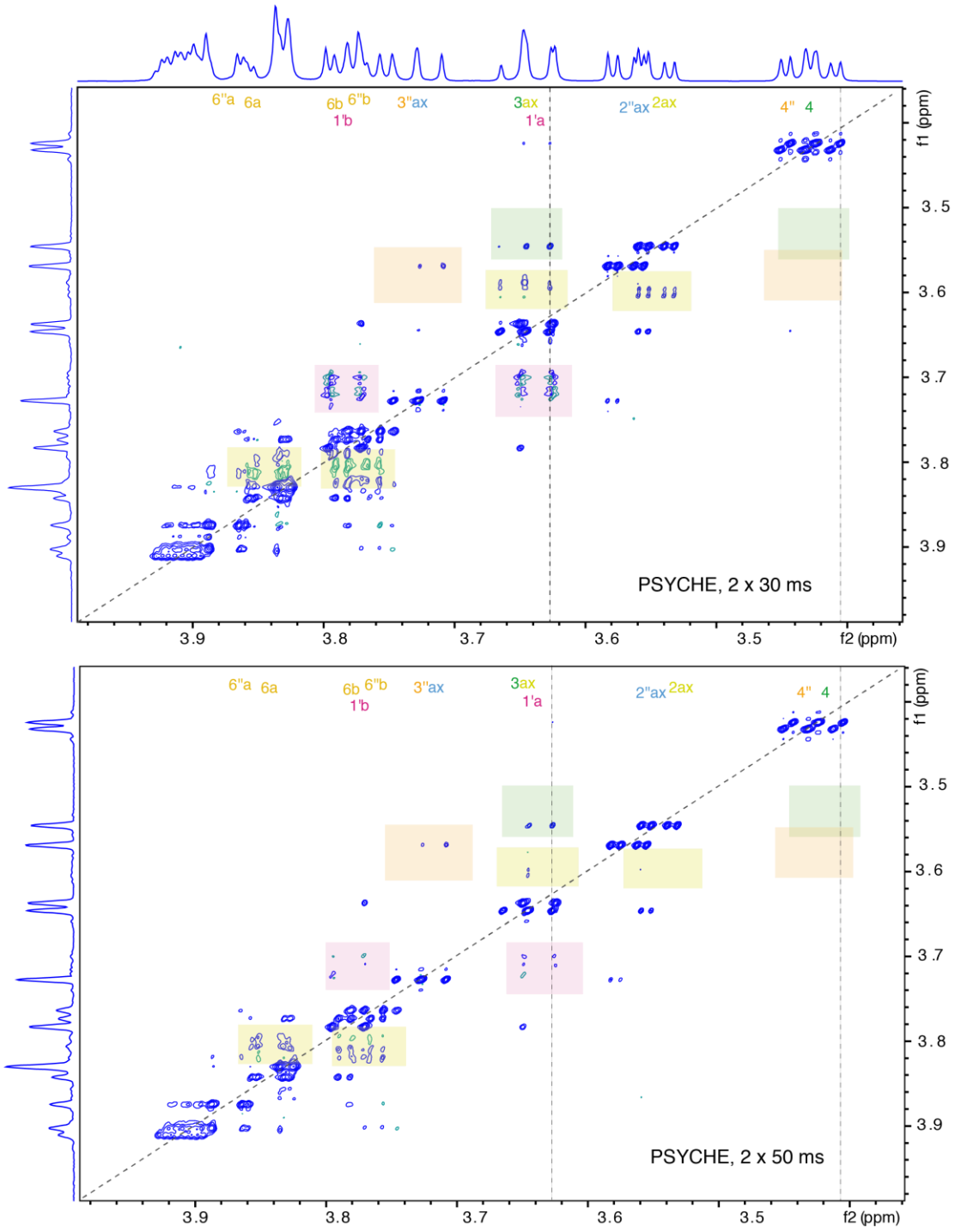

Figure 35. The comparison of PSYCHE-DIAG spectra acquired with different durations of the decoupling element: 2x7 ms, 2x15 ms, 2x30 ms, 2x50 ms; the strength of the gradient for spatial encoding was kept constant (1%). Spectra were acquired with TD (F2, F1) = (4k, 256), NS = 2. The spectra were processed using SINE window functions.

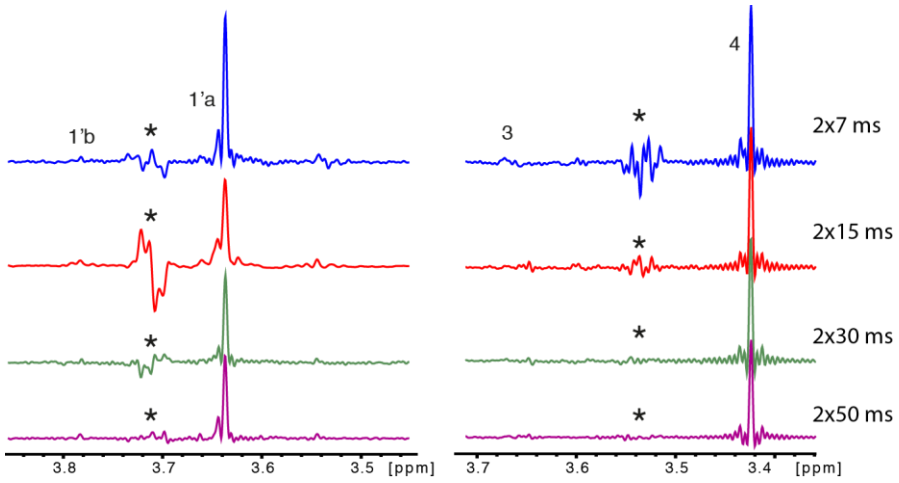

Figure 36. Comparison of F1 cross-sections extracted at position marked by the dashed black lines in figures above and corresponding to protons 1'a and 4, respectively. The asterisk marks the artifact in between coupled spins. It can be seen that the intensity of these artifacts does not change linearly with the duration of the PSYCHE element.

A rationalization of the generation of undesired terms within the PSYCHE element and the efficiency of their dephasing with respect to the parameters of the PSYCHE element (duration of chirps, its relation to the strength of the encoding gradient etc.) will be studied in future work. Spinach simulations will facilitate the examination of these transfers now when the theoretical background has been established as presented in this thesis and will facilitate the design of simulations and experimental tests.

VI. Complementarity of the decoupling elements with respect to strong coupling

It is generally assumed that if $\Delta\delta \leq J$ the spins are classified as very strongly coupled, however, already with $\Delta\delta \leq 10J$, strong coupling features can be recognized in the spectra.

There is a considerable number of strongly coupled spins in the carbohydrate melezitose, for example, the fructofuranosyl ring of the sugar is an example of ABMXY system (H-$3', 4', 5', 6'_a, 6'_b$). The chemical shifts and couplings in this system are summarized in Table 1.

Table 1. Scalar couplings (Hz) present in the glucopyranosyl ring of melezitose.

Melezitose							
ring A, glucopyranosyl							
Signal	$1_a^{'}$	$1_b^{'}$	$3^{'}$	$4^{'}$	$5^{'}$	$6_a^{'}$	$6_b^{'}$
δ	3.635	3.785	4.2985	4.2845	3.904	3.835	3.831
$1_a^{'}$							
$1_b^{'}$	12.3						
$3^{'}$							
$4^{'}$			8.5				
$5^{'}$							
$6_a^{'}$					7.6		
$6_b^{'}$					2.4	12.4	

Table 2. Ratio $\Delta\delta$/J. If lower than 10, it indicates strong coupling interaction.

Melezitose							
ring A, glucopyranosyl							
Signal	$1_a^{'}$	$1_b^{'}$	$3^{'}$	$4^{'}$	$5^{'}$	$6_a^{'}$	$6_b^{'}$
δ	3.635	3.785	4.2985	4.2845	3.904	3.835	3.831
$1_a^{'}$							
$1_b^{'}$	6.1						
$3^{'}$							
$4^{'}$			0.8				
$5^{'}$							
$6_a^{'}$					4.5		
$6_b^{'}$					15.2	0.2	

It can be seen that the protons 3' and 4' are very strongly coupled, with $\Delta\delta = 6.98\,Hz$ and $J_{4'-3'} = 8.50\,Hz$. Such strongly coupled spins are not expected to be decoupled by neither the PSYCHE nor the *nemoZS* elements. In fact, the 1D and 2D multiplet shows completely mixed transitions.

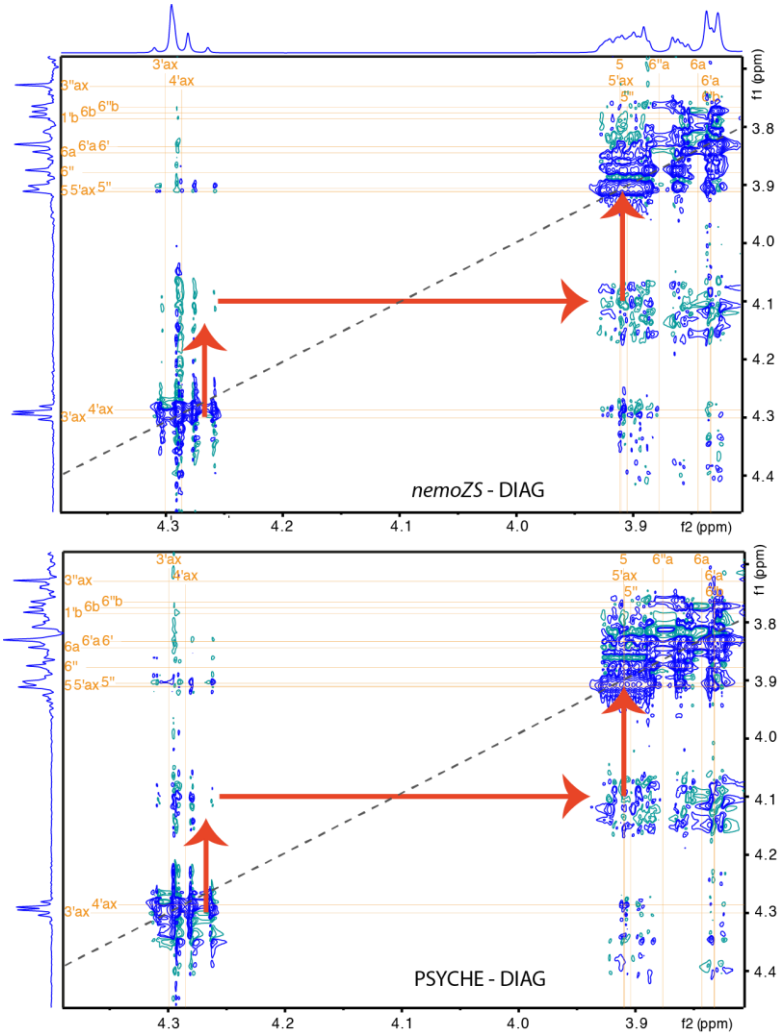

Figure 37. Enlarged regions of DIAG spectra decoupled in F1 with nemoZS and PSYCHE showing the very strongly coupled 3' and 4' and the dispersive artifacts correlating these signals with their partner 5'.

The BIRD-decoupling is perfectly complementary in this case to *nemoZS* and PSYCHE, as the satellites 3' and 4' are not strongly coupled and they do not interact with any neighboring spins neither. When broadband ^{13}C decoupling is used during the acquisition, the signal will be decoupled in F1, but the strong coupling interaction will still be present and observed in the direct dimension, as we "cut off" the effect of the ^{13}C. Without ^{13}C decoupling during acquisition, the first order multiplets can be eventually disclosed by profiting from the presence of the ^{13}C isotope in both dimensions, Figure 38 d, f.

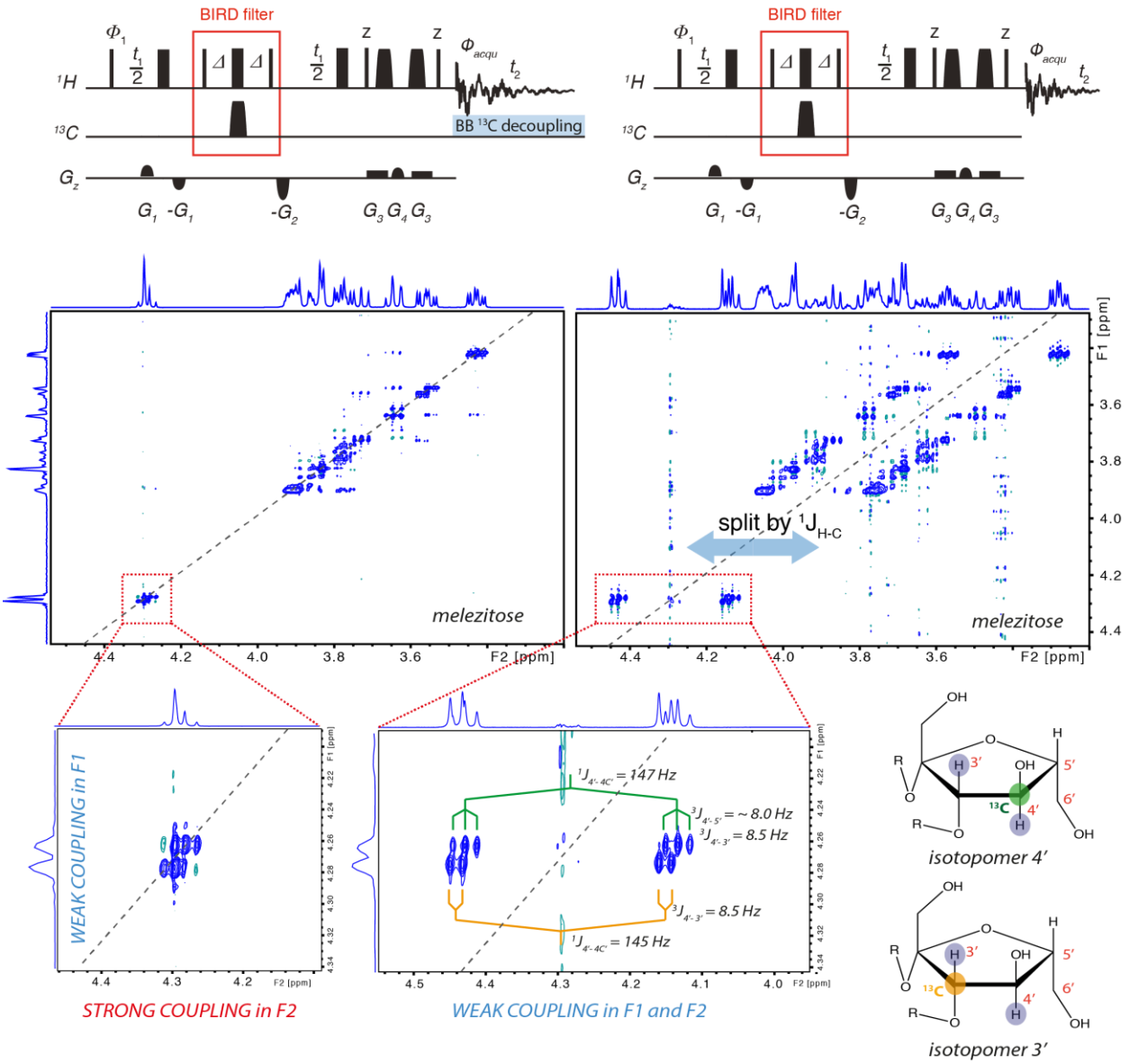

Figure 38. Enlarged region of the BIRD-decoupled DIAG spectrum showing signals 3' and 4' well resolved in the F1 dimension, but still manifesting second order effects in the F2 dimension. The spectrum on the left was acquired with TD(F2, F1) = 8k, 512 and AQ(F2,F1) = 3.15, 0.2 s (it should be noted that the AQ should not be as long if ^{13}C broadband decoupling is active during acquisition, this dataset was run unintentionally with these parameters). The spectrum on the right was acquired with TD(F2, F1) 4k, 512 and AQ(F2,F1) = 1.58, 0.2 sec. The spectrum shown in the right bottom enlargement acquired with TD(F2, F1) =8k, 512 and AQ(F2,F1) = 3.15, 0.2 s.

The coupling constant $J_{4'-3'}$ can be then measured experimentally from the non-^{13}C-decoupled BIRD-DIAG experiment. The coupling can be measured precisely from the 3' diagonal signal splitted only by this coupling and appearing as a doublet with $J_{4'-3'} = 8.5$ Hz. The diagonal signal 4' is splitted by two coupling constants: $J_{4'-3'}$ and $J_{4'-5'}$. The latter cannot be measured precisely due to limit in resolution in F2 (the spectrum was acquired with the

following parameters in the F2 direct dimension: TD = 2048, SW = 1.3 ppm, AQ = 1.58 s). It is clear however that the two couplings are very similar, since the signal 4' shows a triplet pattern. Previously, these couplings could not be observed with the precision provided by our experiment and it was reported that: "… the relevant coupling constants were obtained through computer-aided simulations, because classical calculation procedures failed. The values [are] $J_{4'-3'} = 7.6$ Hz and $J_{5'-3'} = 8$ Hz[55].

Subsequently, the BIRD-decoupled CLIP-COSY can be acquired in order to provide the cross-peaks in the form of multiplets splitted not only by homonuclear J_{H-H} couplings, but additionally by heteronuclear couplings through 2 or 3 bonds, $^{2,3}J_{C-H}$. It is particularly interesting in this experiment to be able to reveal the cross-peaks that lie very close to the diagonal (situation common when spins are strongly coupled). Normally in such situations, diagonal peaks severely overlap with their corresponding cross-peaks. In our experiment, the diagonal signals are displaced far apart from the diagonal by the $^{1}J_{C-H}$ coupling, (Figure 39).

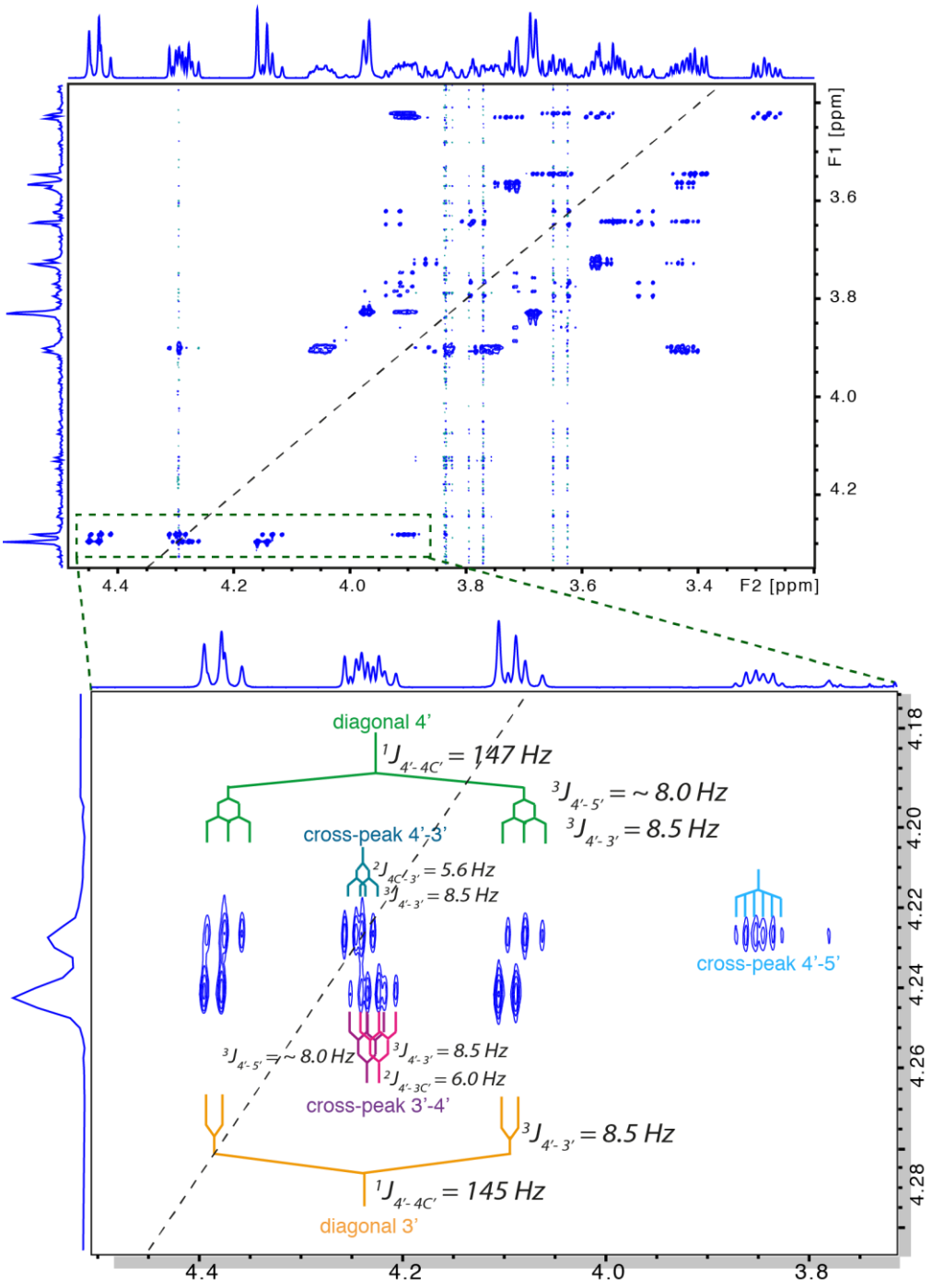

Figure 39. BIRD-decoupled CLIP-COSY spectrum without broadband ^{13}C decoupling during acquisition (top); enlargement showing multiplets splitted by homo- and heterenuclear couplings.

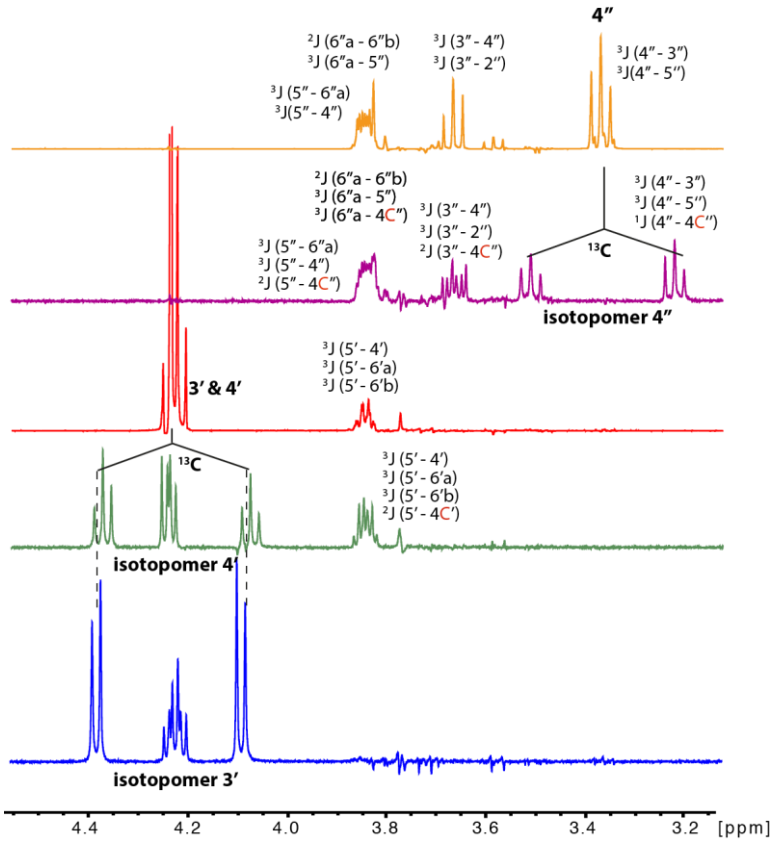

Figure 40. Examples of cross-sections extracted along F2 from the BIRD and PSYCHE-decoupled CLIP-COSY experiments and coupling constants that contribute to the splitting of the respective signals.

In certain cases, the additional split generated by the presence of the ^{13}C isotope in a spin system may be used to a great advantage to obtain information about the heteronuclear couplings, which may give additional insights into the structure of the molecule. However, often, the additional splitting of proton signals having very similar chemical shift by the long range $J_{C,H}$ couplings, such as the protons 5" and 6"a (Figure 40, second cross-section from the top) may lead to an extensive overlap (with respect to standard protons spectra) and eventually a failure in revealing the coupling constants.

It is noteworthy that in correlation experiments like the BIRD-decoupled CLIP-COSY or TOCSY and with the broadband decoupler active during acquisition, cross-peaks lying above and below the diagonal originate from transfers of magnetization within a given pair of proton spins, where the pair belongs to a different spin system when the cross-peak along F1 and F2 is generated, respectively. This loss of symmetry in the magnetization transfers may lead to a different lineshape of cross-peaks on both sides of the diagonal (in addition to different multiplicity – the cross-peaks symmetry known from typical 2D experiments is lost when F1-decoupled).

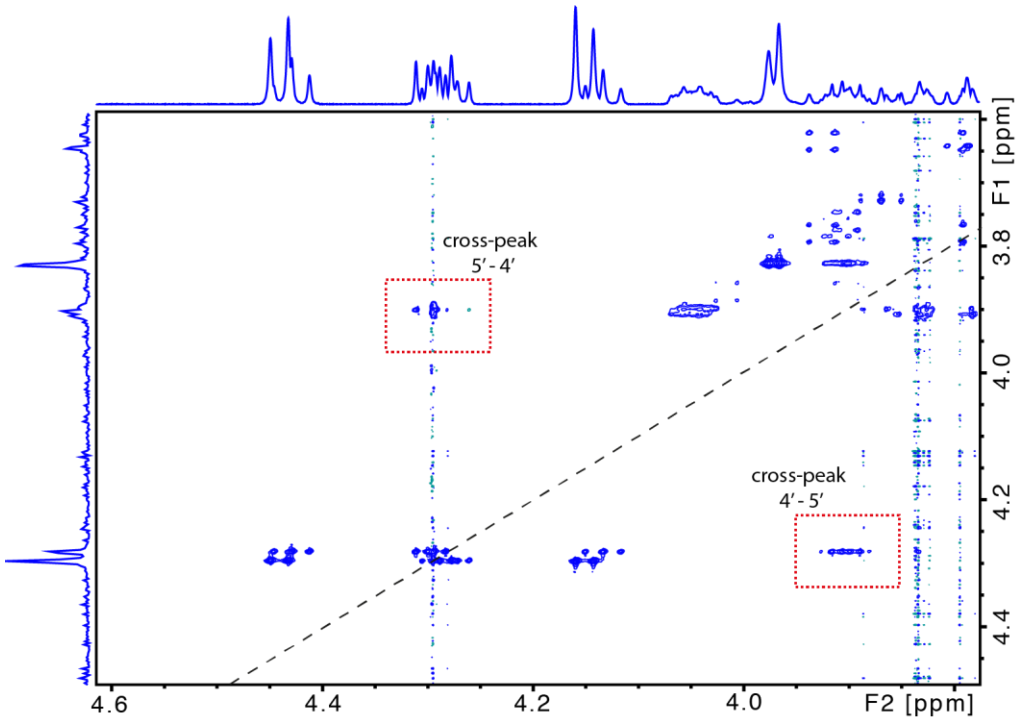

Figure 41. Fragment of BIRD-decoupled CLIP-COSY spectrum showing the cross-peak 4'-5' on both sides of the diagonal. When above it, the cross-peak results from a transfer of magnetization from strongly coupled 3' and 4'. When below the diagonal, it results from transfers from the weakly coupled isotopomers 3' and 4'.

The BIRD-decoupling based experiments (BIRD-DIAG, BIRD-CLIP-COSY, BIRD-TOCSY) are essential to retrieve the coupling constants in such seriously mixed signals as 3' and 4'. However, applying the BIRD method to decouple very crowded proton spectra may sometimes be adverse. This can occur when the distance between a satellite and its coupling partner approximately matches half of the large heteronuclear coupling: the strong coupling interaction between *the part* of the broad multiplet of the satellite and the partner will take effect and complicate the spectrum. An illustrative example of this situation was found in a spectrum of strychnine, where one part of the diagonal signal of isotopomer 3 (splitted by the large $^{1}J_{CH}$ heteronuclear coupling) shows a strong coupling interaction with the signal of the isotopomer 2, (see red circles in Figure 42)).

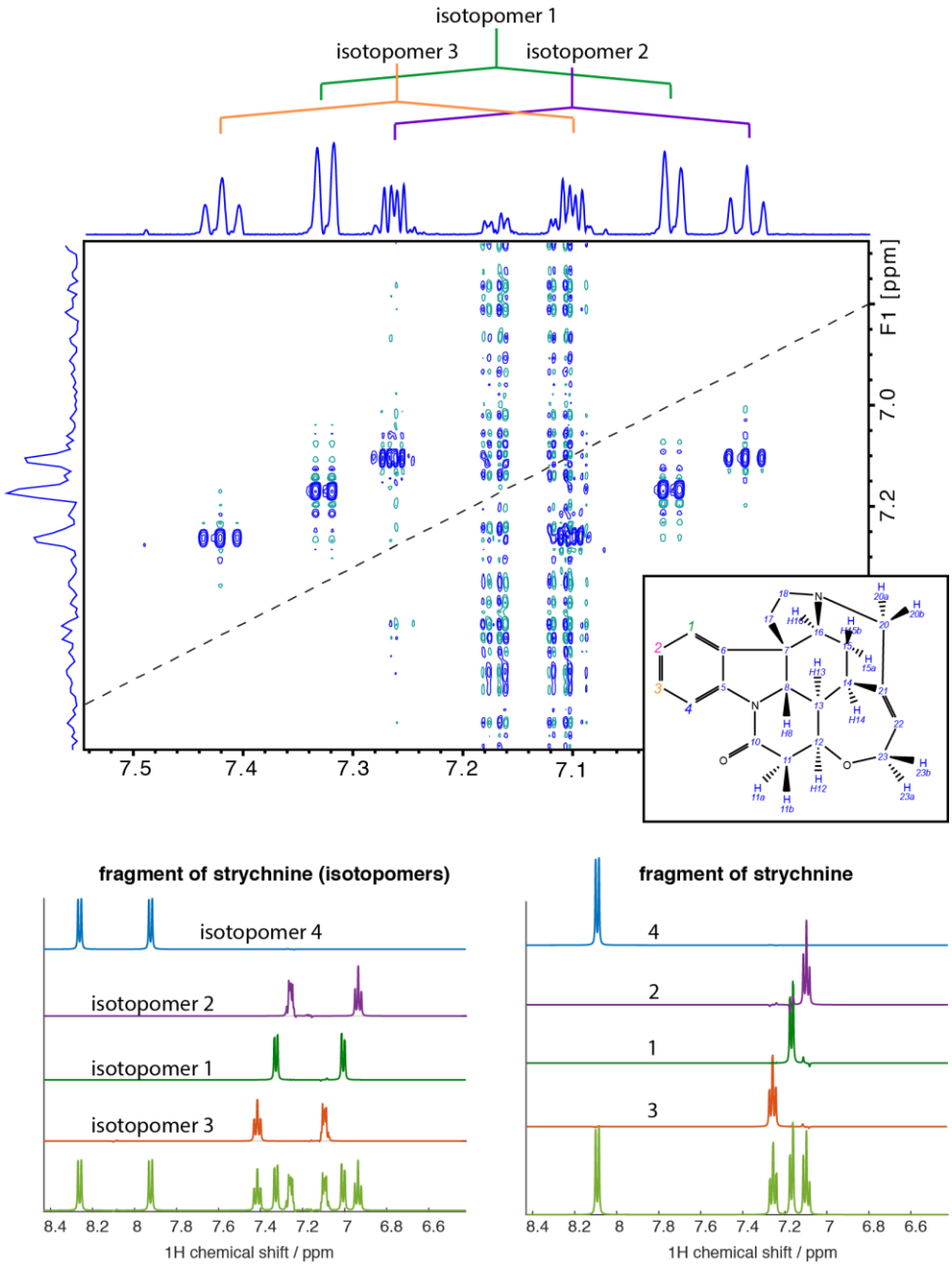

Figure 42. Fragment of a 2D F1-BIRD-decoupled DIAG spectrum of strychnine showing the aromatic protons 1, 2 and 3 splitted by the large $^{1}J_{CH}$ ~ 145 Hz couplings (top) and the Spinach simulations of 1D spectra of this spin system in the presence/absence of ^{13}C isotope.

Coming back to the melezitose, the fructofuranosyl ring was used as a model to reproduce, by simulation, the artifacts that result from spin interactions in isotopomers. First, the coupling constants and chemical shifts were adjusted according to a simple manual fitting of a one-dimensional simulated spectrum (Mnova) with the experimental one. Then, the

spectrum was simulated using Spinach, assuming the strong coupling Hamiltonian, and theoretically decomposed, as discussed in Section II.H and shown in Figure 10 for two strongly coupled spins.

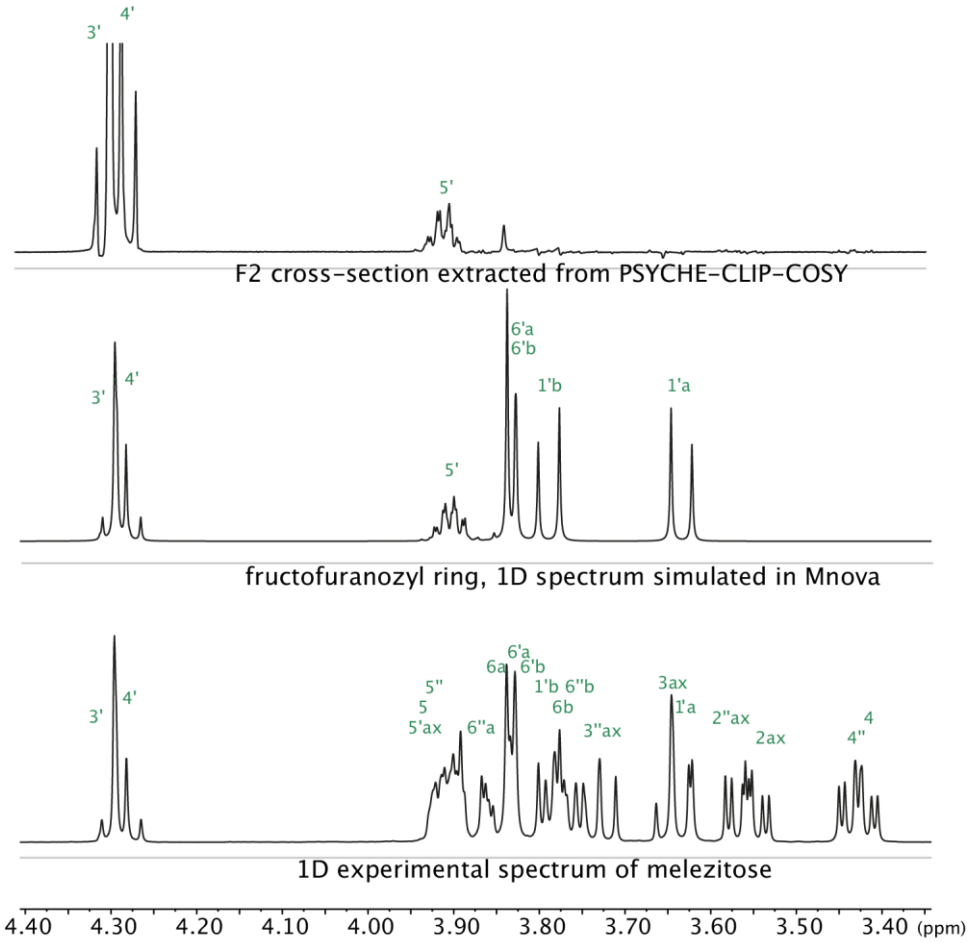

Figure 43. The F2-trace extracted from PSYCHE-CLIP-COSY at $\delta \approx 4.285$ ppm showing the mixed 3' and 4' diagonal signals and the cross-peak 4'-5' (top), Mnova simulation of the fructofuranosyl ring with a simple manual fitting (middle) and the experimental 1D spectrum (bottom).

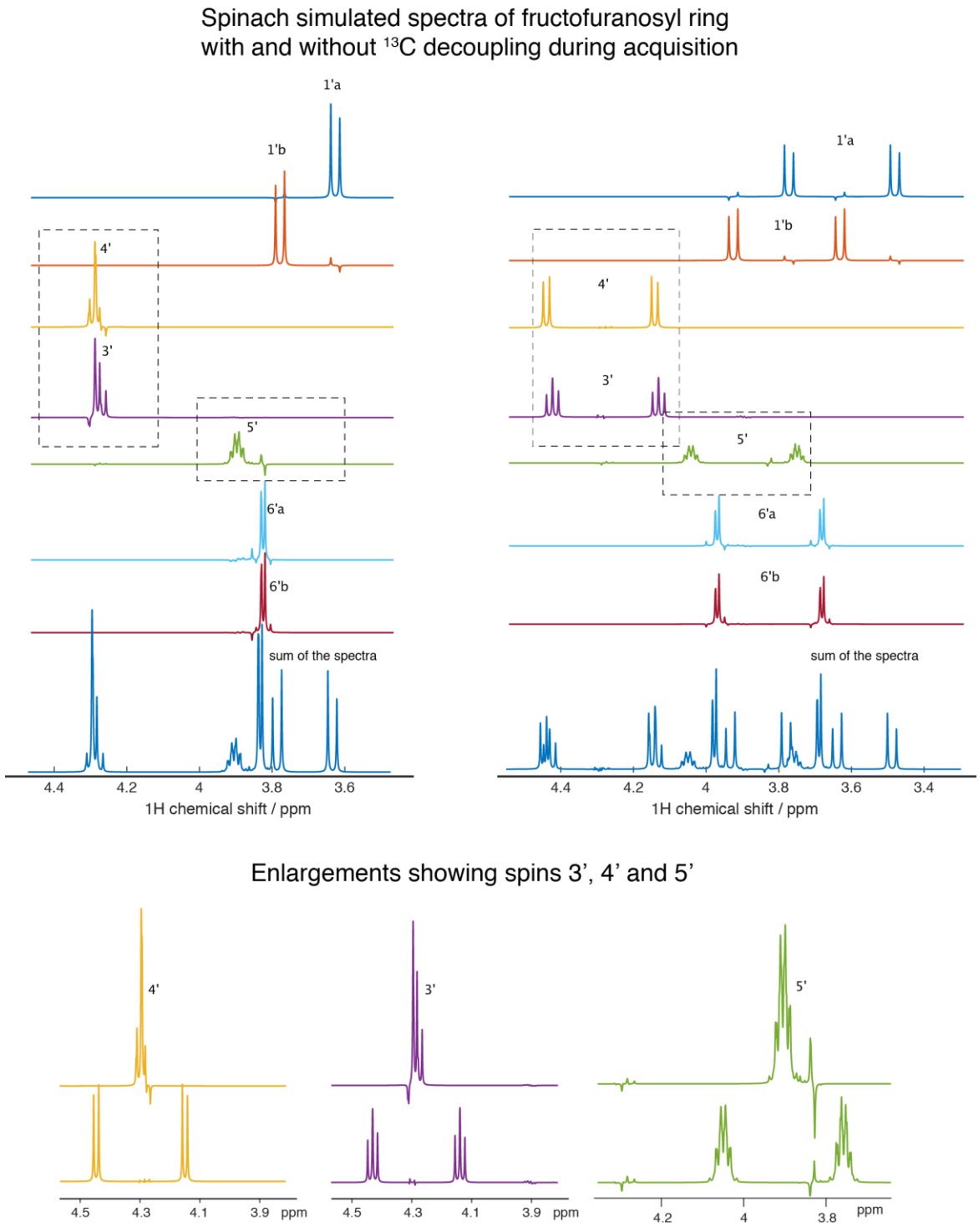

Figure 44. Simulated 1D spectra of the fructofuranosyl ring; the 1D spectra were "theoretically" decomposed into spectra with selective excitation (performed sequentially for each spin in the spin system), in order to show the transfers between strongly coupled spins. When keeping the ^{13}C in the spin system, each selectively excited spectrum corresponds to a distinct isotopomer.

In the two-dimensional spectra, the artifacts resulting from these transfers will evolve in the indirect dimension according to their frequency in given intervals of the pulse sequence. The fact that several spins may be strongly coupled and that each pulse and delay contributes to the rotation of this magnetization according to the Hamiltonian of the interaction (or in other words there is the constantly changing commutation relationship between the propagator and the density matrix describing the magnetization), the magnetization turns out to not only appear in between the coupled spins, but it is observed as being distributed over the F1 indirect dimension, as shown in Figure 45.

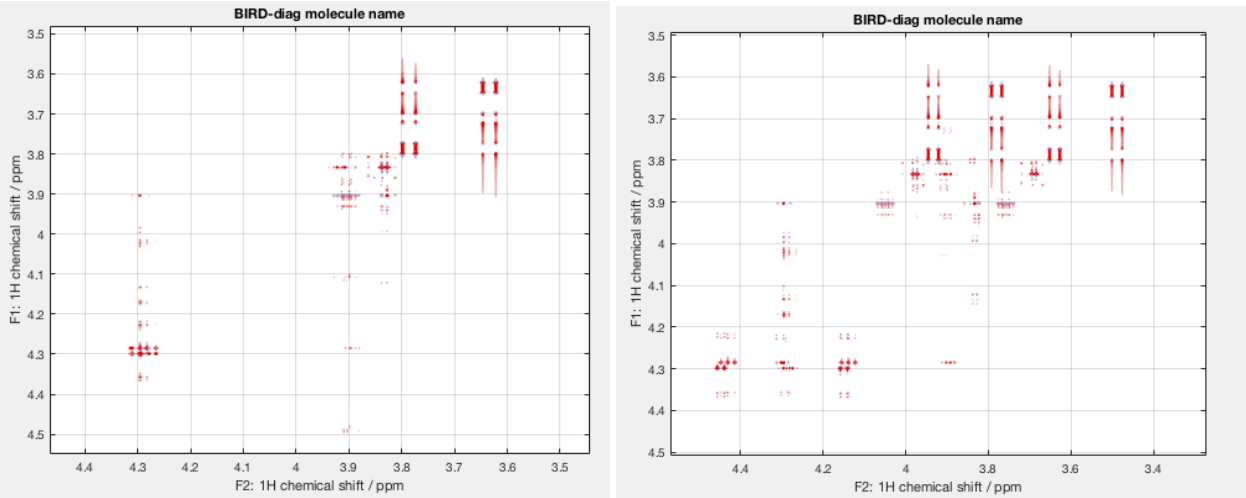

Figure 45. Simulation of BIRD-DIAG spectra with and without ^{13}C decoupling during acquisition.

It is noteworthy that the spectra shown on the left side of Figure 44 would correspond to cross-sections extracted along the F2 dimension of a DIAG experiment, if (and only if) the strong coupling interaction was not existing in the F1 dimension. The reason is that the 1D spectra shown in Figure 44 are perfectly separated (they were simulated by applying a theoretical pulse selectively to one proton). If strong coupling would exist in F1, the lineshapes of signals extracted from the spectrum would be additionally distorted. The F1-BIRD-decoupled experiments give the possibility to have an access to cross-sections of a 2D spectrum, from which the strong coupling interactions can be examined as in the theoretical spectra, since in F1 the spins are not mixed in the same way as in F2.

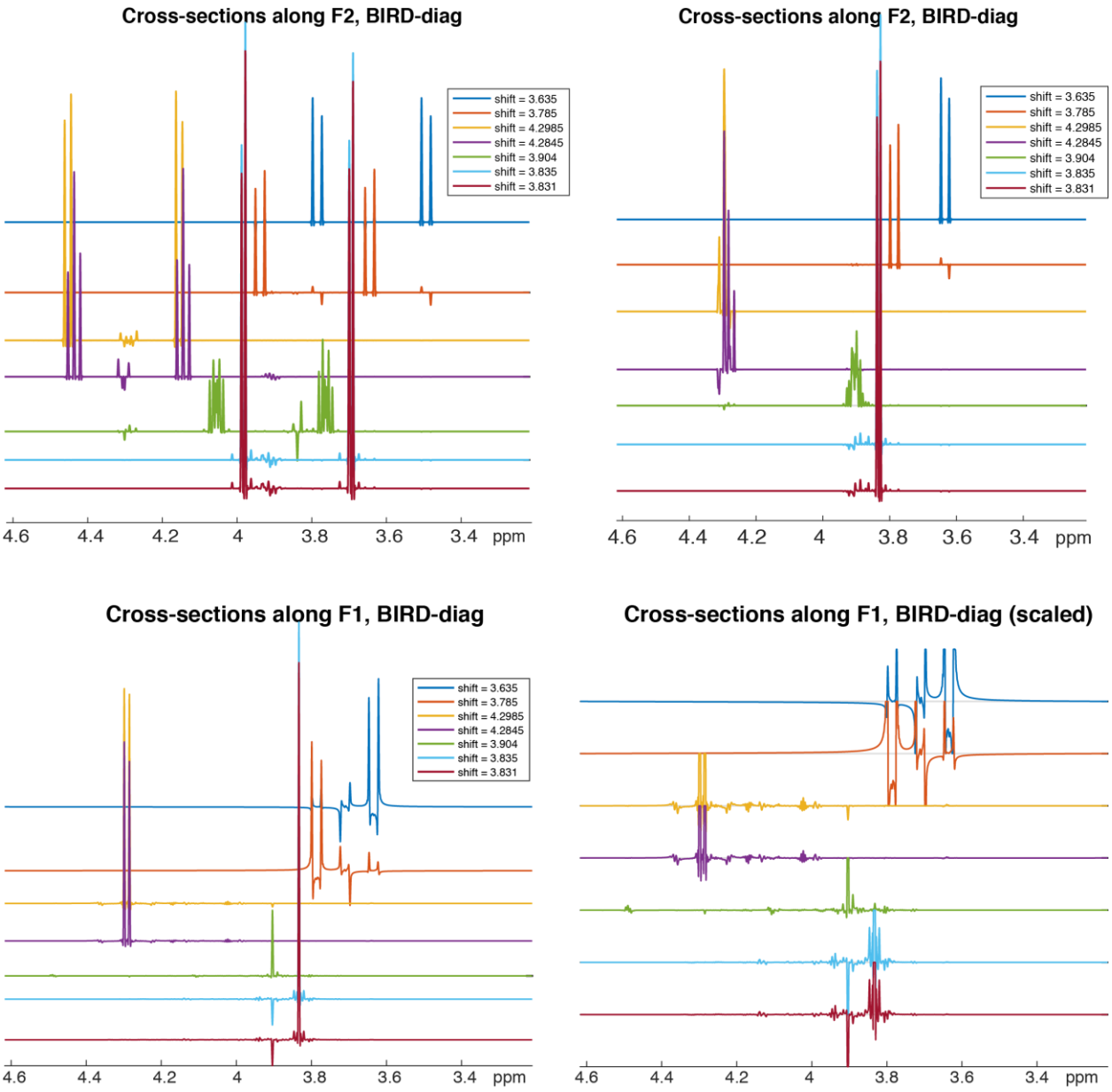

Figure 46. Cross-sections extracted from Spinach simulations of 2D BIRD-decoupled DIAG spectra.

Simulated spectrum in Figure 47 can be compared to the experimental one in Figure 38.

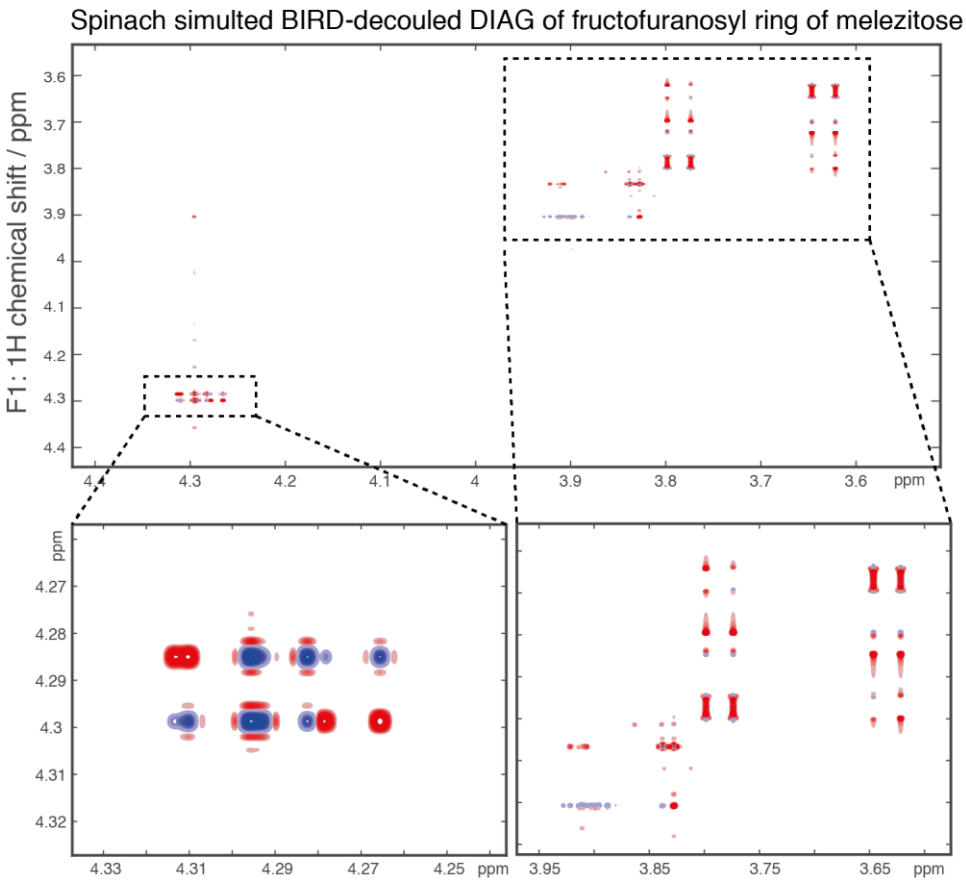

Figure 47. Enlarged region of the BIRD-decoupled DIAG spectrum showing signals 3' and 4' splitted by the large carbon coupling in F2 dimension and manifesting the first order structure in both dimensions. (a) experimental signal, (b) simulated signal.

VII. Conclusions and Perspectives

The initial aim of the work was to assemble an uniform set of experiments for fast and simplified assignment of resonances with the possibility to precisely measure couplings, even in cases where it is greatly impeded, such as strong coupling.

There is a plethora of different methods to achieve the simplification of spectra by homonuclear decoupling or other techniques – band-selective spectroscopy, *J*-resolved spectroscopy, *z*-COSY, *E*-COSY, etc. Thus, producing such a simplification was not a goal of the research in itself. Rather, it seemed necessary to evaluate the performance of the different methods in different situations. This task turned out to be quite demanding, taking into account how detailed the comparison needs to be to examine methods that all lead to similar results and overall successful homodecoupling. What sets them apart is the different mechanism that they are based on and performance in cases when spins are strongly coupled.

The study of the strong coupling artifacts in the F1-decoupled two-dimensional (correlation) experiments was organized in a way as to find a link between the features observed in 1D spectra (mainly the "roof effect" and intensity distortions), the family of *J*-resolved experiments (for which quite a significant amount of literature data is available) and the 2D experiments developed in our group.

Since the exact mechanism of the PSYCHE method and its performance in the context of different experiments was not thoroughly studied and reported, it became a great part of this work to understand it and estimate the sources of artifacts that were observed in the spectra. Moreover, since the element was introduced quite recently, it has not been much modified. One motivation in this project was to explore possibilities of improving its performance.

For that purpose, a basic theoretical ground has been prepared and the key rules binding the modern NMR methods have been revised and discussed. This was a first necessary step to be able to develop a package of simulations of the studied experiments. The main usage of spin simulation programs is to strengthen the link between the appearance of the spectrum and its formal description. The theoretical description facilitates significantly the search for improved solutions in NMR methodology.

The theoretical considerations developed in this thesis should be useful to better design the simulations and to get more precise information about the simulated system. That would eventually and tentatively lead to proposing solutions for further improvement of the existing methods.

Some difficulties encountered in the development of this project were, among others: making the link in applicability of analysis performed for 2-3 spins in much larger spin systems and the considerable time of the simulations treating explicitly the spatial encoding. Moreover,

quite a basic knowledge of the spin dynamics of this thesis author was hindering the capacity to relate the appearance of the simulated signals to their origin in a more systematic way by the decomposition of the simulation into smaller elements.

Bibliography

[1] R. R. Ernst, H. Primas, *Helv. Phys. Acta* **1963**, *36*, 583.
[2] W. P. Aue, J. Karhan, R. R. Ernst, *J. Chem. Phys.* **1976**, *64*, 4226.
[3] J. R. Garbow, D. P. Weitekamp, A. Pines, *Chem. Phys. Lett.* **1982**, *93*, 504.
[4] M. Foroozandeh, R. W. Adams, M. Nilsson, G. A. Morris, *J. Am. Chem. Soc.* **2014**, *136*, 11867.
[5] J. A. Aguilar, A. A. Colbourne, J. Cassani, M. Nilsson, G. A. Morris, *Angew. Chem. Int. Ed. Engl.* **2012**, *51*, 6460.
[6] J. A. Aguilar, S. Faulkner, M. Nilsson, G. A. Morris, *Angew. Chem. Int. Ed. Engl.* **2010**, *49*, 3901.
[7] J. A. Aguilar, M. Nilsson, G. Bodenhausen, G. A. Morris, *Chem. Commun.* **2012**, *48*, 811.
[8] J. A. Aguilar, M. Nilsson, G. A. Morris, *Angew. Chem. Int. Ed. Engl.* **2011**, *50*, 9716.
[9] M. Foroozandeh, R. W. Adams, N. J. Meharry, D. Jeannerat, M. Nilsson, G. A. Morris, *Angew. Chem. Int. Ed. Engl.* **2014**, *53*, 6990.
[10] A. Cotte, D. Jeannerat, *Angew. Chem. Int. Ed. Engl.* **2015**, *54*, 6016.
[11] L. Paudel, R. W. Adams, P. Kiraly, J. A. Aguilar, M. Foroozandeh, M. J. Cliff, M. Nilsson, P. Sandor, J. P. Waltho, G. A. Morris, *Angew. Chem. Int. Ed. Engl.* **2013**, *52*, 11616.
[12] M. Foroozandeh, P. Giraudeau, D. Jeannerat, *ChemPhysChem* **2011**, *12*, 2409.
[13] M. Foroozandeh, P. Giraudeau, D. Jeannerat, *Magn. Reson. in Chem.* **2013**.
[14] M. Foroozandeh, L. Castañar, L. G. Martins, D. Sinnaeve, G. D. Poggetto, C. F. Tormena, R. W. Adams, G. A. Morris, M. Nilsson, *Angew. Chem. Int. Ed. Engl.* **2016**, *128*, 15808.
[15] L. Castañar, P. Nolis, A. Virgili, T. Parella, *Chem. Eur. J.* **2013**, *19*, 15472.
[16] M. R. Koos, G. Kummerlowe, L. Kaltschnee, C. M. Thiele, B. Luy, *Angew. Chem. Int. Ed. Engl.* **2016**, *55*, 7655.
[17] K. Zangger, H. Sterk, *J. Magn. Reson.* **1997**, *124*, 486.
[18] M. J. Thrippleton, J. Keeler, *Angew. Chem. Int. Ed. Engl.* **2003**, *42*, 3938.
[19] N. Giraud, M. Joos, J. Courtieu, D. Merlet, *Magn. Reson. Chem.* **2009**, *47*, 300.
[20] D. Jeannerat, *Encyclopedia of Magnetic Resonance*, Wiley, Chichester, **2011**.
[21] B. Luy, *J. Magn. Reson.* **2009**, *201*, 18.
[22] K. Takegoshi, K. Ogura, K. Hikichi, *Journal of Magnetic Resonance (1969)* **1989**, *84*, 611.
[23] H. J. Hogben, M. Krzystyniak, G. T. Charnock, P. J. Hore, I. Kuprov, *J. Magn. Reson.* **2011**, *208*, 179.
[24] I. Kuprov, *Magn. Reson. Chem.* **2018**, *56*, 415.
[25] M. J. Thrippleton, R. A. Edden, J. Keeler, *J. Magn. Reson.* **2005**, *174*, 97.
[26] J. M. Nuzillard, *J. Magn. Reson* **2007**, *187*, 193.
[27] M. Goldman, *Quantum Desription of High-Resolution NMR in Liquids*, Oxford University Press, **2002**.
[28] C. Bauer, R. Freeman, T. Frenkiel, J. Keeler, A. J. Shaka, *J. Magn. Reson.* **1984**, *58*, 442.
[29] Ē. Kupče, J. Boyd, I. D. Campbell, *J. Magn. Reson. Ser. B* **1995**, *106*, 300.
[30] M. Foroozandeh, R. W. Adams, P. Kiraly, M. Nilsson, G. A. Morris, *Chem. Commun.* **2015**, *51*, 15410.

[31] J. Keeler, *Understanding NMR Spectroscopy*, John Wiley & Sons, West Sussex, England, **2005**.
[32] C. Griesinger, O. W. Soerensen, R. R. Ernst, *The Journal of Chemical Physics* **1986**, *85*, 6837.
[33] R. R. Ernst, G. Bodenhausen, A. Wokaun, *Principles of Nuclear Magnetic Resonance in One and Two Dimensions*, Clarendon Press, Oxford, **1987**.
[34] H. Oschkinat, A. Pastore, P. Pfändler, G. Bodenhausen, *J. Magn. Reson.* **1986**, *69*, 559.
[35] M. Rance, P. E. Wright, *Journal of Magnetic Resonance (1969)* **1986**, *66*, 372.
[36] L. Braunschweiler, G. Bodenhausen, R. R. Ernst, *Mol. Phys.* **1983**, *48*, 535.
[37] L. Braunschweiler, R. R. Ernst, *J. Magnetic. Reson.* **1983**, *53*, 521.
[38] L. Braunschweiler, R. R. Ernst, *Journal of Magnetic Resonance (1969)* **1983**, *53*, 521.
[39] J.-M. Nuzillard, *Molecular Physics* **2007**, *105*, 2243.
[40] J. B. Murdoch, A. H. Lent, M. R. Kritzer, *J. Magn. Reson.* **1987**, *74*, 226.
[41] J. Pauly, P. Le Roux, D. Nishimura, A. Macovski, *IEEE Trans Med Imaging* **1991**, *10*, 53.
[42] M. Brucka, Kirill F. Sheberstov, D. Jeannerat, *Magn. Reson. Chem.* **2018**, *56*, 1021.
[43] O. W. Soerensen, C. Griesinger, R. R. Ernst, *J. Am. Chem. Soc.* **1985**, *107*, 7778.
[44] A. J. Pell, J. Keeler, *J. Magn. Reson.* **2007**, *189*, 293.
[45] A. J. Pell, R. A. E. Edden, J. Keeler, *Magn. Reson. Chem.* **2007**, *45*, 296.
[46] A. Tal, L. Frydman, *Prog. Nucl. Magn. Reson. Spectrosc.* **2010**, *57*, 241.
[47] M. Foroozandeh, G. A. Morris, M. Nilsson, *Chem. Eur. J.* **2018**, *24*, 13988.
[48] https://www.spectroscopynow.com/details/ezine/1468fb7be24/PSYCHE-NMR-High-resolution-not-all-in-the-mind.html?tzcheck=1
[49] A. Lupulescu, G. L. Olsen, L. Frydman, *J. Magn. Reson.* **2012**, *218*, 141.
[50] N. Giraud, L. Béguin, J. Courtieu, D. Merlet, *Angew. Chem. Int. Ed. Engl.* **2010**, *49*, 3481.
[51] M. Foroozandeh, R. W. Adams, P. Kiraly, M. Nilsson, G. A. Morris, *Chem. Commun.* **2015**, *51*, 15410.
[52] W. P. Aue, E. Bartholdi, R. R. Ernst, *J. Chem. Phys.* **1976**, *64*, 2229.
[53] P. Kiraly, M. Foroozandeh, M. Nilsson, G. A. Morris, *Chem. Phys. Lett.* **2017**, *683*, 398.
[54] J. A. Aguilar, R. Belda, B. R. Gaunt, A. M. Kenwright, I. Kuprov, *Magn. Reson. Chem.* **2018**, *56*, 969.
[55] M. Anteunis, A. de Bruyn, G. Verhegge, *Carbohyd. Res.* **1975**, *44*, 101.

Appendix

A. Experimental details

All spectra were recorded at 298 K on a Bruker DRX 500 spectrometer with a 5-mm DCH ^{13}C–^{1}H cryogenic probe equipped with a *z*-gradient coil. The durations of the 90° pulses were 10.0 and 10.3 μs for ^{1}H and ^{13}C, respectively. The relaxation delay was set to 2 s. The pulses used for homonuclear decoupling were centered in the middle of the detected window.

For the ZS-decoupled spectra, the selective refocusing pulses applied during the encoding gradient (G_s) were Rsnob[41] pulses. For the modulation generating non-equidistantly separated irradiation sites, the lists of frequencies contained two blocks of n = 50 irradiation sites, where, in each block, the distance between first and second site was (1/3)Δ (where Δ = SW/n) and SW = 20 ppm. The distance was gradually incremented up to (2/3)Δ. Such a modulated pulse covered 20 ppm, but homogenous coverage was ensured over 10 ppm. The encoding gradient in this case was calculated to cover a spectral domain of 10 ppm, equal to the one covered by each block of irradiations, which was 0.78 G cm^{-1} (1.3 % of the maximum strength). The duration of the Rsnob pulse was 120 ms with refocusing bandwidth of 156 and 78 Hz, respectively. The power of the modulated pulses was set by calibrating the non-modulated pulses using the Shape Tool (part of Bruker's Topspin 3.5 software), which resulted in calculated change of power level with respect to the 10.0 μs hard 90° pulse on the ^{1}H channel The calculated powers were finally increased by a factor corresponding to the 50 irradiation sites.

For the PSYCHE decoupling experiments, most of the time the two 10 kHz saltire chirps[30] had (each) a duration of 15 ms 20% smoothing. In some tests chirps with duration (each) of 7, 30, and 50 ms were also employed. The power of each double saltire chirp is set automatically by the pulse program, but was verified using the following calculations [5]: (a) A single adiabatic phase modulated chirp (sweeping from low to high frequency) was generated according to the desired durations (7, 15, 30, and 50 ms, respectively), bandwidth (10 kHz), and number of points (14,000) and saved; the same was repeated for a chirp sweeping from high to low frequency. The two phase modulated chirps sweeping in opposite directions were added by using the Manipulate/Add Shapes option in the Shape Tool by aligning to the center of the shape and scaling to 100%. (b) Such a single but now amplitude modulated (saltire) non-adiabatic chirp was integrated by using Analysis/Integrate Shape (analyze integr3) option in the Shape Tool by introducing duration of the single saltire chirp (7, 15, 30, and 50 ms, respectively), desired flip angle (20°), and duration of the hard 90° pulse on the ^{1}H channel

(10.0 μs). (c) Finally, the obtained change of power level (dB) was added to the power of the hard 90° pulse on the ^{1}H channel (−11.05 dB). The power of the double saltire chirp element was set to the resulting value. During the chirp pulses, a constant field gradient of 0.58 G cm^{-1} (1% of the maximum power) was applied.

B. Pulse programs

1. *nemoZS* - decoupled homonuclear experiments

a) DIAG

```
;bbhd_ZS_diag
;based on TOCSY with ZQ elimination from
;M. J. Thrippleton and J. Keeler
;Angew.Chem.Int.Ed. 42, 3938-3941 (2003).
;with Zangger-Sterk homodecoupling
;J. A. Aguilar, S. Faulkner, M. Nilsson & G. A. Morris,
;Angew. Chem. Int. Ed. 49, 3901-3903 (2010).
;J. A. Aguilar, A. A. Colbourne, J. Cassani, M. Nilsson, G. A. Morris,
;Angew. Chem. Int. Ed., 51, 6460-6463 (2012).
;A. Cotte, A, D. Jeannerat, Angew. Chem. Int. Ed., 54 (20), 6016-6018 (2015).
;avoid selective pulses parameters to be overwritten by inconnmr

;$CLASS=HighRes
;$DIM=2D
;$TYPE=
;$SUBTYPE=
;$COMMENT=

#include <Avance.incl>
#include <Delay.incl>
#include <Grad.incl>

"d0=3u"
"in0=inf1/2"
"in1=2*in0"
"p2=p1*2"
"p22=p32"
"p27=500u"
"d27=500u"
"d13=50u"
"d18=d13+p27+d27"
"d11=30m"
"d12=20u"
"d7=500u"
"d6=d7"

1 ze
2 d11
3 d12 pl1:f1
  d1
  p1 ph1
  d0
; the homodecoupling starts here
```

```
 d13 UNBLKGRAD
 p27:gp3
 d27
 p2 ph6
 d13
 p27:gp3*-1
 d27
 100u pl0:f1
 3u
 (center (p22:gp4) (p32:sp29 ph7):f1)
 100u pl1:f1
 d13
 p27:gp7*-1
 d27
; the homodecoupling ends here
 d0
 p2 ph5
 d18
 3u
 p1 ph2
; magnetisation moved to z
 5u pl0:f1
 300u gron0
 p11:sp1:f1 ph4
 100u groff
 5u pl0:f1
 d6 gron5
 300u gron0
 p12:sp2:f1 ph4
 100u groff
 d7
 5u  pl1:f1
 4u BLKGRAD
 p1 ph3
 ; magnetisation moved to plane for aquisition
 go=2 ph31
 d11 mc #0 to 2 F1PH (ip1, id0&dd1)
exit

ph1=0 2          ;first hard pulse 90
ph2=0 0          ;hard pulse 90 sending magnetization to z for filtering
ph3=0 0          ;hard pulse 90 sending magnetization to plane after filtering
ph4=0            ;sweep pulse as filter
ph5=0 0          ;hard pulse 180
ph6=0 0          ;hard pulse 180 during t1
ph7=0 0          ;selective pulse 180
ph31=0 2

;pl0 : zero power (120 dB)
;pl1 : high power
;p1  : 90 degree high power pulse
;p11 : duration of first sweep
;p12 : duration of second sweep
```

```
;d0  : incremented delay
;d1  : relaxation delay
;d6  : duration of homospoil
;d7  : recovery delay
;sp1 : strength for first sweep
;sp2 : strength for second sweep
;sp29: strength for selective pulse for homodecoupling
;gpz0: gradient strength for ZQ suppression
;gpz3: gradient for selective refocusing
;gpz4: gradient for spatial encoding
;gpz5: gradient strength for homospoil
;gpz7: gradient for selective refocusing
;in0 : 1/(2 * SW) = DW
;nd0 : 2
;NS  : 2 * n
;DS  : 8
;td1 : number of t1 increments
;MC2 : States-TPPI

;for z-only gradients:
;gpz0: 5%
;gpz3: 30%
;gpz4: 1%
;gpz5: 40%
;gpz7: 60%

;use gradient files:
;gpnam3: SMSQ10.100
;gpnam4: RECT.1
;gpnam7: SMSQ10.100
```

b) CLIP-COSY

```
;bbhd_ZS_clip_cosy
;based on TOCSY with ZQ elimination from
;M. J. Thrippleton and J. Keeler
;Angew.Chem.Int.Ed. 2003, 42, 3938-3941
;with Zangger-Sterk homodecoupling
;clean in-phase transfer according to
;Koos, M. R. M.; Kummerlowe, G.; Kaltschnee, L.; Thiele, C. M.; Luy, B.
;Angew.Chem.Int.Ed. 2016, 55, 7655-7659

;$CLASS=HighRes
;$DIM=2D
;$TYPE=
;$SUBTYPE=
;$COMMENT=

#include <Avance.incl>
#include <Delay.incl>
#include <Grad.incl>

"d0=3u"
"in0=inf1/2"
"in1=2*in0"
"p2=p1*2"
"p22=p32"
"p27=500u"
"d27=500u"
"d13=50u"
"d18=d13+p27+d27"
"d11=30m"
"d12=20u"
"d7=500u"
"d6=d7"

1 ze
2 d11
3 d12 pl1:f1
  d1
  p1 ph1
  d0
; the homodecoupling starts here
  d13 UNBLKGRAD
  p27:gp3
  d27
  p2 ph6
  d13
  p27:gp3*-1
  d27
  100u pl0:f1
  3u
  (center (p22:gp4) (p32:sp29 ph7):f1)
```

```
  100u pl1:f1
  d13
  p27:gp7*-1
  d27
; the homodecoupling ends here
  d0
  p2 ph5
  d18
  3u
  p1 ph2
; magnetisation moved to z
  5u pl0:f1
  300u gron0
  p11:sp1:f1 ph4
  100u groff
  5u pl1:f1
; the in-phase transfer starts here
  p1 ph2
  d20
  p2 ph8
  d20
  p1 ph8
  d20
  p2 ph8
  d20
  p1 ph2
; the in-phase transfer ends here
  5u pl0:f1
  d6 gron5
  300u gron0
  p12:sp2:f1 ph4
  100u groff
  d7
  5u pl1:f1
  4u BLKGRAD
  p1 ph3
; magnetisation moved to plane for detection
  go=2 ph31
  d11 mc #0 to 2 F1PH (ip1, id0)
exit

ph1=0 2          ;first hard pulse 90
ph2=0 0          ;hard pulse 90 sending magnetization to z for filtering
ph3=0 0          ;hard pulse 90 sending magnetization to plane after filtering
ph4=0            ;sweep pulse as filter
ph5=0 0          ;hard pulse 180
ph6=0 0          ;hard pulse 180 during t1
ph7=0 0          ;selective pulse 180
ph8=1            ;hard pulses in CLIP transfer
ph31=0 2
```

;pl0 : zero power (120 dB)
;pl1 : high power
;p1 : 90 degree high power pulse
;p11 : duration of first sweep
;p12 : duration of second sweep
;d0 : incremented delay
;d1 : relaxation delay
;d6 : duration of homospoil
;d7 : recovery delay
;d20: CLIP delay: 1/(4J(HH))

;sp1 : strength for first sweep
;sp2 : strength for second sweep
;sp29: strength for selective pulse for homodecoupling
;gpz0: gradient strength for ZQ suppression
;gpz3: gradient for selective refocusing
;gpz4: gradient for spatial encoding
;gpz5: gradient strength for homospoil
;gpz7: gradient for selective refocusing
;in0 : 1/(2 * SW) = DW
;nd0 : 2
;NS : 2 * n
;DS : 8
;td1 : number of t1 increments
;MC2 : States-TPPI

;for z-only gradients:
;gpz0: 5%
;gpz3: 30%
;gpz5: 40%
;gpz7: 60%

;use gradient files:
;gpnam3: SMSQ10.100
;gpnam4: RECT.1
;gpnam7: SMSQ10.100

2. *PSYCHE* - decoupled homonuclear experiments

a) DIAG

```
;bbhd_psyche_diag
;based on TOCSY with ZQ elimination from
;M. J. Thrippleton and J. Keeler
;Angew. Chem. Int. Ed. 42, 3938-3941 (2003).
;with PSYCHE homodecoupling
;J. A. Aguilar, S. Faulkner, M. Nilsson & G. A. Morris,
;Angew. Chem. Int. Ed. 49, 3901-3903 (2010).
;J. A. Aguilar, A. A. Colbourne, J. Cassani, M. Nilsson, G. A. Morris,
;Angew. Chem. Int. Ed., 51, 6460-6463 (2012).
;M. Foroozandeh, R. W. Adams, N. J. Meharry, D. Jeannerat, M. Nilsson, G. A. Morris, Angew. Chem. Int. Ed. Engl. 53, 6990 (2014).
;A. Cotte, A, D. Jeannerat, Angew. Chem. Int. Ed., 54 (20), 6016-6018 (2015).
;avoid selective pulses parameters to be overwritten by inconnmr

;automatic calculation of power for the chirps

#include <Avance.incl>
#include <Delay.incl>
#include <Grad.incl>

"d0=3u"
"in0=inf1/2"
"in1=2*in0"
"p2=p1*2"
"p22=p32"
"p27=500u"
"d27=500u"
"d13=50u"
"d18=d13+p27+d27"
"d11=30m"
"d12=20u"
"d7=500u"
"d6=d7"

"cnst50=(cnst20/360)*sqrt((2*cnst21)/(p32/2000000))"
"p30=1000000/(cnst50*4)"
"cnst31=(p30/p1)*(p30/p1)"
"spw29=plw1/cnst31"

1 ze
2 d11
3 d12 pl1:f1
d1
p1 ph1
d0
; the homodecoupling starts here
d13 UNBLKGRAD
```

```
p27:gp3
d27
p2 ph6
d13
p27:gp3
d27
p27:gp7
d27
100u pl0:f1
3u
(center (p22:gp4) (p32:sp29 ph7):f1)
100u pl1:f1
d13
p27:gp7
d27
d27
d27
; the homodecoupling ends here
d0
p2 ph5
d18
3u
p1 ph2
; magnetisation moved to z
5u pl0:f1
300u gron0
p11:sp1:f1 ph4
100u groff
5u pl0:f1
d6 gron5
300u gron0
p12:sp2:f1 ph4
100u groff
d7
5u  pl1:f1
4u BLKGRAD
p1 ph3
; magnetisation moved to plane for detection
go=2 ph31
d11 mc #0 to 2 F1PH (ip1, id0&dd1)
exit

ph1=0 2  ;first hard pulse 90
ph2=0 0  ;hard pulse 90 sending magnetization to z for filtering
ph3=0 0  ;hard pulse 90 sending magnetization to plane after filtering
ph4=0    ;sweep pulse as filter
ph5=0 0  ;hard pulse 180
ph6=0 0  ;hard pulse 180 during t1
ph7=0 0  ;selective pulse 180
ph31=0 2

;pl0 : zero power (120 dB)
;pl1 : high power
```

```
;p1  : 90 degree high power pulse
;p11 : duration of first sweep
;p12 : duration of second sweep
;d0  : incremented delay
;d1  : relaxation delay
;d6  : duration of homospoil
;d7  : recovery delay
;sp1 : strength for first sweep
;sp2 : strength for second sweep
;sp29: strength for PSYCHE double chirp element for homodecoupling
;gpz0: gradient strength for ZQ suppression
;gpz3: gradient for selective refocusing
;gpz4: gradient for PSYCHE element
;gpz5: gradient strength for homospoil
;gpz7: gradient for selective refocusing
;cnst20: desired flip angle for PSYCHE pulse element (degrees) (normally 10-25)
;cnst21: bandwidth of each chirp in PSYCHE pulse element (Hz) (normally 10000)
;p32: duration of double-chirp pulse element
;in0 : 1/(2 * SW) = DW
;nd0 : 2
;NS  : 2 * n
;DS  : 8
;td1 : number of t1 increments
;MC2 : States-TPPI

;for z-only gradients:
;gpz0: 5%
;gpz3: 30%
;gpz4: 1-3%
;gpz5: 40%
;gpz7: 60%

;use gradient files:
;gpnam3: SMSQ10.100
;gpnam4: RECT.1
;gpnam7: SMSQ10.100
```

b) CLIP-COSY

```
;bbhd_psyche_clip_cosy
;based on TOCSY with ZQ elimination from
;M. J. Thrippleton and J. Keeler
;Angew.Chem.Int.Ed. 2003, 42, 3938-3941
;with PSYCHE homodecoupling;clean in-phase transfer according to
;Koos, M. R. M.; Kummerlowe, G.; Kaltschnee, L.; Thiele, C. M.; Luy, B.
;Angew.Chem.Int.Ed. 2016, 55, 7655-7659

;$CLASS=HighRes
;$DIM=2D
;$TYPE=
;$SUBTYPE=
;$COMMENT=

#include <Avance.incl>
#include <Delay.incl>
#include <Grad.incl>

"d0=3u"
"in0=inf1/2"
"in1=2*in0"
"p2=p1*2"
"p22=p32"
"p27=500u"
"d27=500u"
"d13=50u"
"d18=d13+p27+d27"
"d11=30m"
"d12=20u"
"d7=500u"
"d6=d7"
"d20=1/(4*cnst22)"

"cnst50=(cnst20/360)*sqrt((2*cnst21)/(p32/2000000))"
"p30=1000000/(cnst50*4)"
"cnst31=(p30/p1)*(p30/p1)"
"spw29=plw1/cnst31"

1 ze
2 d11
3 d12 pl1:f1
d1
p1 ph1
d0
; the homodecoupling starts here
d13 UNBLKGRAD
p27:gp3
d27
```

```
p2 ph6
d13
p27:gp3
d27
p27:gp7
d27
100u pl0:f1
3u
(center (p22:gp4) (p32:sp29 ph7):f1)
100u pl1:f1
d13
p27:gp7
d27
d27
d27; the homodecoupling ends here
d0
p2 ph5
d18
3u
p1 ph2; magnetisation moved to z
5u pl0:f1
300u gron0
p11:sp1:f1 ph4
100u groff
5u pl1:f1; the in-phase transfer starts here
p1 ph2
d20
p2 ph8
d20
p1 ph8
d20
p2 ph8
d20
p1 ph2; the in-phase transfer ends here
5u pl0:f1
d6 gron5
300u gron0
p12:sp2:f1 ph4
100u groff
d7
5u pl1:f1
4u BLKGRAD
p1 ph3
go=2 ph31
d11 mc #0 to 2 F1PH (ip1, id0)
exit

ph1=0 2          ;first hard pulse 90
ph2=0 0          ;hard pulse 90 sending magnetization to z for filtering
ph3=0 0          ;hard pulse 90 sending magnetization to plane after filtering
ph4=0            ;sweep pulse as filter
ph5=0 0          ;hard pulse 180
ph6=0 0          ;hard pulse 180 during t1
```

```
ph7=0 0            ;PSYCHE pulse element
ph8=1              ;hard pulses in CLIP transfer
ph31=0 2

;pl0 : zero power (120 dB)
;pl1 : high power
;p1  : 90 degree high power pulse
;p11 : duration of first sweep
;p12 : duration of second sweep
;d0  : incremented delay
;d1  : relaxation delay
;d6  : duration of homospoil
;d7  : recovery delay
;d20: CLIP delay: 1/(4J(HH))
;cnst22: homonuclear J(HH) coupling
;sp1 : strength for first sweep
;sp2 : strength for second sweep
;sp29: strength for PSYCHE double chirp element for homodecoupling
;gpz0: gradient strength for ZQ suppression
;gpz3: gradient for selective refocusing
;gpz4: gradient for spatial encoding
;gpz5: gradient strength for homospoil
;gpz7: gradient for selective refocusing
;in0 : 1/(2 * SW) = DW
;nd0 : 2
;NS  : 2 * n
;DS  : 8
;td1 : number of t1 increments
;MC2 : States-TPPI
;cnst20: desired flip angle for PSYCHE pulse element (degrees) (normally 10-25)
;cnst21: bandwidth of each chirp in PSYCHE pulse element (Hz) (normally 10000)
;p32: duration of double-chirp pulse element

;for z-only gradients:
;gpz0: 5%
;gpz3: 30%
;gpz4: 1-3%
;gpz5: 40%
;gpz7: 60%

;use gradient files:
;gpnam3: SMSQ10.100
;gpnam4: RECT.1
;gpnam7: SMSQ10.100
```

3. *BIRD* – decoupled homonuclear experiments

a) DIAG

```
;bbhd_BIRD_diag
;based on TOCSY with ZQ elimination from
;M. J. Thrippleton and J. Keeler
;Angew.Chem.Int.Ed. 42, 3938-3941 (2003).
;with BIRD homodecoupling
;using 1H broadband homodecoupling during acquisition
;using dwellmode explicit
;CH2 groups may be left as doubletts with 2J(HH) spliting
;J.A. Aguilar, M. Nilsson & G.A. Morris, Angew. Chem. 123, 9716-9717 (2011)
;P. Sakhaii, B. Haase & W. Bermel, J. Magn. Reson. 199, 192-198 (2009)

;$CLASS=HighRes
;$DIM=2D
;$TYPE=
;$SUBTYPE=
;$COMMENT=

#include <Avance.incl>
#include <Grad.incl>
#include <Delay.incl>
#include <De.incl>

"d0=3u"
"in0=inf1/2"
"p2=p1*2"
"p4=p3*2"
"p27=500u"
"p29=300u"
"d2=1s/(cnst2*2)"
"d6=d7"
"d7=500u"
"d11=30m"
"d12=20u"
"d13=50u"
"d14=2*d0+p4"
"d18=d13+p27+d27"
"d27=500u"

"l1=l0-1"
"DELTA2=d2-larger(p2,p14)/2"
;"TAU=p14"
"TAU=larger(p2,p14)"
"DELTA1=TAU/2"
"TAU1=p2"
"l30=0"

1 ze
  d11 pl12:f2
```

```
2 d11 do:f2
3 d12 pl1:f1
 d1
      (p1 ph1):f1
 d2 pl0:f2
 if "l30 %2 == 0"
            {
            (center (p2 ph1):f1 (p14:sp3 ph6):f2 )
            }
 else
            {
            (center (p2 ph1):f1 (TAU):f2 )
            }
      4u iu30
      d0
; the homodecoupling starts here
      d13 UNBLKGRAD
      p27:gp3
            d27
      p2 ph6
      d13
      p27:gp3*-1
      d27
      3u
      4u
; the BIRD filter starts here
      (p1 ph7)
      DELTA2
      (center (p2 ph7) (p14:sp3 ph6):f2 )
      DELTA2
      (p1 ph7)
      d2
; the BIRD filter ends here
      d13
      p27:gp7 *-1
      d27
; the homodecoupling ends here
      d0
      4u
      p2 ph5
      d18
      3u
      4u
      p1 ph3
; magnetisation moved to z
      5u pl10:f1
      300u gron0
      p11:sp1:f1 ph4
      100u groff
      5u pl10:f1
      d6 gron5
      300u gron0
      p12:sp2:f1 ph4
```

```
      100u groff
      d7
      5u  pl1:f1
      4u pl12:f2
      4u
      p1 ph3
; magnetisation moved to plane for detection
      go=2 ph31 cpd2:f2
      d11 do:f2 mc #0 to 2 F1PH(ip1, id0)
exit

ph1=0
ph2=0
ph3=3
ph4=0
ph5=0
ph6=0
ph7=0 0 1 1 2 2 3 3
ph23=0
ph25=1
ph30=0
ph31=0 2 2 0

;pl1 : f1 channel - power level for pulse (default)
;pl2 : f2 channel - power level for pulse (default)
;pl12: f2 channel - power level for CPD/BB decoupling
;sp3: f2 channel - shaped pulse (180 degree inversion)
;spnam3: Crp60,0.5,20.1 (Crp80,0.5,20.1)
;p1 : f1 channel -  high power pulse
;p2 : f1 channel - 180 degree high power pulse
;p14: f2 channel - 180 degree shaped pulse for inversion
;     = 500usec for Crp60,0.5,20.1
;d1 : relaxation delay
; 1-5 * T1
;d2 : 1/(2J)XH
;d11: delay for disk I/O  [30 msec]
;cnst2: = J(XH)
;NS  : 2 * n
;DS  : 8
;cpd2: decoupling according to sequence defined by cpdprg2
;pcpd2: f2 channel - 90 degree pulse for decoupling sequence

;for z-only gradients:
;gpz0: 5%
;gpz3: 30%
;gpz4: 1-3%
;gpz5: 40%
;gpz7: 60%

;use gradient files:
;gpnam3: SMSQ10.100
;gpnam4: RECT.1
;gpnam7: SMSQ10.100
```

b) CLIP-COSY

```
;bbhd_BIRD_CLIP_COSY
;based on TOCSY with ZQ elimination from
;M. J. Thrippleton and J. Keeler
;Angew.Chem.Int.Ed. 42, 3938-3941 (2003)
;with BIRD homodecoupling
;using 1H broadband homodecoupling during acquisition
;using dwellmode explicit
;CH2 groups may be left as doubletts with 2J(HH) spliting
;J.A. Aguilar, M. Nilsson & G.A. Morris, Angew. Chem. 123, 9716-9717 (2011)
;P. Sakhaii, B. Haase & W. Bermel, J. Magn. Reson. 199, 192-198 (2009)

;$CLASS=HighRes
;$DIM=2D
;$TYPE=
;$SUBTYPE=
;$COMMENT=

#include <Avance.incl>
#include <Grad.incl>
#include <Delay.incl>
#include <De.incl>

"d0=3u"
"in0=inf1/2"
"p2=p1*2"
"p4=p3*2"
"p27=500u"
"d27=500u"
"d13=50u"
"d18=d13+p27+d27"
"d11=30m"
"d12=20u"
"d7=500u"
"d6=d7"
"d14=2*d0+p4"
"d2=1s/(cnst2*2)"
"p29=300u"

"l1=l0-1"
"DELTA1=d7-12u"
"DELTA2=d2-larger(p2,p14)/2"
"TAU=p14"
"TAU1=p2"
"l30=0"

1 ze
  d11 pl12:f2
2 d11 do:f2
3 d12 pl1:f1
  d1
```

```
 (p1 ph1):f1
 d2 pl0:f2
 if "l30 %2 == 0"
   {
   (center (p2 ph1):f1 (p14:sp3 ph6):f2 )
   }
 else
   {
   (center (p2 ph1):f1 (TAU):f2 )
   }
 4u iu30
 d0
; the homodecoupling starts here
 d13 UNBLKGRAD
 p27:gp3
 d27
 p2 ph6
 d13
 p27:gp3*-1
 d27
 3u
 4u
; the BIRD filter starts here
 (p1 ph7)
 DELTA2
 (center (p2 ph7) (p14:sp3 ph6):f2 )
 DELTA2
 (p1 ph7)
 d2
; the BIRD filter ends here
 d13
 p27:gp7 *-1
 d27
; the homodecoupling ends here
 d0
 4u
 p2 ph5
 d18
 3u
 4u
 p1 ph3
; magnetisation moved to z
 5u pl10:f1
 300u gron0
 p11:sp1:f1 ph4
 100u groff
 5u pl1:f1
; the in-phase transfer starts here
 p1 ph2
 d20
 p2 ph8
 d20
 p1 ph8
```

```
  d20
  p2 ph8
  d20
  p1 ph2
; the in-phase transfer ends here
  5u pl10:f1
  d6 gron5
  300u gron0
  p12:sp2:f1 ph4
  100u groff
  d7
  5u  pl1:f1
  4u pl12:f2
  4u BLKGRAD
  p1 ph3
;
  go=2 ph31 cpd2:f2
  d11 do:f2 mc #0 to 2 F1PH(ip1, id0)
exit

ph1=0
ph2=0
ph3=3
ph4=0
ph5=0
ph6=0
ph7=0 0 1 1 2 2 3 3
ph8=1               ;hard pulses in CLIP transfer
ph23=0
ph25=1
ph30=0
ph31=0 2 2 0

;pl1 : f1 channel - power level for pulse (default)
;pl2 : f2 channel - power level for pulse (default)
;pl12: f2 channel - power level for CPD/BB decoupling
;sp3: f2 channel - shaped pulse (180degree inversion)
;spnam3: Crp60,0.5,20.1 (Crp80,0.5,20.1)
;p1 : f1 channel -  high power pulse
;p2 : f1 channel - 180 degree high power pulse
;p14: f2 channel - 180 degree shaped pulse for inversion
;     = 500usec for Crp60,0.5,20.1
;p16: homospoil/gradient pulse                    [1 msec]
;p29: gradient pulse 3                          [300 usec]
;d1 : relaxation delay; 1-5 * T1
;d2 : 1/(2J)XH
;d11: delay for disk I/O                         [30 msec]
;d16: delay for homospoil/gradient recovery
;d62: length of block between decoupling pulses : = aq/l0 [< 20-25 msec]
;d63: = d62/2
;cnst2: = J(XH)
;l0 : number of blocks during acquisition time
;adjust to get d62 as required
```

;ns: 1 * n, total number of scans: NS * TD0
;ds: >= 16
;cpd2: decoupling according to sequence defined by cpdprg2
;pcpd2: f2 channel - 90 degree pulse for decoupling sequence

;for z-only gradients:
;gpz1: 20%
;gpz2: 80%
;gpz3: 60%
;gpz4: 3%
;gpz5: 5%

;use gradient files:
;gpnam1: SMSQ10.100
;gpnam2: SMSQ10.100
;gpnam3: SMSQ10.100
;gpnam4: SMSQ10.50
;gpnam5: SMSQ10